ENGINEERING RESEARCH INSTITUTE · UNIVERSITY OF MICHIGAN

MODERN ICING TECHNOLOGY

LECTURE NOTES

by

MYRON TRIBUS

Project M992-E

AIR RESEARCH AND DEVELOPMENT COMMAND, USAF
CONTRACT AF 18(600)-51, E. O. No.462 Br-1

January, 1952

FOREWORD

These notes are the outgrowth of a seminar on icing information given at the University of Michigan in the Fall of 1951. They are intended to be useful to persons interested in entering the icing field who require a single source where either the basic information or suitable references may be found.

This first edition was rather hurriedly put together for use in a second seminar in February, 1952. Corrections and suggested additions will be most welcome.

Myron Tribus
Director of Icing Research
University of Michigan

TABLE OF CONTENTS

TABLE OF CONTENTS (cont)

CHAPTER I

AN INTRODUCTION TO THE ICING PROBLEM

The type of icing with which we will be concerned in this and subsequent chapters occurs when an airplane flies through a region containing supercooled water droplets. These supercooled water droplets are in an unstable thermodynamic state and upon impinging upon the airplane turn to ice. The resultant ice formation clings tenaciously to the airplane surfaces, adding weight and deforming the aerodynamic shape. Our interest lies in the details of the ice formation process and the methods available for protecting the airplane from its harmful effects. The carburetor icing problem is not considered in this work.

In the first chapter we will consider the circumstances which bring about an icing condition in the atmosphere, typical ice formations on aircraft, and some of the schemes which have been proposed or are used to eliminate the ice. This chapter is intended to serve as an introduction to the field of airplane icing.

Water may be cooled below its freezing point to a surprising degree. Figure I-1 shows the results of experiments carried out by Dorsch and Hacker of the NACA.[1]* This figure shows clearly that small drops of water do not always freeze at 32°F but tend to remain liquid to quite low temperatures. Frank[2] reports supercooled water at -72°C. Once the small drops have turned to ice, however, the melting always occurs at 32°F as reported by Dorsch and Hacker. Figure I-2 shows some typical observed values of supercooled water drops found in the atmosphere.

*Superior figures in the text refer to the references at the end of each chapter.

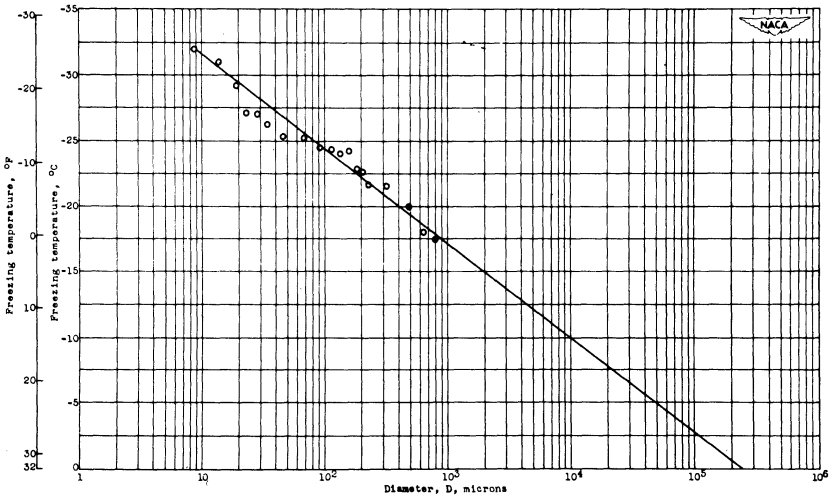

Figure I-1. Curve from Reference 3 showing average freezing temperature of various sized drops observed in Reference 1.

We have a fairly satisfactory qualitative view of why the supercooling occurs. In a drop of water below the freezing point the most stable thermodynamic state for the water molecules (plus their surroundings) is the solid state, wherein the water molecules are oriented in an ice crystal structure. However, in order to form this structure it is necessary for several water molecules to come together in the proper orientation and with the proper energy. The odds against this happening are rather large, though from the Second Law of Thermodynamics point of view we should expect that eventually the drop would freeze. We may, however, help matters along by putting something in the water to act as a nucleus upon which the ice crystals may grow. Such a nucleus will be effective to the degree that it matches the ice crystal structure or permits the crystal to start at a corner or surface defect.[2] Thus, the best nucleus for ice, is a small crystal of ice. Another suitable nucleus is a silver iodide crystal since the structure of silver iodide resembles that of ice. There are enough kinds of materials which may nucleate supercooled water, that ordinary water usually contains sufficient nuclei to prevent undercooling. Not all nuclei are expected to be equally effective. Those which resemble the ice crystal only weakly are expected to be less effective than those which are identical. In the presence of these "weaker" nuclei the freezing point should be lower than 32°F. This concept of the specific nature of a nucleating substance is supported by observations which show that the freezing point is unchanged by successive melting and freezing of an individual drop.[1] Levine[3] has examined the statistical problem of distributing a finite number of specific nuclei in a large volume of water and then dividing the water into a large

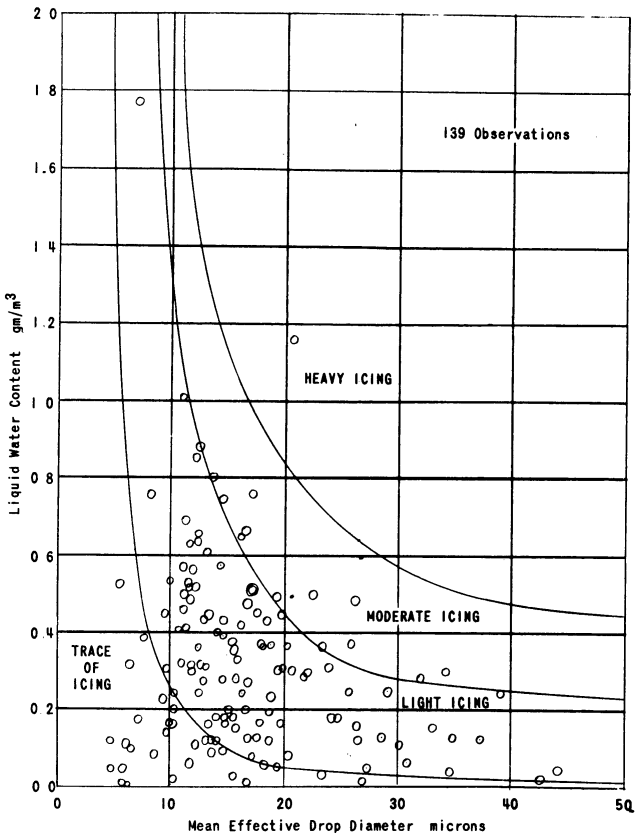

Figure I-2. Liquid water content as related to mean effective drop diameter for flight observations between 5000 and 10,000 feet pressure altitude in the temperature range 15° to 20°F.

number of small droplets. The results of his analysis indicate that the smaller the drop the smaller the probability it will contain a particular nucleating substance. The statistical treatment renders plausible the linear relation between freezing temperature depression and logarithm of diameter (Figure I-1), though the slope and intercept are not predictable by this method. More work certainly remains to be accomplished on the nature of ice nuclei.

In view of the above experimental evidence, then, it is not surprising that clouds of supercooled water droplets are often encountered in the atmosphere. When these water droplets are intercepted by the leading edges of the wings and empennage, as well as all the other components, nuclei present on the surface initiate the transition from liquid to solid. Once a thin film of ice is deposited, succeeding water droplets strike an ice surface and freeze at a rate limited by the heat transfer process rather than the process of initiating an ice crystal.

Before taking up the details of the ice formation and removal, we might, in passing, note that atmospheric icing conditions may be dispelled by providing ice nuclei to "trigger" the unstable supercooled cloud. Silver iodide crystals introduced into a cloud of supercooled droplets will convert the water droplets into snow. The water will condense on these nuclei and form ice crystals. The vapor pressure of ice is lower than that of water, hence the snow grows at the expense of the water drops. Modern rainmaking operations[4] are based upon this principle.

It is now worthwhile to look at some typical ice formations on aircraft. Figures 3, 4, 5, 6, and 7 show typical examples of airplane icing.

Airplane icing is serious for several reasons:

1) The airplane is increased in weight. An ice accretion of 30 lbs per minute on a DC-3-type airplane is not unusual.

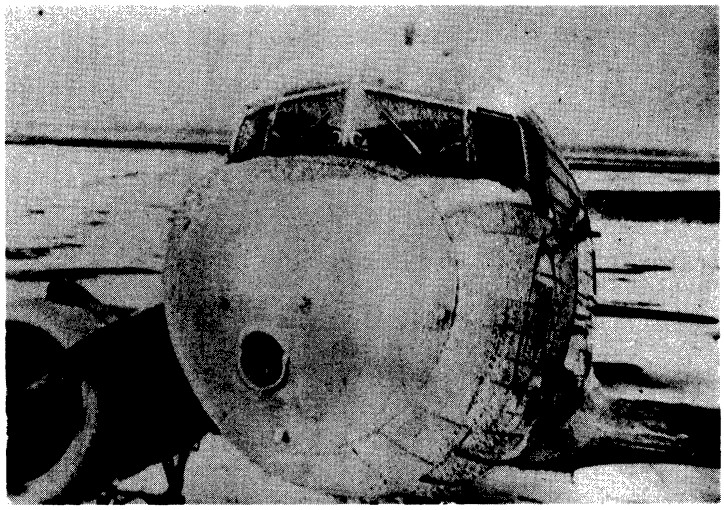

Figure I-3. Ice formations on an airliner forced down by a freezing rain.

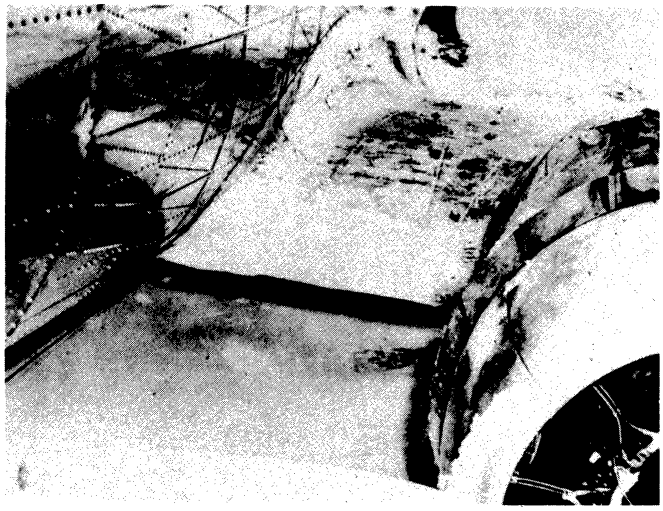

Figure I-4. A view of the wing root of the airplane shown in Figure 3.

2) The airfoil contour is changed. The lift coefficient can be very rapidly reduced by deformation of the wind profile.

3) Ice breaking off the wing may damage tail surfaces. Propellers cast off ice which may damage the fuselage.

4) Air intakes may become clogged. Oil coolers, radiators, jet engine inlets may be stopped up.

5) Ice loads may break the antenna wires.

6) The ice coating on the windshield obstructs vision.

7) Instruments which rely upon air pressure become unreliable. Ice may close over pitot tubes or interfere with pitot-tube readings. Fuel vents may be closed over.

8) The ice loads may set up vibrations in antenna masts.

Figure I-5. A typical "mild" icing condition on the wing root of a B-24-type bomber. (175 mph, 6000 ft, -3°C, drop diameter = 17 microns (avg), 0.2 grams of liquid water per cubic meter of air.

9) Ice formations on various protuberances on the airplane increase the overall drag of the airplane. This effect is more serious in older-style airplanes where the rivet heads stick out from the skin and serve as individual ice collectors.

The system used for ice protection will depend not only upon the particular component but also upon the degree of ice protection desired. Any one airplane is in icing conditions only a small fraction of the time, and, depending on the bias of the designer and the demands of the customer, either emergency or "complete" protection will be provided.

The earliest type of wing de-icers were the rubber "inflatable-shoe" type. This de-icer is alternately inflated and deflated to crack the ice loose. These were practically the only de-icers used in the U. S. and Europe until 1938.5

In the latter part of 1938, the Germans brought out the Ju 88G, which had the wings heated with hot air. Gradually, the Germans replaced their

Figure I-6. Ice formations on an unheated propeller. (Photo, Courtesy Propeller Laboratory, Wright Field, Ohio)

"rubber-shoe" equipped planes with heated wings, and at the close of World War II they used thermal means exclusively.

Experiments with thermal ice protection were conducted by the NACA[7] as early as 1931, when Theodorsen and Clay built a small steamheated model Clark Y airfoil, mounted it on a Fairchild monoplane, and flew it both with water sprays and in natural icing conditions. Some of the predictions in Reference 7 on the behavior of thermal de-icing equipment have been accurately borne out in the intervening twenty years, as will be discussed later.

Several experimental airplanes have been built and flown by the NACA[9-11] The first U. S. mass-produced heated-wing-equipped airplane was the Consolidated

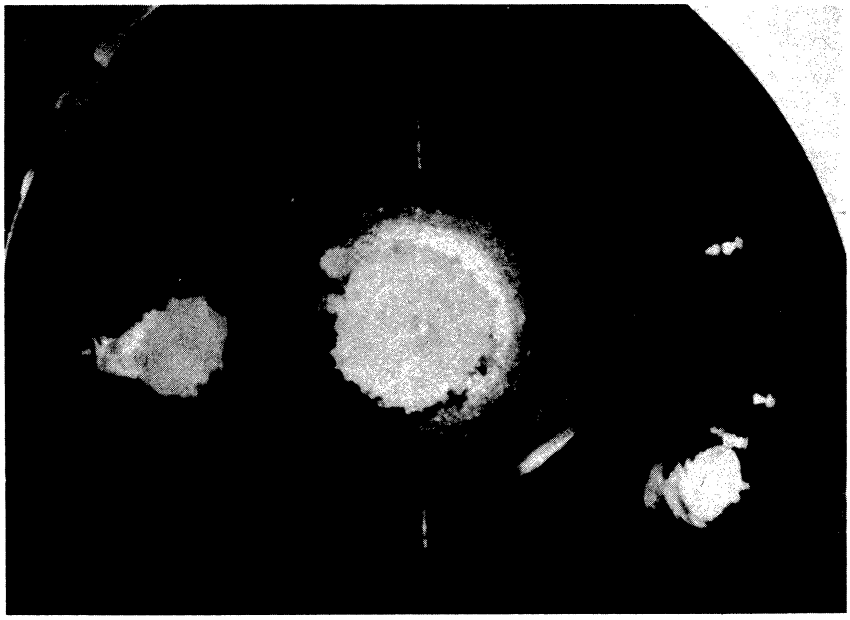

Figure I-7. Ice formations on an unheated jet engine after 36 minutes of icing (Reference 10).

B-24 bomber, which reached production at San Diego March 6, 1944. Since then most new aircraft have featured one form or other of thermal ice-prevention system.

The British equipped some of their bombers with leading edges containing porous metal. Alcohol or glycerol was pumped out these porous leading edges to depress the freezing point of the water and thus release the ice. The system was not satisfactory.

The heated wing was by far the most successful system and today most new aircraft employ air-heated wings for ice protection. Figures 8 and 9 show typical heated-wing systems. The heat supply in an airplane such as the B-24 employed exhaust-gas heat exchangers. In the DC-6 heated-wing separate gasoline-burning combustion heaters are used, as a weight saving has been found through simplification of the exhaust system without heat exchangers. In some jet airplanes the hot air is obtained from the last stage of the compressor. This source of air is expensive, particularly since bleeding 1 per cent of the engine air produces approximately a 2 per cent loss in thrust, but the simplifications in control, installation, maintenance, and fabrication have made the method attractive to the airplane designers, and the overall loss in performance has been acceptable

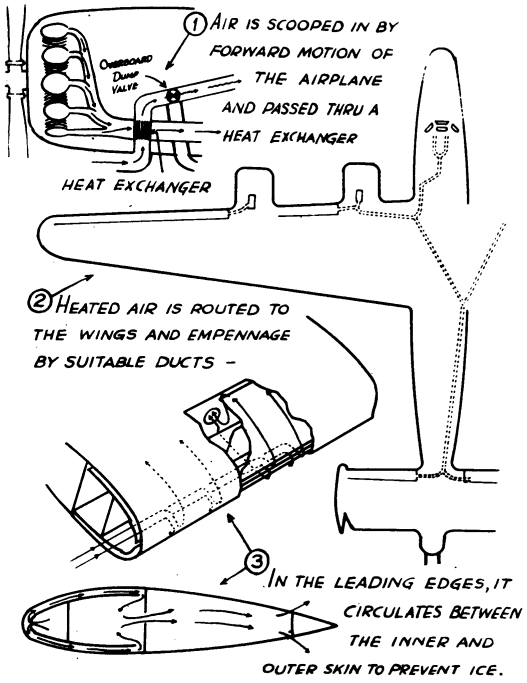

Figure I-8. Typical flow system for a hot-air-type heated wing.

Towards the end of World War II the Germans began to experiment with de-icing methods which were expected to be more economical in their operation. Figures 10 and 11 show two of these schemes. In this country some interest has recently been shown in the intermittently heated systems, as will be seen in a later chapter.

Propeller ice-protection systems have received their share of attention. Early systems of ice protection utilized alcohol "feed shoes". These were dispensing systems which distributed the alcohol along the rotating blades. The alcohol systems were a nuisance but did give protection. Great care is required in the preparation of the slinger rings and shoes lest the alcohol be wasted. If the alcohol vapors are taken into the ventilating system, there is a danger of pilot intoxication. In battle the alcohol tanks are a fire hazard. The alcohol feed shoes have generally been replaced by electrically heated

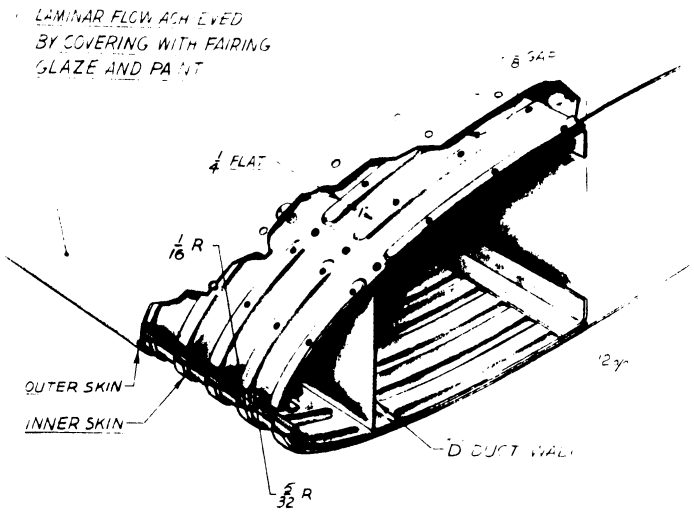

Figure I-9. Typical double-skin construction.

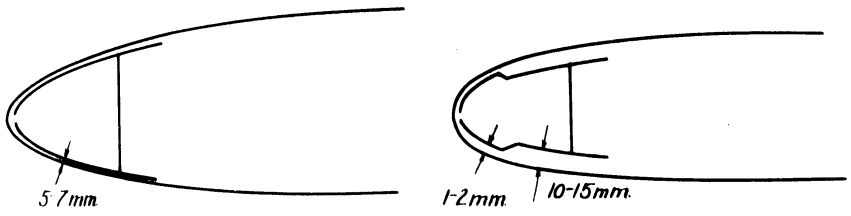

Conventional Heated Wing. Constant gap thickness.

"Economical" De-Icer. Narrow gap (High Intensity Heating) at nose, wide gap (Low Intensity) from 3 to 10% chord.

Figure I-10. German proposal for an "economical" de-icer. Ice formations outside the wide gap were expected to be shed periodically (Reference 5).

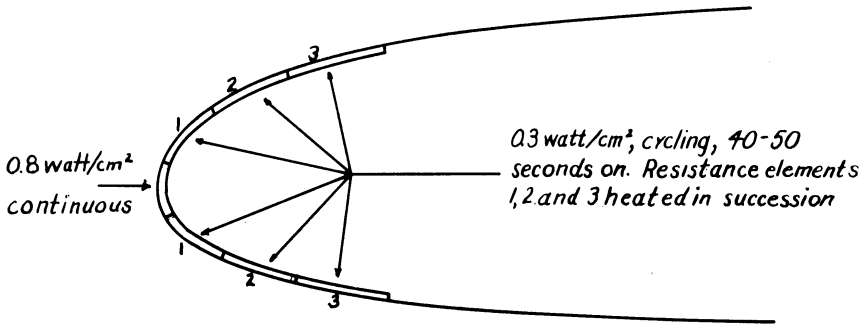

Figure I-11. Messerschmidt scheme for cyclic electrical wing de-icing. For the empennage half these quantities of heat were employed. Resistance elements were approximately six feet in spanwise direction. Different spanwise sections were to be heated at a time.

propellers. The ice is allowed to form and then is shed when the heaters are intermittently energized. As will be shown later, this intermittent operation requires much less energy than continuous heating. Experimental hot-air-heated propellers have been built but none have been reported in operation.[11-13]

A helicopter hot-air system has been described by Katzenberger of Sikorsky Aircraft.[6] The principles of this system are the same as for the heated wing. The rotating mechanism introduces a difficulty in getting the air into the blades without leakage. The rotor acts as a pump to draw air through the heater and duct system. Figure 12 shows a photograph of the test installation made by Sikorsky.

The windshields of aircraft require ice protection. Prior to 1941, most airplane windshields were protected by alcohol spray systems which operated in conjunction with the windshield wipers. United Air Lines pioneered the use of double-paned windshields with hot air flowing between the two layers of glass. These double-paned windshields introduce multiple reflections, particularly during night landings, and are difficult to keep clean, but have otherwise been satisfactory.

Recently the trend has been toward glass with a thin layer of metal laid over to the surface to act as an electrical resistance-heating element.

The important problem here is one of thermal shock. As an airplane suddenly enters or leaves a cloud the thermal stresses may crack the glass.

Jet engines are particularly susceptible to icing difficulties. A jet engine inlet may become iced over a few minutes. The accident in 1951, in which five jet fighters were lost, attests to the seriousness of the jet-engine icing problem. The details of jet-engine anti-icing systems have not been published; however, NACA reports have described both electrical and hot-air systems for engine inlets.[8]

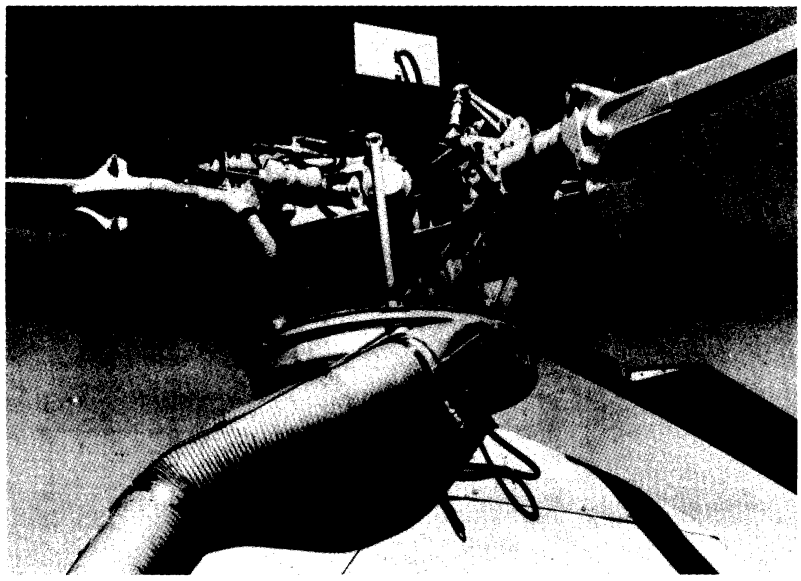

Figure I-12. Experimental installation of hot-air heating system on the hollow-bladed rotor of a helicopter. The box on the top is a temperature recorder. Hot air enters the rotating collector and is ducted to the individual blades by flexible ducting (Reference 6).

REFERENCES

1. Dorsch, R. G., and Hacker, Paul T., "Photomicrographic Investigation of Spontaneous Freezing Temperatures of Supercooled Water Droplets". NACA TN 2142. July, 1950.

2. Frank, F. C., "Molecular Structure of Deeply Supercooled Water". Nature, March 2, 1946, p. 267.

3. Levine, J., "Statistical Explanation of Spontaneous Freezing of Water Droplets". NACA TN 2234. December, 1950.

4. Schaefer, V. J., "Man-Made Snow". Mech. Eng., January, 1947.

5. Tribus, M., "A Review of Some German Developments in Airplane Anti-Icing". Trans ASME, July, 1947, p. 505.

6. Katzenberger, E. F., "An Investigation of a Rotor Blade Thermal Ice Prevention System for the H-5 Helicopter". IAS Preprint 333, January, 1951.

7. Theodorsen, Theodore, and Clay, William C., "Ice Prevention on Aircraft by Means of Engine Exhaust Heat and a Technical Study of Heat Transmission from a Clark Y Airfoil". NACA Report 403, 1931.

8. Hacker, P. T., Dorsch, R. G., Gelder, T. F., Lewis, J. P., Chandler, H. C., and Koutz, S. L. "Ice Prevention for Turbojet Transport Airplane". Sherman M. Fairchild Fund Paper No. FF-1, IAS, March 24, 1950.

9. Ambrosio, A., "Statistical Analysis of Meteorological Icing Conditions". Department of Engineering, University of California, Los Angeles. December, 1950.

10. Samolewicz, J. J., and Macaulay, G. A., "Notes on Some Charge Heating Anti-Icing Tests with an Axial Flow Turbo Jet". Report No. ME-173 Nat. Res. Counsil of Canada, December, 1948.

11. Carson, B. W., and Maynard, J. D., "Investigation of the Effect of a Tip Modification and Thermal De-Icing Air Flow on Propeller Performance", NACA TN 1111, July, 1946.

12. Gray, V. H., and Campbell, R. G., "A Method for Estimating Heat Requirements for Ice Prevention on Gas Heated Hollow Propeller Blades". NACA TN 1494, December, 1947.

13. Mulholland, D. R., and Perkins, P. J., "Investigation of Effectiveness of Air Heating a Hollow Steel Propeller for Protection Against Icing".
Part I NACA TN 1586, May 1948.
Part II NACA TN 1587, May 1948.
Part III NACA TN 1588, May 1948.

CHAPTER II

TRAJECTORIES OF WATER DROPS AROUND STREAMLINED BODIES

The Icing of a Cylinder

The first step in an attack upon the icing problem is the analysis of the icing rates to be expected upon a particular surface.

Consider first the icing of right circular cylinder placed transverse to the air stream. Figure II-1 shows the streamlines for an incompressible non-viscous fluid flowing past a cylinder. A spherical water drop in the fluid stream will not follow the stream lines, but due to its inertia will follow a trajectory which is less curved. Figure II-2 shows a typical water-drop trajectory.

The drop trajectory shown in Figure II-2 was calculated as follows: Consider a drop in air, let

u_a, v_a = components of air velocity

u_d, v_d = components of drop velocity.

Then let

$(u_a - u_d)$, $(v_a - v_d)$ = components of P , the relative drop velocity.

The relative velocity of the droplet gives rise to a drag force

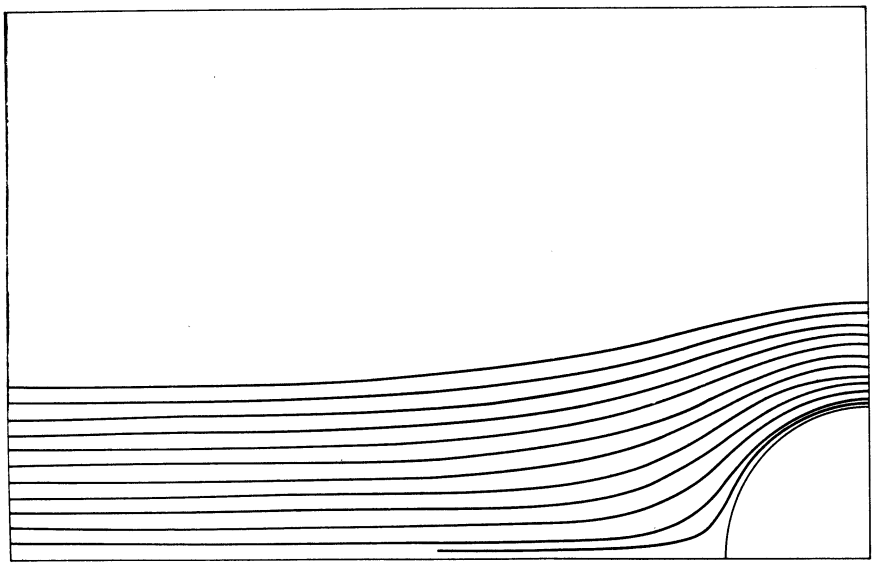

Figure II-1. Flow field ahead of a cylinder.

$$F_x = \frac{1}{2}\rho_a \pi a^2 C_D P (u_a - u_d)$$

$$F_y = \frac{1}{2}\rho_a \pi a^2 C_D P (v_a - v_d) \quad ,$$

where

a = drop radius

C_D = drag coefficient

ρ_a = air density .

These components of drag give rise to accelerations according to Newton's equation.

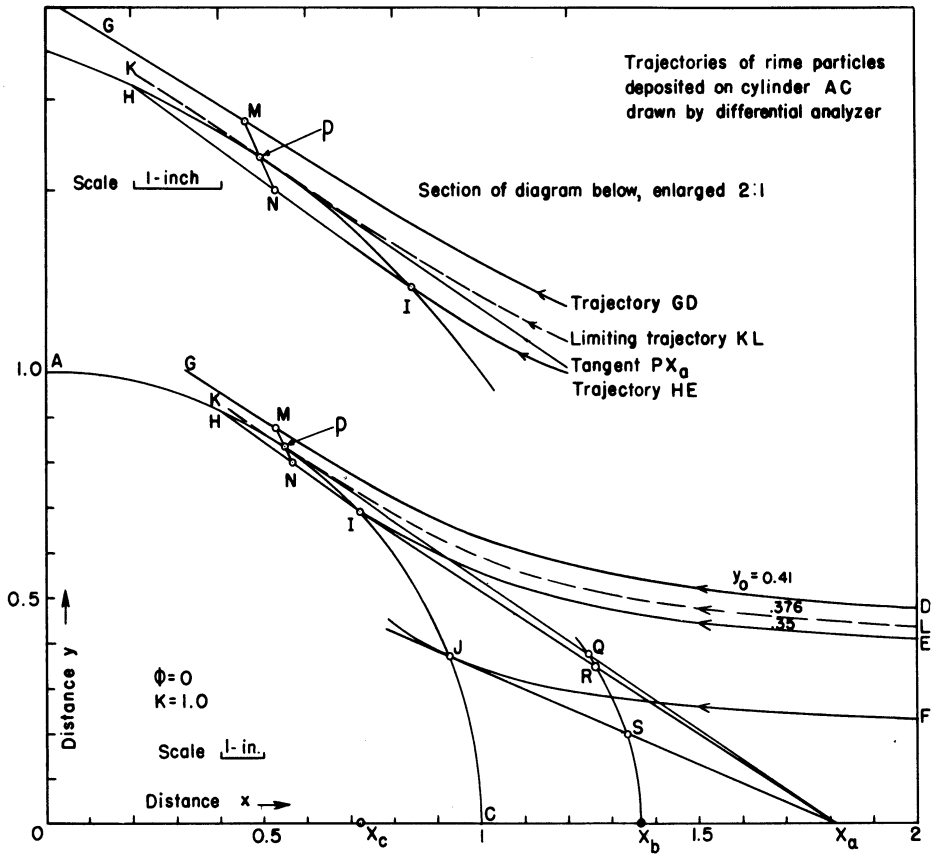

Figure II-2. Typical water drop trajectory drawn by Differential Analyzer (Reference 2).

$$F_x = m a_x = \frac{4}{3} \pi a^3 \rho_d \frac{d u_d}{dt}$$

$$F_y = m a_y = \frac{4}{3} \pi a^3 \rho_d \frac{d v_d}{dt} ,$$

where

ρ_d = drop density .

Equating the forces yields:

$$\frac{d u_d}{dt} = \frac{3}{8} \frac{\rho_a}{\rho_d} \frac{P(u_a - u_d)}{a} C_D$$

$$\frac{d v_a}{dt} = \frac{3}{8} \frac{\rho_a}{\rho_d} \frac{P(v_a - v_d)}{a} C_D .$$

The trajectory of the drop is obtained by integrating the following equations simultaneously:

$$(x - x_o) = \int \left\{ \int \frac{3}{8} \frac{\rho_a}{\rho d} (u_a - u_d) \frac{P C_D}{a} dt \right\} dt$$

$$(y - y_o) = \int \left\{ \int \frac{3}{8} \frac{\rho_a}{\rho d} (v_a - v_d) \frac{P C_D}{a} dt \right\} dt \quad .$$

The first integration yields the drop velocity and the second integration the drop displacement. To lessen the number of calculations required the equations are rendered dimensionless as follows:

$$\frac{x}{C} = \frac{x_o}{C} + \int \left\{ \int \left(\frac{9 \rho a \, C}{\rho d \, a} \right) \left(\frac{C_D \, P}{24 \, U} \right) \left(\frac{u_a - \dot{x}}{U} \right) d\left(\frac{Ut}{C} \right) \right\} d\left(\frac{Ut}{C} \right)$$

$$\frac{y}{C} = \frac{y_o}{C} + \int \left\{ \int \left(\frac{9 \rho_a \, C}{\rho d \, a} \right) \left(\frac{C_D \, P}{24 \, U} \right) \left(\frac{v_a - \dot{y}}{U} \right) d\left(\frac{Ut}{C} \right) \right\} d\left(\frac{Ut}{C} \right) \quad .$$

Now let

$$\psi = \frac{9 \rho_a \, C}{\rho_d \, a} \quad , \quad R_p = \frac{2a \, \rho_a \, P}{\mu_a} \quad , \quad R_u = \frac{2a \, \rho_a \, U}{\mu_a} \quad .$$

μ_a = air viscosity

C = a significant dimension in the flow field

U = free stream velocity

$$\frac{x}{C} = \frac{x_o}{C} + \int \left\{ \frac{\psi}{R_u} \int \left(\frac{C_D \, R_p}{24} \right) \left(\frac{u_a - \dot{x}}{U} \right) d\left(\frac{Ut}{C} \right) \right\} d\left(\frac{Ut}{C} \right)$$

$$\frac{y}{C} = \frac{y_o}{C} + \int \left\{ \frac{\psi}{R_u} \int \left(\frac{C_D \, R_p}{24} \right) \left(\frac{v_a - \dot{y}}{U} \right) d\left(\frac{Ut}{C} \right) \right\} d\left(\frac{Ut}{C} \right) \quad .$$

The integration of these equations must be accomplished step-wise, graphically, or via a differential analyzer, since C_D is a function of R_p and, except for very simple cases, $\frac{u_a}{U}$ and $\frac{v_a}{U}$ are rather complicated functions of $\frac{x}{C}$ and $\frac{y}{C}$.

For the cylinder, then, it follows that the trajectories, i.e., the loci of $\frac{x}{C}$, $\frac{y}{C}$ from these equations, are functions of ψ and R_p .

In the special case that $(C_D R_p/24) = 1$, the region of Stokes' law, the term in $R_u = R_p(U/P)$ does not appear inside the integral and the trajectories are functions of one parameter only, i.e., ψ/R_u .

Albrecht[1] was the first to calculate the trajectories around a cylinder for the case of the Stokes' law regime. Later Langmuir and Blodgett, using a differential analyzer, calculated trajectories for the case where C_D varies with R_p as determined experimentally for large spheres.[2] In this same report they calculated trajectories past ribbons and spheres, the results of which will be considered later.

From these trajectories certain specific items of information emerge. The first is known as the "percentage catch" and sometimes the "collection efficiency". Figure II-3 illustrates the physical significance of this term. All the

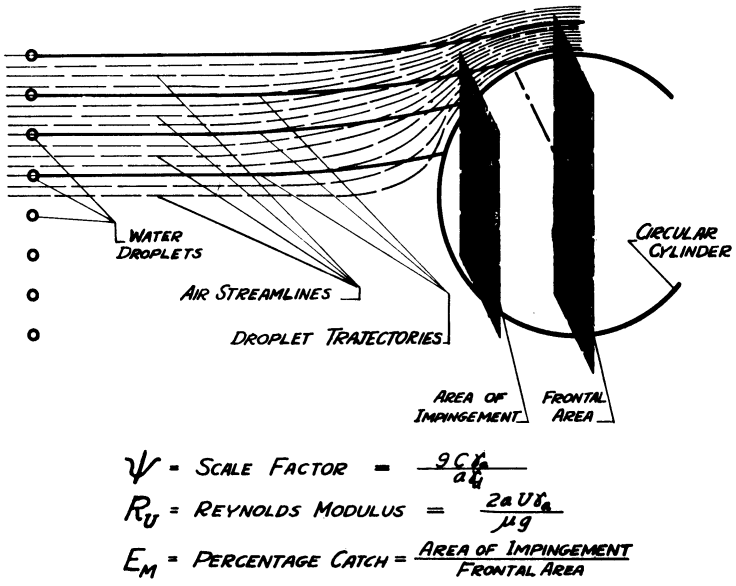

Figure II-3. Graphical representation of parameters used in trajectory work.

drops which lie within the limiting trajectories strike the cylinder. Those drops which lie outside these trajectories do not strike the cylinder but are blown around it. The ratio of the original y coordinate of the "tangent trajectory" to the cylinder radius defines the "percentage catch" which, expressed as a fraction, is given the symbol E_M.

Another property of interest is the area over which the cylinder is wetted. The angle measured from the stagnation line to the tangent trajectory is given the symbol θ_m. All drops which strike the cylinder do so within $\pm \theta_m$.

A third property of trajectories is the intensity of catch at the stagnation line, β_o . (The symbols are all from Langmuir and Blodgett.)

The catch rate may be computed from the percentage catch by

$$W = E_M U (2C) L w ,$$

where

W = catch rate (lbs/sec)

E_M = "fractional catch"

U = velocity (ft/sec)

C = cylinder radius (ft)

L = cylinder axial length (ft)

w = liquid water content of atmosphere (lbs/ft^3)

The intensity of catch along the stagnation line is given by

$$\frac{dW}{dA} = \beta_o U w$$

dW/dA = intensity of catch, lbs/sec ft^2 .

Because of certain end uses for their data, Langmuir and Blodgett plotted the quantities E_M, θ_m, and β_o versus two parameters defined as follows:

$$K = Ru/\psi \qquad \phi = Ru \cdot \psi$$

Figures II-4a to II-6b show graphs of E_M θ_m, β_o, and relative velocity V_1 versus K and ϕ. The relative velocity is the fraction of free stream velocity possessed by the drops as they strike the stagnation point, $\theta = 0$.

For values of $K \leq 1/8$, $E_M = 0$ on a cylinder. Since K contains the cylinder radius C in the denominator, it follows that for a given icing condition there is a maximum size of cylinder which will collect ice! This effect of size was not always appreciated. The author once participated in a test flight where the heat supply to the wings was being continuously diminished to find the

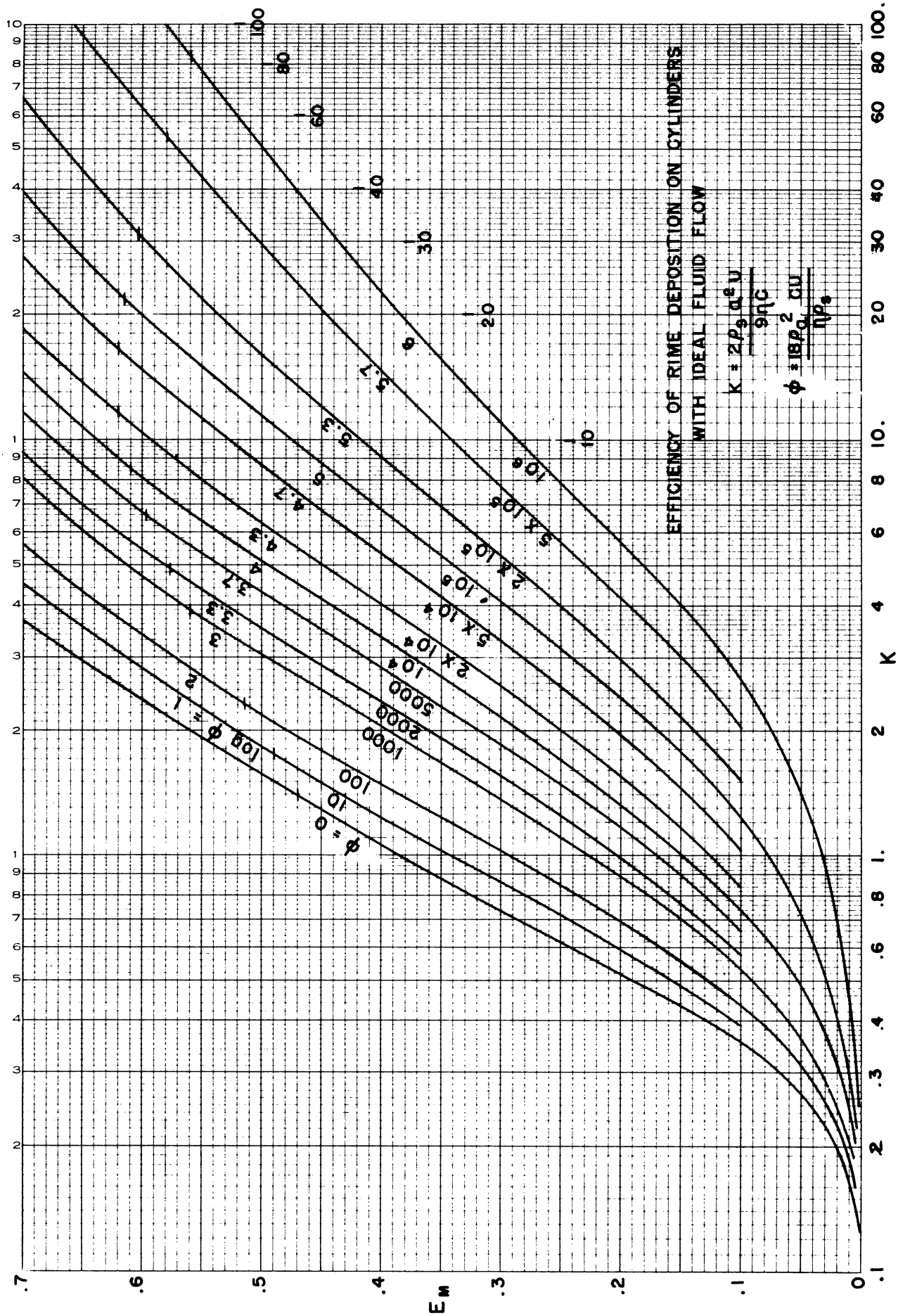
EFFICIENCY OF RIME DEPOSITION ON CYLINDERS
WITH IDEAL FLUID FLOW
$K = \frac{2\rho_s a^2 U}{9\mu C}$
$\phi = 18\frac{\rho_a}{\rho_s}\frac{a^2}{D^2}\frac{\alpha U}{\nu}$
K
E_M
ϕ
$\phi = 0$
$\phi = 10$
$\phi = 100$
$\phi = 1000$
$\phi = 2000$
$\phi = 5000$
$\phi = 10^4$
$\phi = 2 \times 10^4$
$\phi = 5 \times 10^4$
$\phi = 10^5$
$\phi = 2 \times 10^5$
$\phi = 5 \times 10^5$
$\phi = 10^6$
$\log \phi = 1$
$\log \phi = 2$
$\log \phi = 3$
$\log \phi = 4$
$\log \phi = 5$
$\log \phi = 6$
$\log \phi = 7$

Figure II-4a

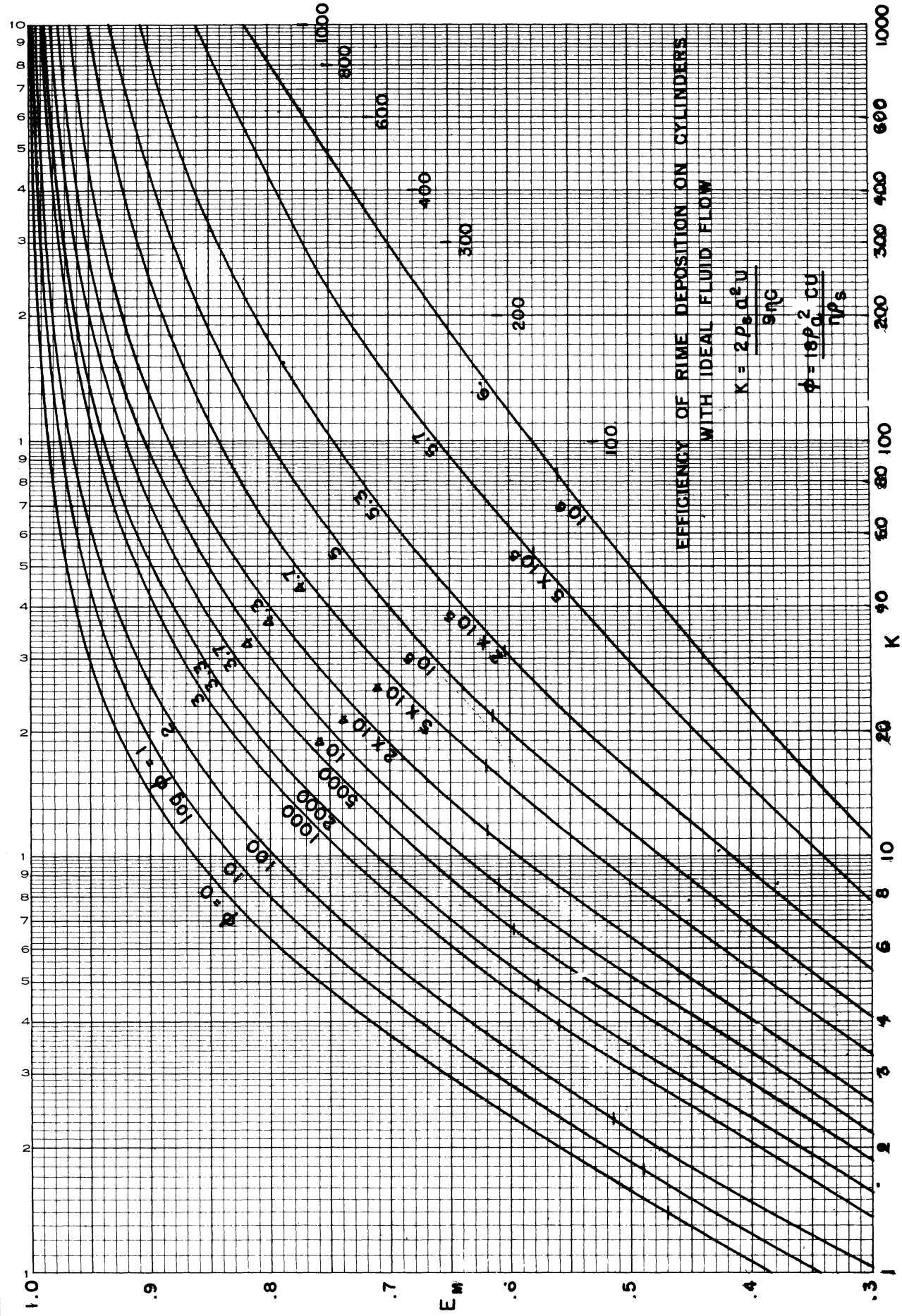
EFFICIENCY OF RIME DEPOSITION ON CYLINDERS
WITH IDEAL FLUID FLOW
$K = \frac{2\rho_s d^2 U}{9\mu D}$
$\phi = \frac{18\rho_a^2 CU}{\rho_s}$
E_M
K
1000
800
600
400
300
200
100
90
80
70
60
50
40
30
20
10
9
8
7
6
5
4
3
2
1
1.0
.9
.8
.7
.6
.5
.4
.3

Figure II-4b

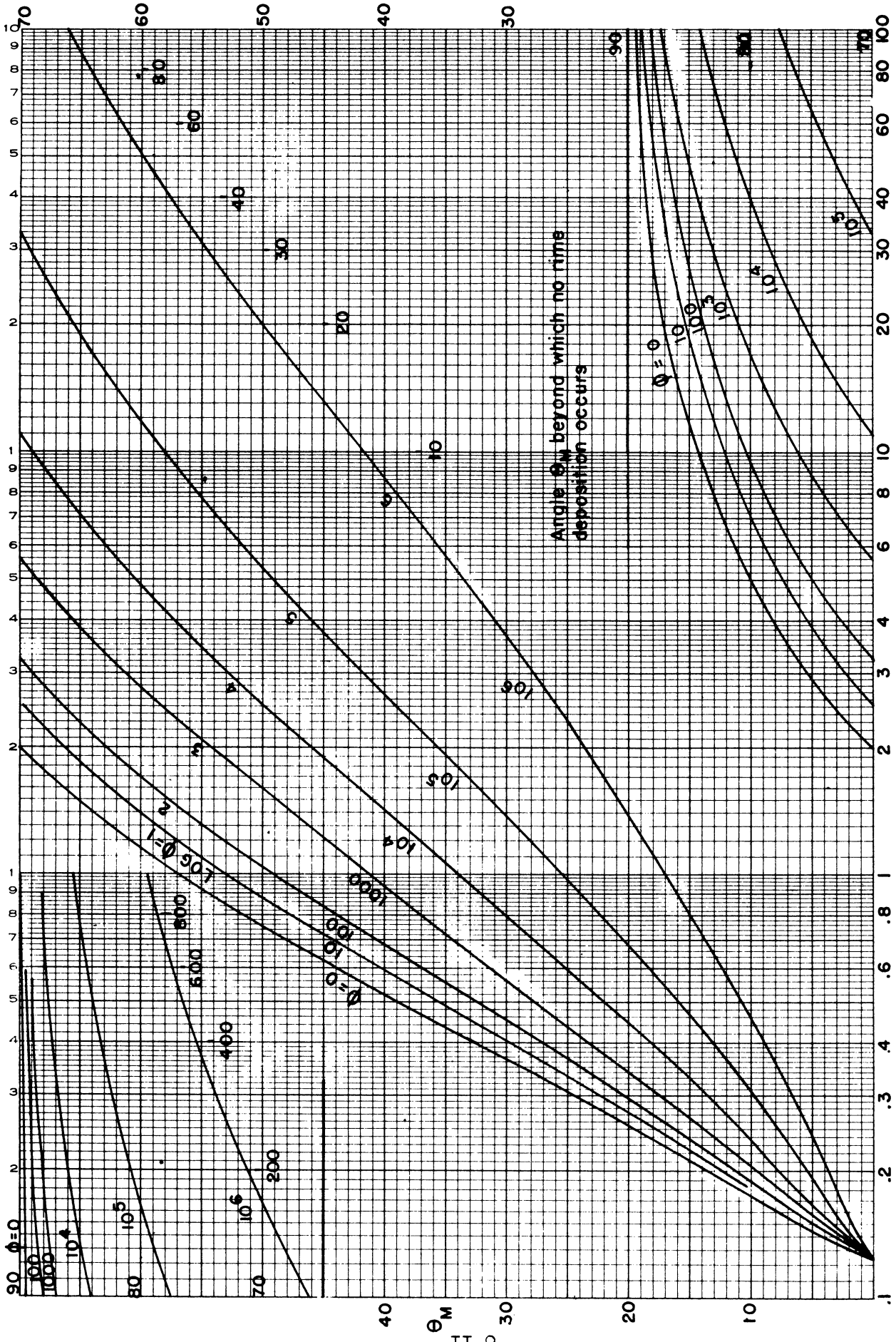
Angle θ_M beyond which no rime deposition occurs
θ_M
K
$\phi = 0$
$\phi = 1$
$\phi = \infty$

Figure II-5

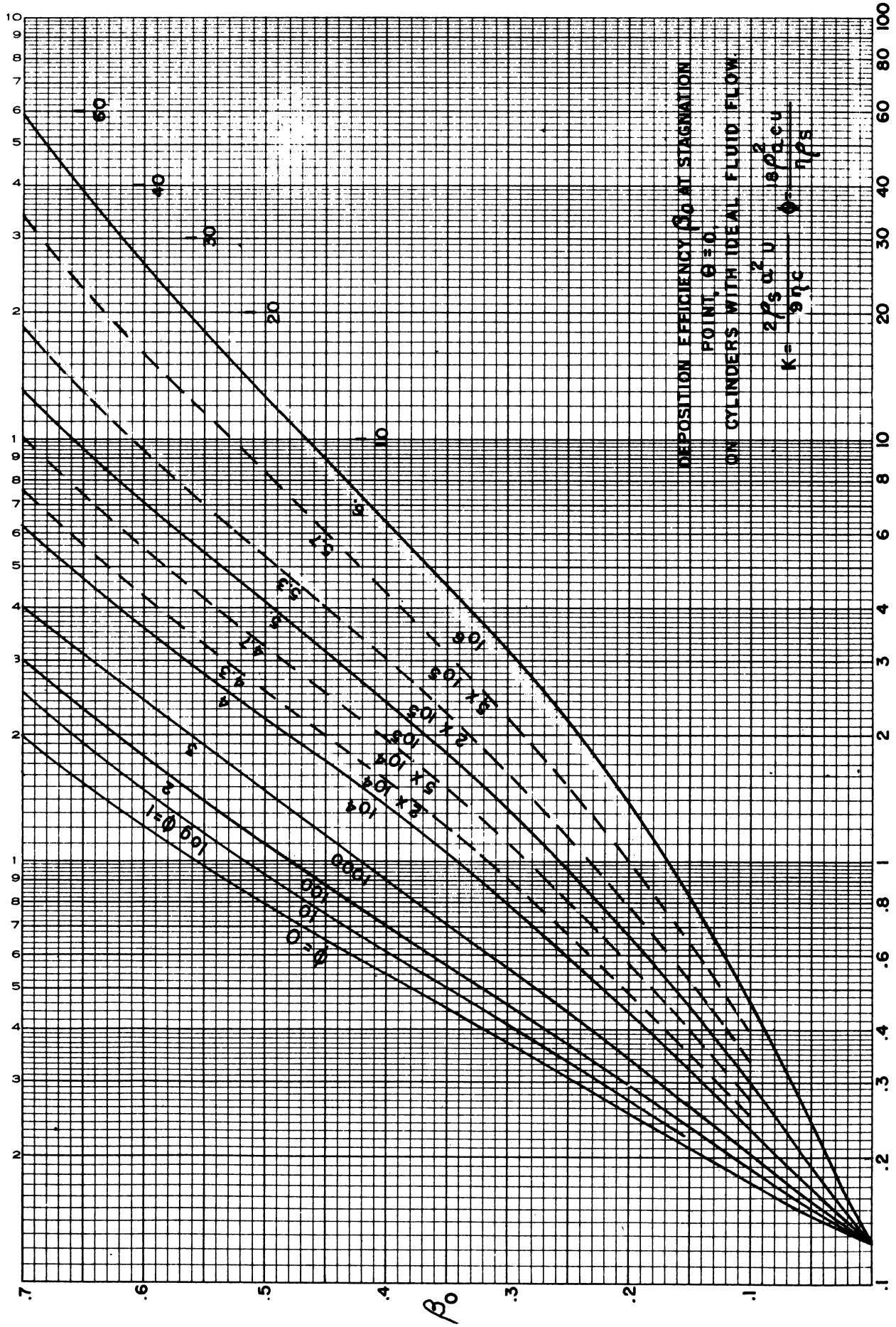
DEPOSITION EFFICIENCY β_0 AT STAGNATION POINT, $\theta = 0$, ON CYLINDERS WITH IDEAL FLUID FLOW
$K = \frac{2\rho_s a^2 U}{9\eta c} = \frac{18\rho_s a c_u}{\eta \rho_s}$
β_0

Figure II-6a

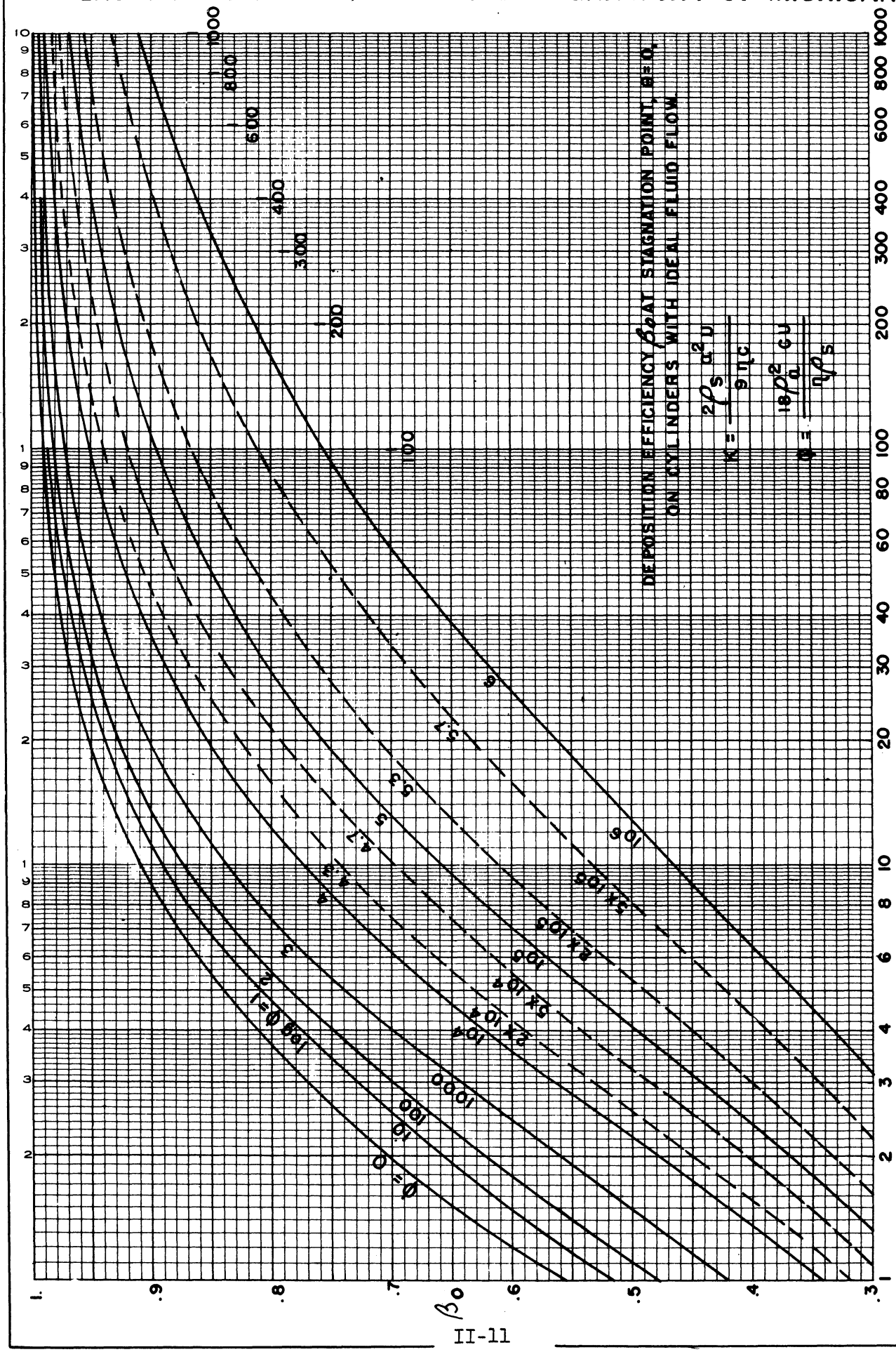
DEPOSITION EFFICIENCY β_o AT STAGNATION POINT, $\theta = 0$,
ON CYLINDERS WITH IDEAL FLUID FLOW
$K = \frac{2\rho_s a^2 U}{9\mu c}$
$\Phi = \frac{18\rho_a^2 c U}{\eta \rho_s}$
β_o
K
$\psi = 0$
$\psi = .001$
$\psi = .01$
$\psi = .1$
$\psi = .2$
$\psi = .3$
$\psi = .4$
$\psi = .5$
$\psi = .6$
$\psi = .7$
$\psi = .8$
$\psi = .9$
$\psi = 1.0$

Figure II-6b

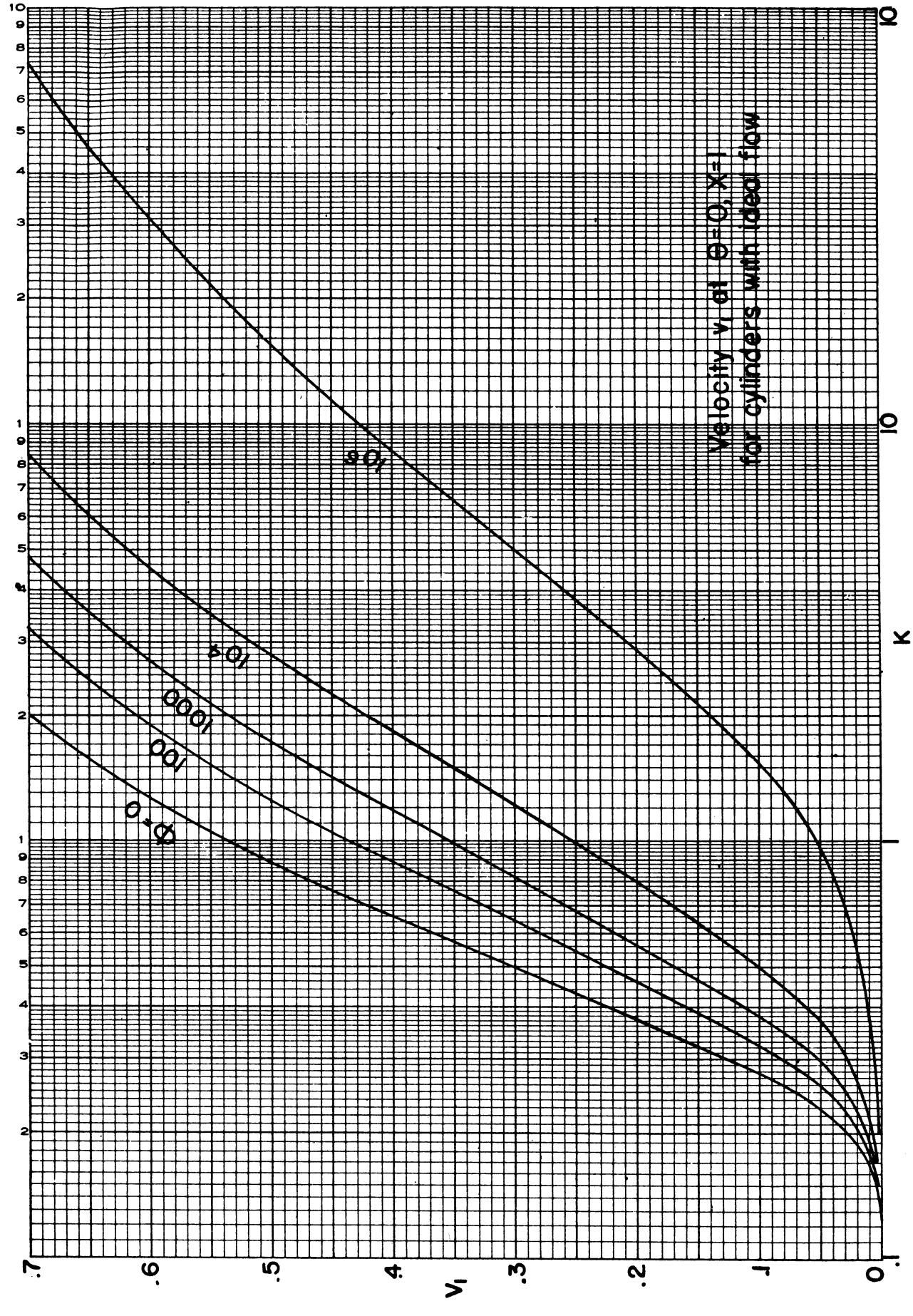
Velocity v_1 at $\theta=0, X=1$
for cylinders with ideal flow
v_1
K
.7
.6
.5
.4
.3
.2
.1
0
10
1
.01
.001
.0001
.00001

Figure II-7a

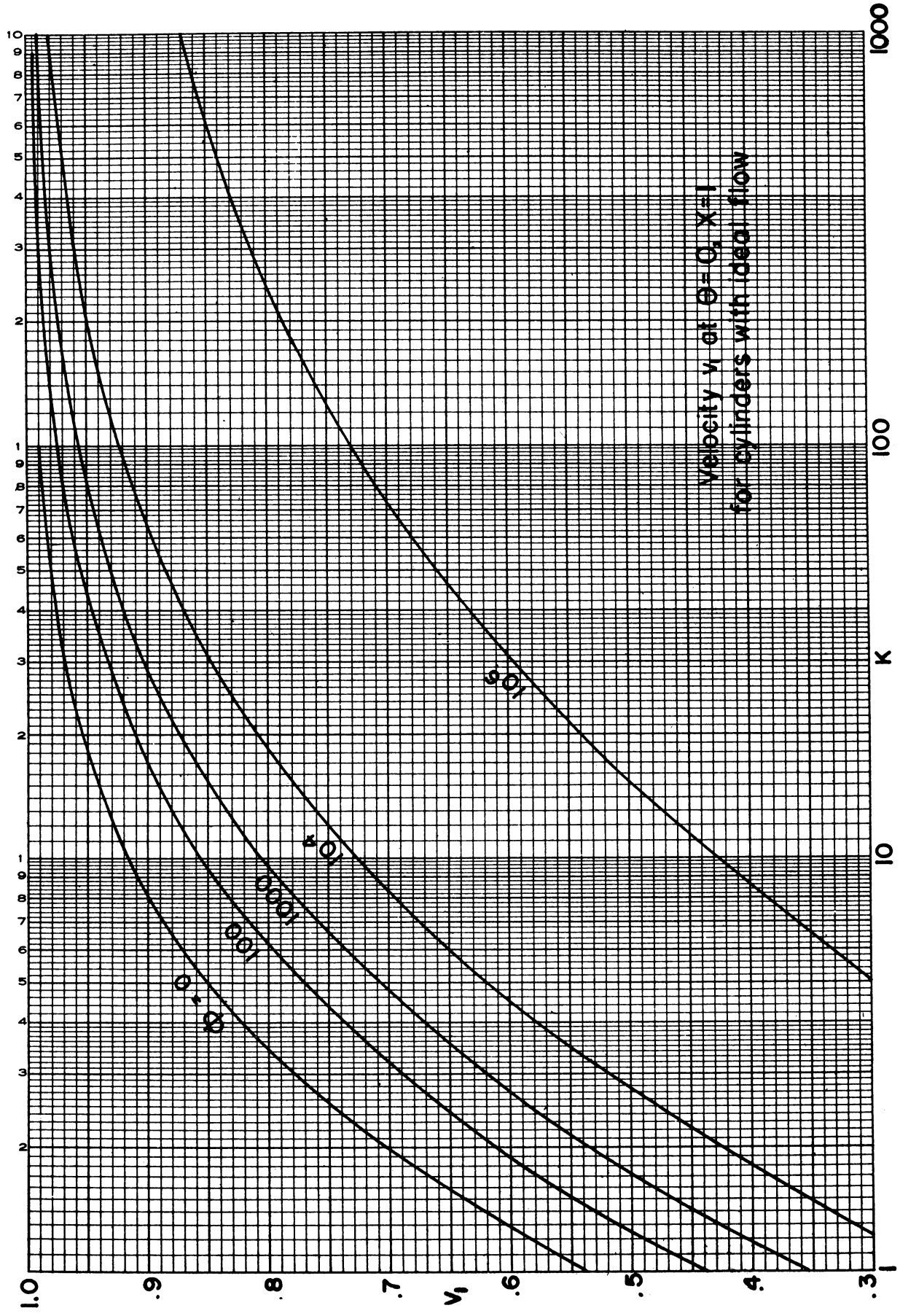
Velocity v_1 at $\theta=0$, $X=1$
for cylinders with ideal flow
1000
100
10
1
K
.001
.01
.1
1.0
.9
.8
.7
.6
.5
.4
.3
v_1

Figure II-7b

minimum heat required to prevent ice. When the heat supply was reduced to zero, the wings still remained ice-free. Meanwhile the antenna wires and mast were icing rapidly. It is now known that this effect may occur when the drops are small. The wing, having a large radius of curvature tended to deflect the drops while the antenna mast had, in effect, a high value of K and therefore a high collection efficiency.

Experimental Verification

Figures II-8a and II-8b show ice accretions on cylinders and spheres which verify qualitatively the trajectory data given by Langmuir and Blodgett. The best check of the calculations may be made using a cylinder, since the cylinder may be rotated and will remain cylindrical while icing.

A quantitative verification of the trajectory data has been obtained by mounting cylinders on a common axis and exposing them to the icing windstream. These cylinders are of different sizes and are rotated to preserve the cylindrical shape during the icing. The unknown properties of the windstream are the liquid-water content (w) and the drop diameter (2a). If the weight of ice catch on each cylinder is divided by the cylinder frontal area, wind velocity and exposure duration and the quotient plotted versus cylinder radius, C, using logarithmic coordinates, we get the results shown in Figure II-9. A graph of E_M versus 1/K with ϕ as a parameter is shown in Figure II-10. An attempt is then made to fit the points of Figure II-9 to the curves of Figure II-10. Since a shift along either logarithmic coordinate corresponds to multiplication by a constant, it is not necessary to know the liquid-water content or drop diameter to do the curve fitting. Figure II-11 shows an example of the "fit". The amount of vertical and horizontal shift permits calculation of the unknown liquid water content and of the drop radius.

Various modifications of the above curve-fitting process have been used, all representing the same basic method. Charts have been prepared in which the curves of E_M versus 1/K have two parameters, one the droplet Reynolds Modulus, Ru, and the other a characterization of the droplet-size distribution. Such curves are given in Reference 3. By matching experimental points to these curves, one obtains not only the liquid-water content and mean drop size but also the approximate drop-size distribution.* Figure II-12 shows an example of such a

* Lewis and Hocker, NACA TN 1904 "Observations of Icing Conditions Encountered in Flight During 1948" comment that the rotating-cylinder method when used in the manner described yields "indications of drop-size distribution (that) are so unreliable that they are of little or no value". However, the Lewis data under discussion was obtained partly from two-cylinder and partly from four-cylinder apparatus. Such data can often be fitted to any of several curves. Data taken, using six or more cylinders at Mt. Washington, generally can be fitted to one curve only. It seems evident that, if one is attempting to measure three variables, more than two measurements should be made.

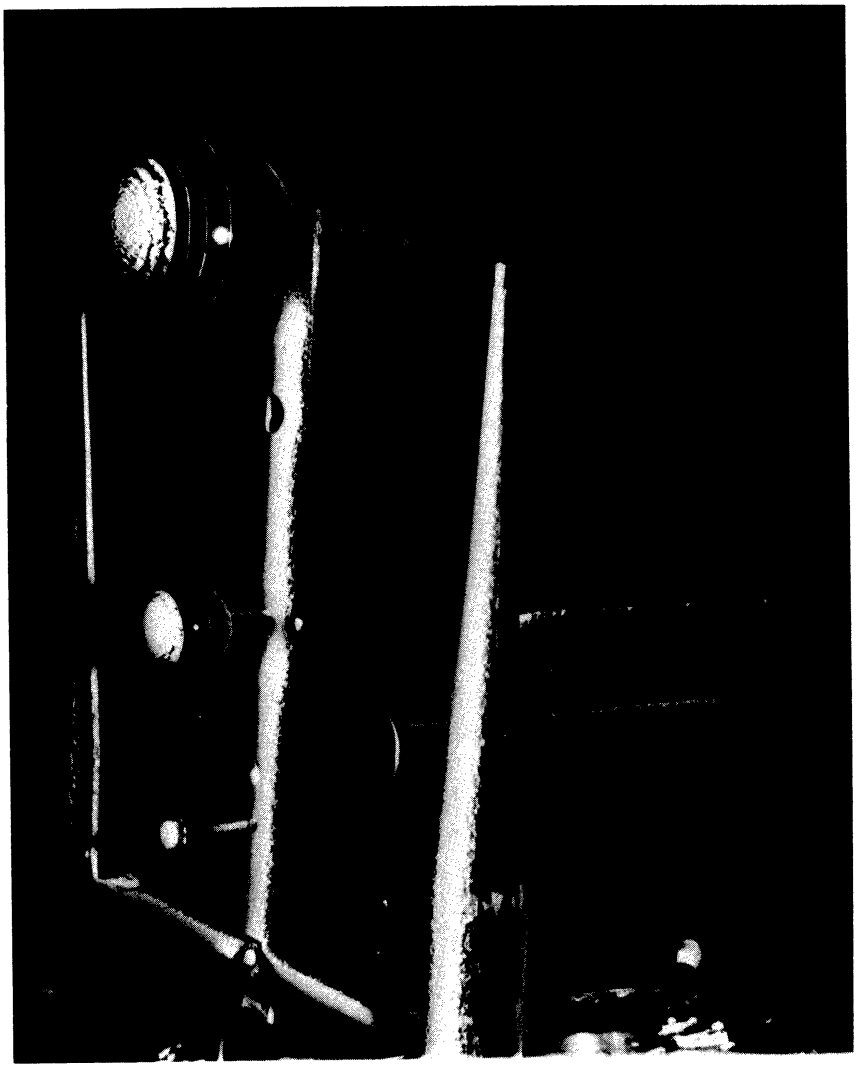

Figure II-8a. Ice accretion obtained by exposure on Mt. Washington, N. H. (Photo, courtesy Victor Clarke, Mt. Washington,Observatory) 15-minute exposure, 7°F, 47 mph, average drop size 12.2 microns diameter, 0.21 grams water/cubic meter of air. April 8, 1946.

fit. The computed drop radius is used to check the correctness of the Ru curve. If an error has been made, the data are fitted to another Ru curve. The convergence of the method is rapid.

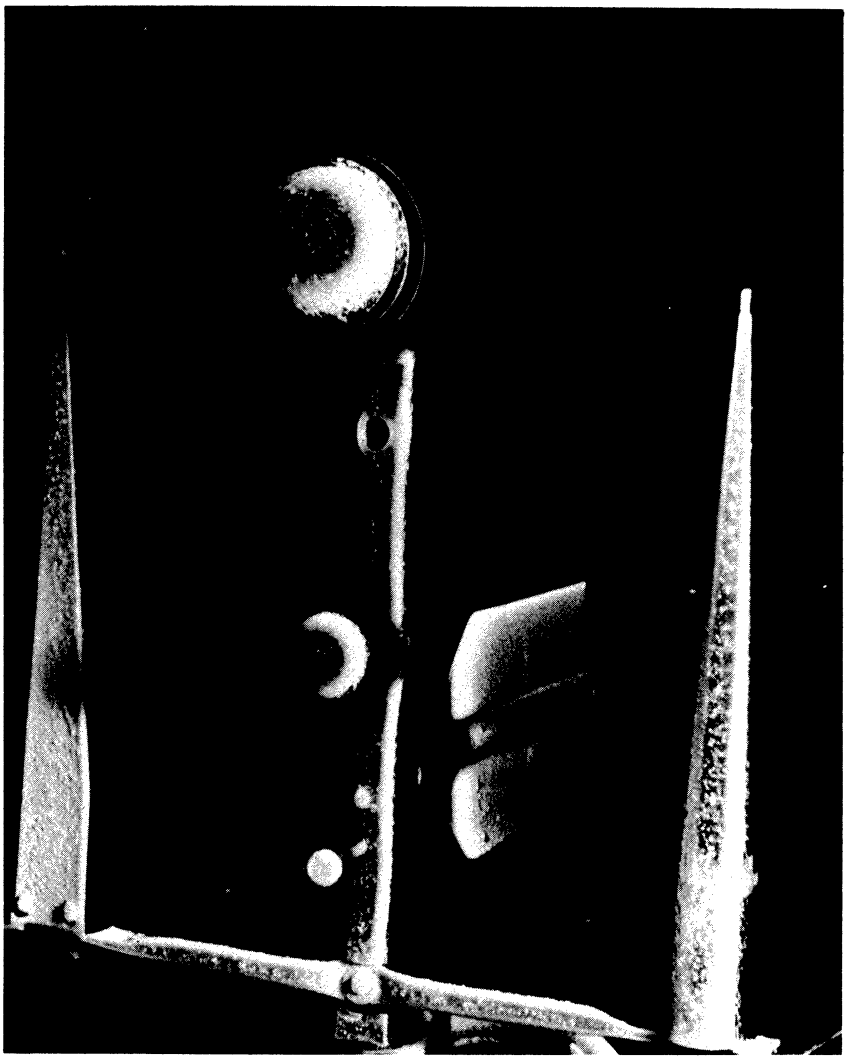

Figure II-8b. Ice accretion on cone, spheres, and tapered flat plate. (Photo, courtesy Victor Clarke, Mt. Washington Observatory) 7-minute exposure, 11°F, 59 mph, average drop size 16.9 microns diameter, 0.66 grams water/cubic meter of air. April 19, 1946.

A Discussion of the Dimensionless Groups Used to Present Trajectory Information

In the initial derivation of the equations for the droplet trajectories, two dimensionless groups appeared, namely, R_u and ψ. The plotting versus K ($= r_u/\psi$) permitted comparison to the Stokes' law solutions. The zero impingement at a critical value of K becomes apparent. The parameter ϕ is useful in work where the droplet diameter is not known ($\phi = Ru \cdot \psi$).

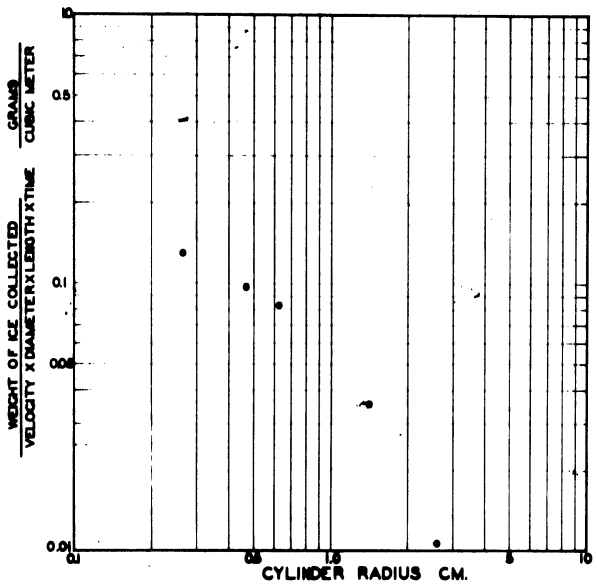

Figure II-9. Experimental points obtained on rotating cylinders.

Figure II-13[4] shows a graph of E_M versus Ru with ψ as a parameter. According to this figure, even at very large values of velocity, E_M does not necessarily approach unity. Plotting with these two parameters permits one to see the effect of velocity.

Drell and Valentine[5] have plotted the data in yet another fashion. Figure II-14 shows a graph of $E_M \psi$ versus ψ for several values of Ru. The product $E_M \psi$ is proportional to catch rate (for given speed, liquid-water content, drop size) and ψ is proportional to cylinder size. This graph shows that for a given icing condition and speed there is one size of cylinder which ices more heavily than any other. Larger cylinders have low-percentage catch; smaller cylinders have less frontal area.

Spheres and Ribbons

Calculations have been made for shapes other than cylinders. Langmuir and Blodgett have published curves showing trajectory information for flow

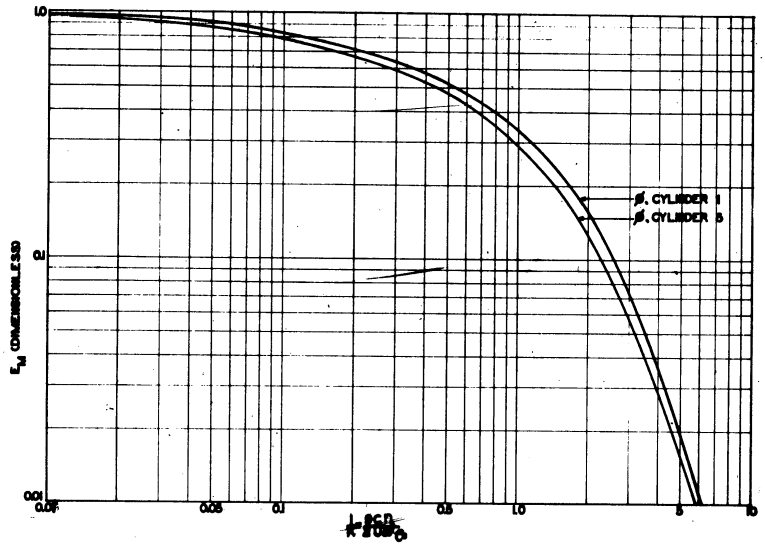

Figure II-10. Replot of data from Reference 2.

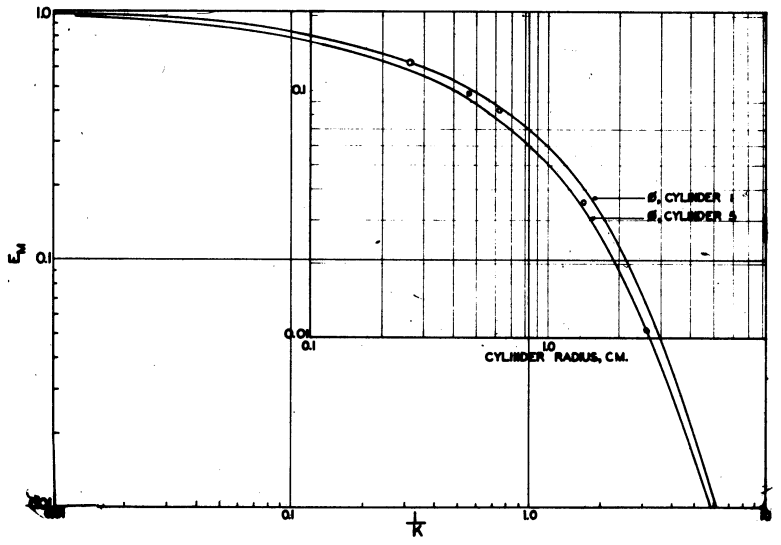

Figure II-11. Comparative fit, Figures II-9 and II-10.

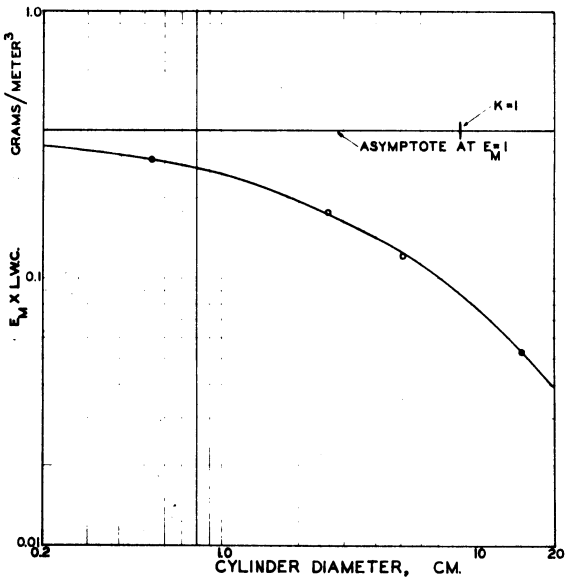

Figure II-12. Comparison between data of Reference 2 and flight measurement (Reference 3).

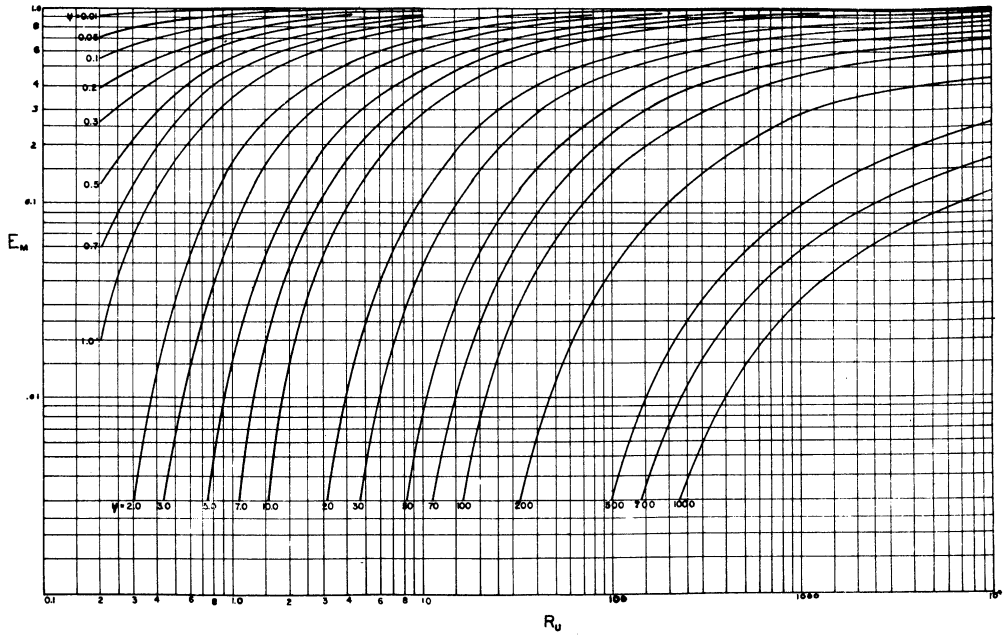

Figure II-13. Replot of data from Reference 2 to show effect of velocity on catch (Reference 4).

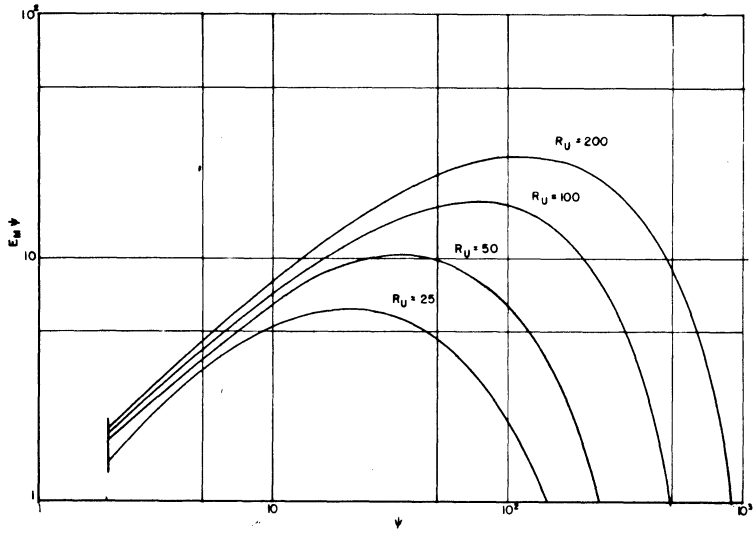

Figure II-14. A replot of Langmuir-Blodgett data using the Drell-Valentine plotting method (Reference 5).

past spheres and ribbons. The sphere data look very much like the cylinder calculations, as illustrated in Figure II-8, showing ice accretions on three spheres exposed atop Mt. Washington, N. H.

The trajectories past ribbons or flat plates perpendicular to the airstream have a different characteristic. The maximum ice accretion does not occur at the stagnation line of the ribbon but occurs on either side of the centerline at a distance Y/b = 0.8 (2b = ribbon width). Figure II-15 shows ice accretions obtained on a flat piece of wood placed transverse to the windstream atop Mt. Washington. The board has a gentle taper which illustrates the effect of size rather well.

The Langmuir and Blodgett report not only presents data on the important parameters E_M , θ_M and β but also contains data on the velocity of the drops upon impact, the angle of impact and the variation of β ($= dE/d\theta$) around the cylinder, sphere or ribbon ($\beta = dE/d(y/b)$). A few results for the case of a viscous fluid (instead of an idealized nonviscous fluid) flowing around a sphere are also given. The serious worker in the icing field should make it a point to study carefully this classical report.

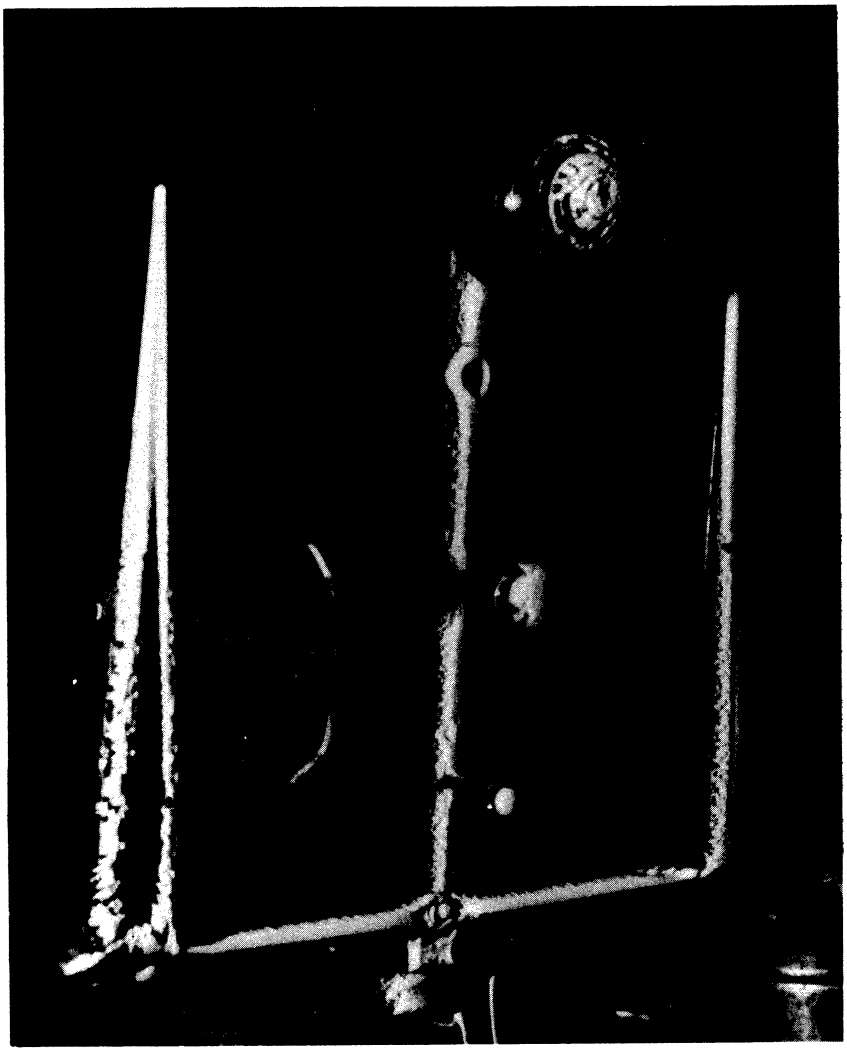

Figure II-15. Icing of different-width "ribbons" is illustrated on tapered board placed flat side towards wind. Note that the maximum ice accretion occurs to either side of the stagnation region. (Photo, courtesy Victor Clarke, Mt. Washington Observatory) 15-minute exposure, 10°F, 67 mph, average drop size 9.4 microns diameter, 0.28 grams liquid water/cubic meter of air. April 7, 1946.

Airfoils

The trajectories about airfoils have been studied by a number of workers. Bergrun[6] has calculated the trajectories about a 12 per cent thick Joukowski profile using a numerical method. He presents curves which are useful if one is forced to resort to hand calculations, though even with these curves, the calculations are long and tedious. Figure II-16 shows some of the results obtained by Bergrun.

Guibert, Janssen, and Robbins[7] have calculated the trajectories for a symmetrical 15 per cent thick Joukowski airfoil at 0, 2 and 4° angle of attack. They also calculated the trajectories for a cambered 15 per cent thick Joukowski profile at 0° angle of attack. In this report[7] data are also given showing the velocity of the drop at impingement.

In work with airfoils most workers have used the chord length of the airfoil as the significant parameter in the dimensionless modulus. Drell and

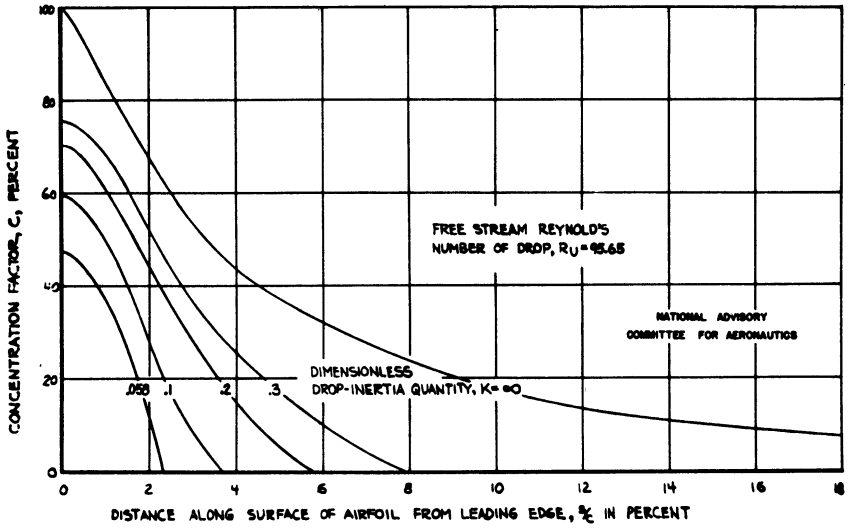

Figure II-16. Distribution of water drop impingement over symmetrical 12 per cent thick Joukowski airfoil. Calculations by Bergrun (Reference 6).

Valentine[5] have shown, however, that if one uses the airfoil thickness as the significant dimension, the data for the various airfoils are brought closer together and the problem of interpolating between airfoils is less difficult. The results are still far from satisfactory, as shown in Figure II-17 but the improvement from the point of view of a designer is significatn. In Figure II-17,

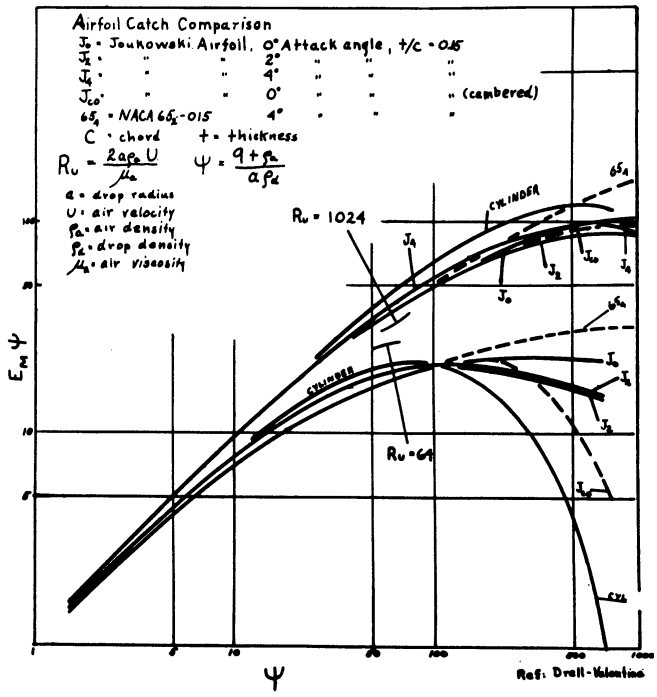

Figure II-17. Replot of available trajectory data using method of Drell and Valentine (Reference 5).

following Drell and Valentine, the product $E_M \psi$ is plotted against ψ since one is more interested in total catch than in fractional catch.

The Supersonic Wedge

Before leaving the trajectory problem, two analytical solutions are of interest. One unpublished solution[8] pertains to the trajectories in supersonic flow about an infinite wedge. The calculation of these trajectories is simple and straightforward.

A wedge travelling at supersonic speeds has a field of flow about it such as shown in Figure II-18. Before the shock wave the flow is uniform. After the shock wave the flow is again uniform but parallel to the wedge surface. Ahead of the shock wave the drops are at rest with respect to the undisturbed air. If the shock wave is treated as a surface of discontinuity and there is no disruption due to the aerodynamic forces, the drop emerges from the shock wave with a finite velocity relative to the flow behind the shock. Now, since the field

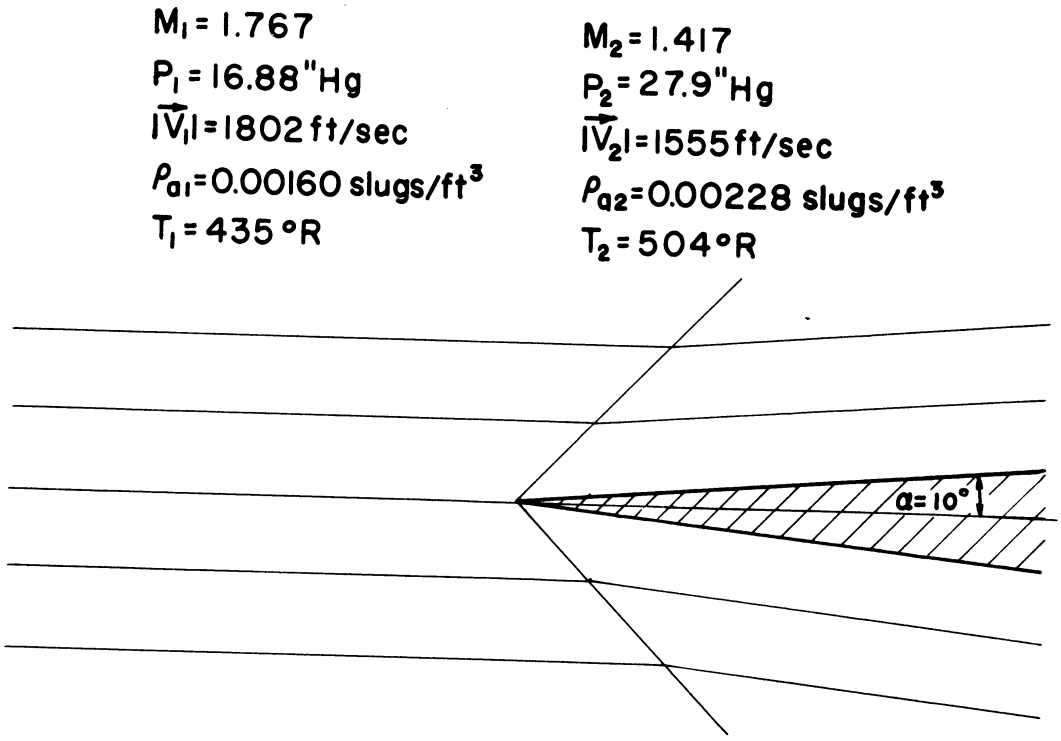

Figure II-18

of flow in front of and behind the shock wave is uniform, we may change the frame of reference and consider a coordinate system which moves with the velocity V of the air stream behind the shock wave. In this frame of reference the air is stationary, and we have then the problem of a drop projected into still air with an initial velocity U.

From Newton's law,

$$F = m \frac{dU}{dt} ,$$

where

$$m = \frac{4}{3} \pi a^3 \rho_d \quad = \text{mass of drop}$$

$$F = -\frac{1}{2} \rho a U^2 C_D \pi a^2 = \text{drag force}$$

ρ_w = water-drop density

ρ_a = air density

a = drop radius

C_D = drag coefficient, drop to air .

The drop velocity as a function of time is given by

$$\frac{dU}{dt} = -\frac{3}{8}\frac{\rho a}{\rho_w}\frac{U^2 C_D}{a} .$$

The drag coefficient, C_D, is a function of the Reynolds Modulus, R; hence, introducing the Reynolds Modulus

$$R = \frac{2\,Ua\,\rho_a}{\mu_a}$$

μ_a = viscosity of air,

$$\frac{dR}{dt} = -\frac{3}{8}\left(\frac{\rho_a}{\rho_w}\right)\frac{C_D}{a}\frac{\mu_a R^2}{2a\,\rho_a} .$$

Finally, then,

$$\int_{R_o}^{R}\frac{dR'}{C_D R'^2} = -\frac{3}{16}\frac{\mu_a t}{a^2 \rho_w} .$$

The right-hand term is a dimensionless measure of the time required for a sphere at initial Reynolds modulus R_o to drop to the speed given by R. The integral may be evaluated graphically from a graph of C_D^{-1} versus 1/R.

After the velocity has dropped low enough for Stokes' law to be valid, the equation above may be integrated directly.

$$C_D = \frac{24}{R}$$

$$\frac{9}{2}\frac{U(t - to)}{a^2 \rho_w} = \int\frac{dR}{R} = \ln\frac{R}{R_o} .$$

The above equation indicates that the drop never comes to rest! Langmuir has pointed out, however, that the drop travels only a finite distance. When the velocity becomes sufficiently low, Brownian movement predominates, and the above equations are no longer descriptive of the motion.

Figure II-19 shows a graph of R versus $U(t-t_o)/4\ a^2\ \rho_w$ for $R_o = 1800$ at $t = t_o$.

A second integration is required to obtain the "range" of the spherical droplet

$$R = \frac{2a\ \rho_a}{\mu_a} \frac{dx}{dt}$$

$$dx = \frac{R \mu_a}{2a\ \rho_a}\ dt \quad .$$

Dividing both sides of the equation by ρ_w a and transposing ρ_a,

$$\frac{\rho_a}{\rho_w}\ d\left(\frac{x}{a}\right) = R\ d\left(\frac{u(t - t_o)}{a^2\ \rho_w}\right).$$

The integration of the above equation may be accomplished since R is known as a function of the dimensionless time. (Curve A, Figure II-19). The results of the second integration are shown as curve B of Figure II-19. The data from these curves may be used to compute the droplet trajectory as follows:

Consider the flow field defined in Figure II-18. The following conditions prevail:

Wedge half angle		10°
Mach number		1.767 (ahead of shock)
Altitude		15,000 ft
Air temperature		-25°F
Drop diameter	20 microns =	6.56×10^{-5} ft
Mach number after shock		1.417
Pressure ratio across shock		1.655*
Air-density ratio across shock		1.428*
Velocity of sound ahead of shock		1021 ft/sec
Shock wave angle		45°
Temperature ratio across shock		1.156*
Ratio of velocities across shock		0.862*

* Items thus marked are calculated from tables in Keenan and Kaye, Gas Tables: Thermodynamic Properties of Air, Products of Combustion and Component Gases, Compressible Flow Functions Wiley, 1948.

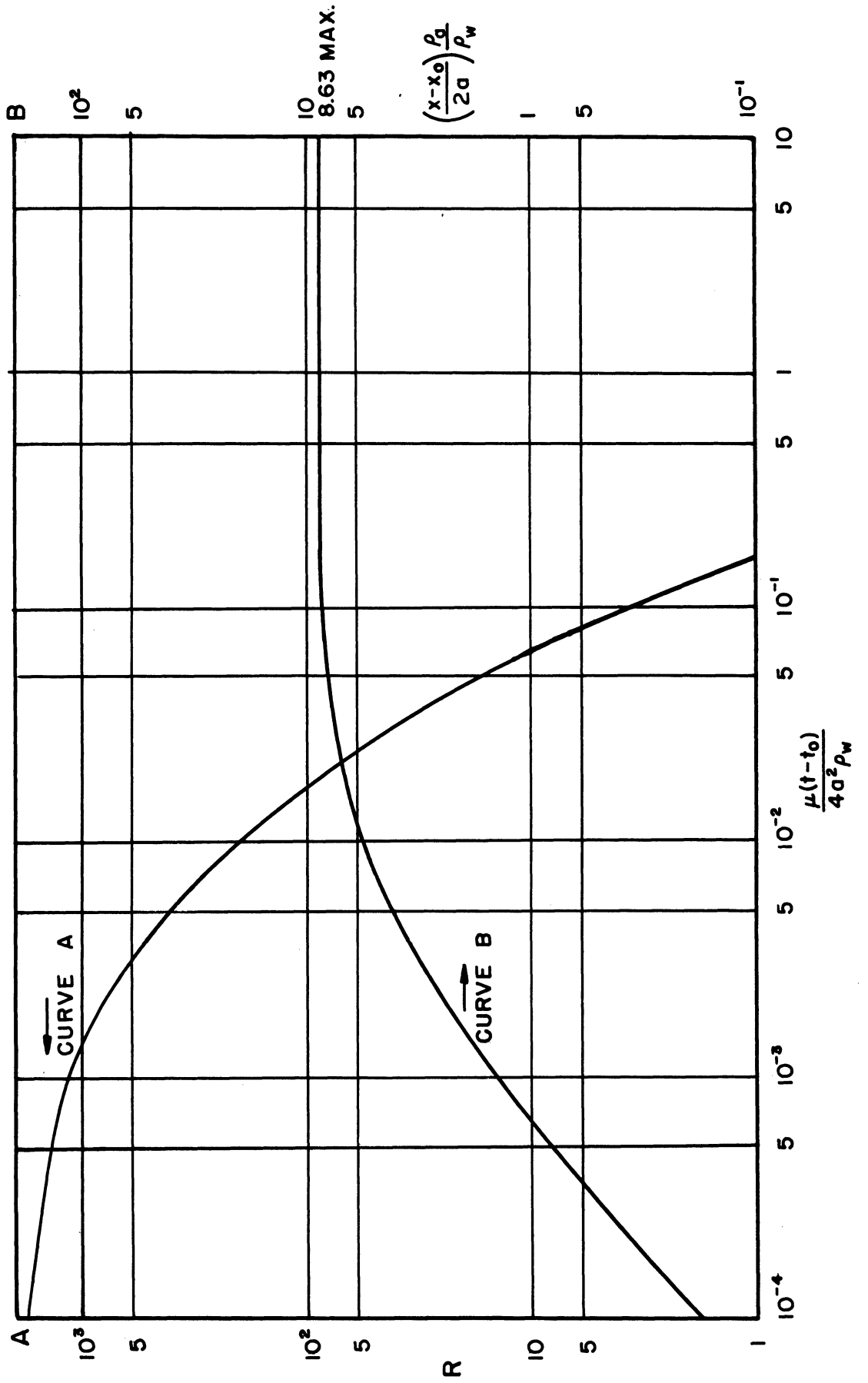
B
10²
5
10
8.63 MAX.
5
1
5
10⁻¹
$\left(\frac{x-x_0}{2a}\right)\frac{\rho_g}{\rho_w}$
10
5
1
5
10⁻¹
5
10⁻²
5
10⁻³
5
10⁻⁴
$\frac{\mu(t-t_0)}{4a^2\rho_w}$
CURVE A
CURVE B
A
10³
5
10²
5
10
5
1
R

Figure II-19

The relative velocity of the drop after the shock is 379 ft/sec calculated from the vector difference between V_1 and V_2. The droplet initial Reynolds modulus is

$$R = \frac{2a\ U\ \rho a}{\mu_a} = 154 \quad .$$

The dimensionless time for a drop to come to this value of R from an initial value $R_o = 1800$ is read from Figure II-19, curve A as 1.25×10^{-2}. Curve B shows that the drop would travel a dimensionless distance (from R = 1800 to R = 154) of 6.10. The maximum range of the drop (from R = 1800 to R = 0) is read from curve B as 8.63. Therefore the range λ of the drop initially at R = 154 is

$$\lambda = \frac{2.53 \times 2a\ \rho_w}{\rho_a}$$

$$\lambda = 0.141 \text{ ft} \quad .$$

The time required to travel half this distance is calculated by entering curves A and B in reverse order. Table I was constructed in this fashion:

TABLE I

Distance Travelled by Droplet Relative to Airstream	Time Required to Traverse this Distance	Time	Distance Relative to Airstream	Distance Moved by Airstream Parallel to Wedge Surface in this time
(dimensionless)	(dimensionless)	(seconds)	(ft)	(ft)
2.53			0.141	
1.90	3.3×10^{-2}	7.46×10^{-4}	0.106	1.16
1.29	1.4	3.16	0.070	0.49
0.63	0.58	1.31	0.035	0.20

The above trajectories may be transformed from the moving coordinate to a coordinate system at rest with respect to the airfoil by straightforward geometrical considerations. Thus we obtain Table II.

TABLE II

Initial Distance of Droplet relative to Wedge Centerline (ft)	Position at which Drop Strikes Wedge feet from Nose (ft)	Average Rate of Ice Accretion between this Point and Nose if Liquid Water Content of Air is 1 gram/m^3 (lbs/hr)	Icing Rate, Average between Nose and this Point (inches/min)
0.035	0.24	60.0	0.20
0.071	0.56	51.0	0.18
0.107	1.27	34.0	0.12
0.143			

Later considerations will show that aerodynamic heating will prevent ice at these conditions, but if the temperature were -40°F, the icing would occur despite the frictional heating.

Trajectories Near a Stagnation Point

G. I. Taylor[9] has found an analytical solution for the case of a drop in the vicinity of a stagnation point and small enough to follow Stokes' law. The solution shows clearly some of the results which occur in the more complicated cases. The equations are:

$$\frac{4}{3}\pi a^3 \rho_w \frac{d u_d}{dt} = \frac{1}{2}\pi a^2 C_D P (u_a - u_d) \rho_a$$

$$\frac{4}{3}\pi a^3 \rho_w \frac{d v_d}{dt} = \frac{1}{2}\pi a^2 C_D P (v_a - v_d) \rho_a \quad ,$$

where

a = drop radius
ρ_d = drop density
u_d = drop x component of velocity
t = time
C_D = drag coefficient, spherical drop to air
P = relative velocity between drop and air
u_a = air x component of velocity
ρ_a = air density
v = y component of velocity

If Stokes' law applies,

$$C_D = \frac{24}{R}$$

$$R = \frac{2\, a\, \rho_d\, P}{\mu_a}$$

R = Reynolds modulus

μ_a = air absolute viscosity .

Substituting for the drag coefficient,

$$\frac{2}{9}\,\frac{\rho_w\, a^2}{\mu_a}\,\frac{d\, u_d}{dt} + u_d = u_a$$

$$\frac{2}{9}\,\frac{\rho_w\, a^2}{\mu_a}\,\frac{d\, v_d}{dt} + v_d = v_a \ .$$

These equations are integrable separately if u_a and v_a, respectively, are functions of x and y only. The velocity field must satisfy the continuity relation

$$\frac{\partial u_a}{\partial x} + \frac{\partial v_a}{\partial y} = 0 \ .$$

Hence, if we seek a solution such that

$$u_a = u_a(x) \qquad \text{and} \qquad v_a = v_a(y) \ ,$$

the only possible sclutions are of the form

$$u_a = C_u - C_1 x$$

$$v_a = C_v + C_1 y \ .$$

These components correspond to streamlines which are right hyperbolae. Figure II-20 shows the flow field which is similar to the flow against a corner or a large flat plate. The flow field is also a good approximation to the immediate vicinity of a stagnation point.

Now let

$$\dot{x} = \frac{d\, u_d}{dt} \qquad \text{and} \qquad \dot{y} = \frac{d\, v_d}{dt} \ ;$$

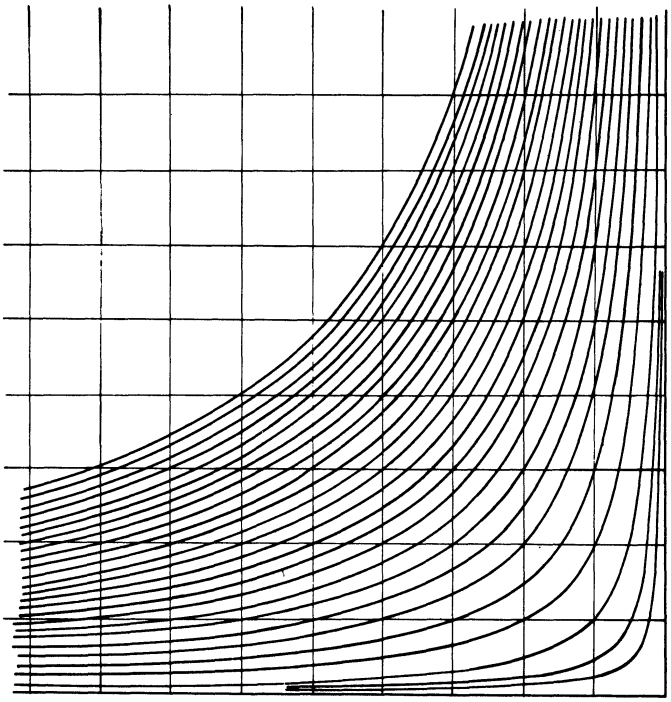

Figure II-20. Flow field in a corner or near stagnation point.

then

$$\frac{2}{9}\,\frac{\rho_w a^2}{\mu_a}\,\ddot{x} + \dot{x} = C_u - C_1 x$$

$$\frac{2}{9}\,\frac{\rho_w a^2}{\mu_a}\,\ddot{y} + \dot{y} = C_v + C_1 y \ .$$

Now let

$$X = x - \frac{C_u}{C_1} \ , \quad Y = y + \frac{C_v}{C_1} \quad \text{and} \quad Z = \frac{9\mu_a t}{2\rho_w a^2} \ ,$$

$$\frac{d^2 X}{d Z^2} + \frac{d X}{d Z} = -\frac{2}{9}\,\frac{C_1 \rho_w a^2}{\mu_a}\,X \ ,$$

$$\frac{d^2 Y}{d Z^2} + \frac{d Y}{d Z} = \frac{2}{9} \frac{C_1 \rho_w a^2}{\mu a} Y$$

If the initial position is X_o , Y_o and the initial velocity (Z scale of time) is X_o' , Y_o' , then the solutions to the above equations are

$$X = e^{-\frac{Z}{2}} \left[\frac{2X_o' + X_o}{\alpha} \sinh \left(\frac{\alpha}{2} Z \right) + X_o \cosh \left(\frac{\alpha}{2} Z \right) \right]$$

$$Y = e^{-\frac{Z}{2}} \left[\frac{2Y_o' + Y_o}{\beta} \sinh \left(\frac{\beta}{2} Z \right) + Y_o \cosh \left(\frac{\beta}{2} Z \right) \right],$$

where

$$X_o' = dX/dZ \quad \text{at} \quad Z = 0$$

$$X_o = X \quad \text{at} \quad Z = 0$$

$$Y_o' = dY/dZ \quad \text{at} \quad Z = 0$$

$$Y_o = Y \quad \text{at} \quad Z = 0$$

$$\alpha = \sqrt{1 - \frac{8}{9} \frac{C_1 \rho_w a^2}{\mu a}}$$

$$\beta = \sqrt{1 + \frac{8}{9} \frac{C_1 \rho_w a^2}{\mu a}}$$

For the case $C_1 > 0$ (Figure II-19) the equation in Y is unaffected by whether $(8/9)(C_1 \rho_w a^2/\mu a)$ is greater or less than unity. The equation in X, however, shows two different behaviors. For small values of drop size, α is real but always less than unity. The equation for X displays an exponential decrease but remains positive for all finite Z, i.e., the drops do not reach the plane X = 0 unless the initial velocity (X_o') is sufficiently large. For large drops α becomes imaginary and the hyperbolic functions become sine and cosine. The drop then exhibits an oscillatory damped motion as in Figure II-21. (The equations do not recognize the existence of the wall at X = 0.)

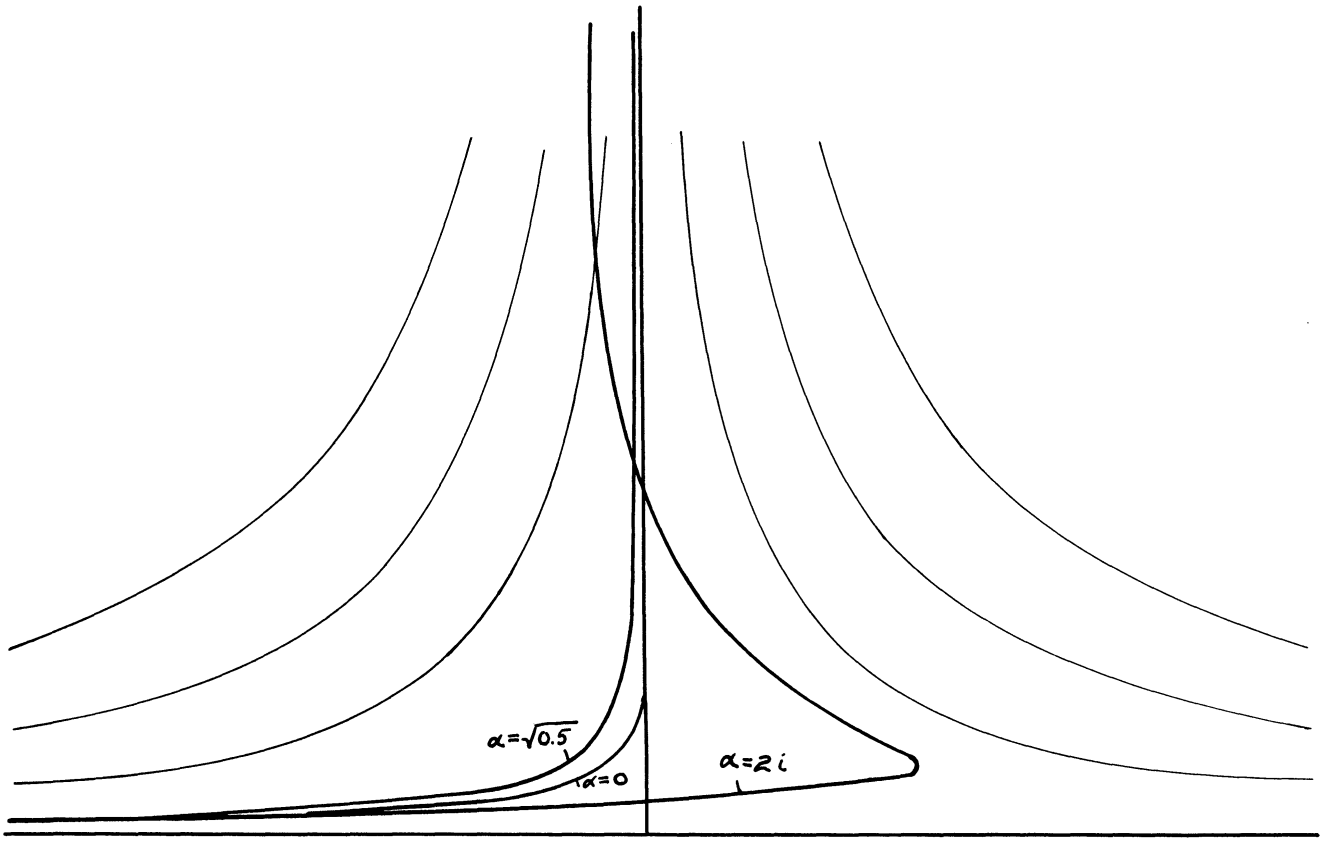

Figure II-21

Returning now to the case of small drops (α real) when Z is large,

$$\sinh \frac{\alpha Z}{2} \longrightarrow \frac{1}{2} e^{\frac{\alpha Z}{2}} \qquad \cosh \frac{\alpha}{2} Z \longrightarrow \frac{1}{2} e^{\frac{\alpha Z}{2}}$$

$$X = e^{(-\frac{1}{2}+\frac{\alpha}{2})Z} \left[\frac{2 X_o' + X_o}{\alpha} + X_o \right] .$$

If the initial position of the drop is a negative coordinate, the initial value X_o' must be positive and at least equal to

$$X_o' = - \frac{\alpha + 1}{2} X_o \quad ,$$

if the drop is ever to reach X = 0. Rewriting the above in terms of the physically significant parameters,

$$\left(\frac{dx}{dt}\right)_{\text{critical}} = \frac{9}{4}\,\frac{\mu_a}{\rho w\, a^2}\left(1 + \sqrt{1 - \frac{8}{9}\,\frac{C_1\,\rho w\, a^2}{\mu_a}}\right)\left(X_o - \frac{C_u}{C_1}\right).$$

The above velocity is the critical one required for a drop to just reach the plane X = 0 from initial position X_o.

Summary of Available Trajectory Data

Table III gives a summary of various trajectory data currently available in the literature.

TABLE III

Shape	Source	Comment
Cylinders	Albrecht, Ref. 1	Stokes' law regime
Cylinders	Glauert, Ref. 11	Stokes' law regime
Cylinders	Kantrowitz, Ref. 10	Oseen's law
Cylinders	Langmuir, Ref. 2	Experimental C_D data
Spheres	Langmuir, Ref. 2	Experimental C_D data
Ribbons	Langmuir, Ref. 2	Experimental C_D data
Stagnation region	Taylor, Ref. 9	Stokes' law
Airfoils	Glauert, Ref. 11	
Uncambered 15% thick Joukowski,	Guibert, Ref. 7	0, 2, and 4° angle of attack
Cambered, 15% thick Joukowski,	Guibert, Ref. 7	0° angle of attack
NACA 65_2-015	Guibert, Ref. 7	0° angle of attack
Uncambered, 12% thick Joukowski	Bergrun, Ref. 6	0° angle of attack
Supersonic wedge	Tribus, Ref. 8	

REFERENCES

1. Albrecht, Fritz, "Theoretische Untersuchungen über die Ablagerung von Staub Strömender Luft und Ihre Anwendung auf die Theorie de Staubfilter". Phys. Zeitschr., vol. 32, (1931) pp. 48-56.

2. Langmuir, Irving, and Blodgett, Katherine, "A Mathematical Investigation of Water Droplet Trajectories". AAF Tech. Rept. 5418, Feb. 1946.

3. Tribus, M., and Tessman, J., "Report on the Development and Application of Heated Wings". AAF Tech. Rept. 4972, Add. 1., Feb. 1946. Wright Field, Ohio.

4. Tribus, M. Young, G. B. W., and Boelter, L. M. K., "Limitations and Mathematical Basis for Predicting Aircraft Icing Characteristics from Scale Model Studies". Trans. ASME, November 1948, p. 977.

5. Drell, Harry, and Valentine, Paul, "Comments on Methods of Calculating Water Catch and a Correlation of Some New Data". Unpublished report, Lockheed Aircraft Company, July 1950.

6. Bergrun, Norman R., "A Method for Numerically Calculating the Area and Distribution of Water Impingement on the Leading Edge of an Airfoil in a Cloud". NACA TN 1397. August 1947. missing in Eng Lib.

7. Guibert, A., Janssen, E., and Robbins, Wm., "Determination of the Rate, the Area, and the Distribution of Impingement of Waterdrops in Various Airfoils from Trajectories Obtained on the Differential Analyzer". NACA RM 9A05 February 1949. An addendum to this report has recently been issued.

8. Tribus, M., and Guibert, A., "The Impingement of Spherical Water Droplets on a Wedge at Supersonic Speeds". University of California, Los Angeles, 1949. Unpublished report.

9. Taylor, G. I., "Notes on Possible Equipment and Technique for Experiments on Icing on Aircraft". R and M No. 2024, January 15, 1940.

10. Kantrowitz, A., "Aerodynamic Heating and Deflection of Drops by an Obstacle in an Air Stream in Relation to Aircraft Icing". NACA TN No. 779, 1940.

11. Glauert, M., "A Method of Constructing the Paths of Raindrops of Different Diameters". R and M No. 2025 (4805) ARC Technical Report, November 1940.

CHAPTER III

REMOVING THE ICE

In the previous chapter we have considered the mechanism of ice deposition on streamlined bodies. There still remain important trajectory problems to be considered, such as new methods of obtaining trajectory data, the influence of compressibility on ice accretion, and the icing characteristics of the new types of airfoils. The previous material, even though it is incomplete, should serve as an introduction and guide to the current literature where new data are constantly being presented.

Detailed studies of what happens to a drop of water just as it strikes an airfoil surface have not been accomplished. Langmuir[1] has suggested that "bounce off" may play an important role, though thus far experiments have not revealed the effect. For a while it was thought that the drops of water might blow off. However, unpublished experiments by Tracy B. Gardner indicate no "blowoff". Gardner used an airfoil with sintered-metal porous strips in the nose region and also inserted in the airfoil surface about one foot back from the leading edge. Water was pumped out through the leading edge and permitted to run along the surface and be collected in the second porous metal strip. The collected water was drained off by suction and compared in quantity with the ejected water. No blowoff was indicated. Figure III-1 shows the apparatus used by Gardner.

Boelter, Johnson, Sanders, and Rubesin[2] have made detailed analyses of the forces which tend to remove a drop from the surface. They have also considered the relation between rate of evaporation and water catch as affecting the percentage of "wetted" area of a wing. The studies were exploratory but did not reveal net forces which would be expected to remove water droplets.

NACA experiments[13], wherein blueprint paper was laid over the wing to reveal those areas which were wetted, showed that in the area of water

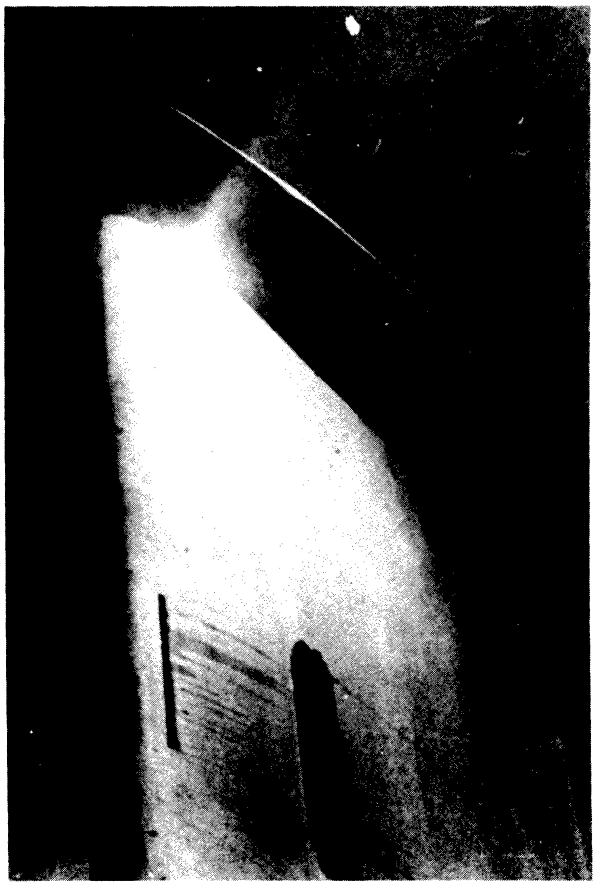

Figure III-1. Runback experiments by Gardner (Reference 12). Water was pumped out of the forward porous metal strip and sucked in at the the rear strip. Note the characteristic rivulet form.

impingement the water covered the entire surface, but aft of this region the water flowed in rivulets. No blowoff was indicated in these traces, either. See Figures III-2a and III-2b.

This evidence has given rise to the general belief that once the drops of water impinge upon the airfoil, they remain on the surface. The drops may evaporate, freeze upon impact, roll along the surface individually (until they blowoff the trailing edge), flow in rivulets, or they may collect in depressions. If the airfoil is heated in one region and not in another, the water may flow back to the unheated regions and cause "runback" or "freeze-back".[3] It must be noted in passing that "bounce off", if it does occur, has thus far not been found.

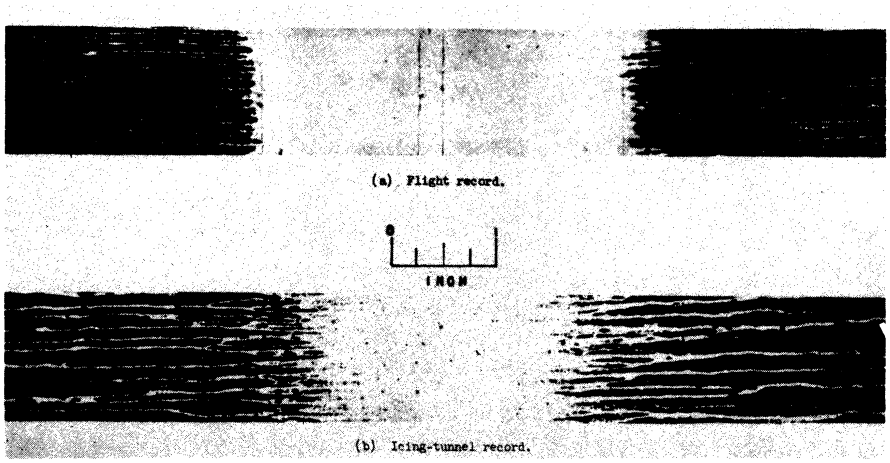

Figure III-2. Records of runback obtained by NACA (a) in flight and (b) in the tunnel. The records were obtained by wrapping a water-sensitive film around the wing leading edge. The wetted areas are clearly visible. The increased turbulence in the tunnel as compared to free flight is evident from the jagged appearance of the rivulets aft of the region of primary impingement (Reference 13).

The designer of an anti-icing system may elect to design his equipment to function in one of several ways:

(a) The entire airfoil surface may be heated above 32°F. The water will then run along the surface and off the trailing edge. This method is most suited to small objects such as jet-engine inlet guide vanes, pitot-tube masts, antennae, and helicopter blades. The method is also used for windshields, though the resultant ice accumulations at the window frames are often objectionable.

(b) The area of water impingement and a short region directly after it may be heated so intensely that all the impinging water is evaporated. This method is used in conventional heated wings. At moderate speeds (200 to 300 mph) the heat requirements are large but not excessive. At higher speeds the energy requirements place a severe burden upon the heat source. The heat may be supplied by hot air, exhaust gases, or electrical resistance heaters.

(c) The surface may be heated intermittently, permitting the ice to gather during the "off" period and melting the interface during the "on" period. This method is especially attractive on

propeller blades where the centrifugal forces are available to release the ice. The method is also used for wings if a "parting strip" at the leading edge is kept warm to prevent "capping". Two methods of heating a wing intermittently have been proposed in Germany and are reported in Reference 4. Electrical energy is usually used, but hot air may be employed intermittently.

(d) The surface may be unheated and the ice permitted to form until removed by mechanical means. The B. F. Goodrich Company markets a inflatable rubber "shoe" which fits over the wing surface and is operated pneumatically. Mechanical systems have an unfortunate history of not operating cleanly; i.e., fragments of ice often stick to the surface. Recently this company has announced some improvements which include a treatment of the rubber to lower the adhesion.[5] Another type of mechanical de-icer is described by Robert Smith-Johannsen.[6] Smith-Johannsen describes the very greatly diminished ice adhesion which occurs when the ice is frozen quickly. He also shows how the presence of impurities will markedly lower the ice adhesion. The "shoeshine de-icer" or "peel-off de-icer", as it was called, consisted of a very thin, less than 5 mm-thick, stainless-steel sheet which was wrapped around the leading edge of the wing and then pulled parallel to the wing surface in much the same fashion as one pulls a rag while shining a shoe. The movement was approximately a half inch. In trials on Mt. Washington the operation was reported as quite successful. The metal was considered preferrable to rubber since the thermal conduction helped remove the heat of fusion of ice and therefore aided quick freezing. Coatings containing special impurities to lower ice adhesion could also be incorporated. The de-icer has not been developed sufficiently for judgment on its efficacy to be made yet.

(e) A melting point depressant may be released in the area of water impingement. This last method has fallen into disfavor. Hardy[7] has shown how the evaporation of the alcohol causes a refrigerating effect and thereby diminishes the alcohol effectiveness. Similarly, special pastes and finishes have been proposed from time to time, but without much success.

(f) The leading edge may be made of a porous material and hot air forced from the interior of the wing. A blanket of warm air is thus created over the icing region. A careful analysis of the method has not yet been made, but preliminary results indicate less hot air is needed than for conventional hot-air anti-icers. This system would not be advisable for a large wing because of the adverse effect

upon the boundary layer, but for a radar housing or other small object it might be very economical. Too few data are now available for adequate appraisal.

(g) Theodorsen and Clay[8] suggested that the leading edge impingement area be heated to just above the freezing point and the "runback" collected in a small trough or slot. Tessman,[5] fifteen years later, made the same suggestion except that porous metal strips were to replace the trough or slot. Insofar as is known the method has never been tried except by Theodoreson and Clay, who reported success.

Heat Transfer Media

Of the various media suitable for transferring heat to the exterior surfaces, air has been the one found most practical. In 1931 the NACA[8] demonstrated a system utilizing alcohol and water. Boiling occurred at the engine exhaust heater and condensation occurred in a small wing model. The alcohol prevented freezing. Systems wherein boiling may occur are usually too heavy for aircraft use because of the high pressures which may occur. Similarly liquids are not practical, particularly since such systems must be leak proof.

The sources of the hot air depend upon the particular airplane. In conventional propeller-driven aircraft with reciprocating engines the source of heat may be the exhaust gases. Although this sort of heat source looks attractive, particularly since the heat seems almost "free", close analysis has shown that considering the overall airplane performance separate gasoline-burning heaters are often superior. Each airplane has its own peculiarities, and where one airplane may utilize the exhaust gases separately for jet-propulsive assistance (as in the Douglas DC-6) and therefore may be unable to accommodate a heat exchanger, another may have a common exhaust manifold which is so located that the addition of a heat exchanger may be made quite easily (as in the Convairliner).

In jet-propelled aircraft the hot air is often taken from the last stage of compression. The hot compressed air may be carried in relatively small conduits since the pressure drop available for distributing the air is high. The performance loss in the engine is serious. An extraction of 1 per cent of the airflow causes approximately a 2 per cent loss in thrust. Some designers have considered extracting air from an early stage of compression and utilizing gasoline-burning heaters for raising the air temperature.

As an example of a comparison between two types of heating systems, Jongeneel and David[10] presented the data of Table I during a symposium on anti-icing in 1946. The data refer to the DC-6-type airplane.

TABLE I

WEIGHT ANALYSIS OF POSSIBLE HEAT SOURCES FOR A 4-ENGINE CARGO AIRPLANE

	(a) Combustion Heaters	(b) Collector Ring	(c) Short Stack	
Total heat required	947,000			BTU/hr
Heat per engine (d)		316,000	316,000	
Fuel weight for 2 hrs	132			lbs
Weight of system, excluding fuel	530	600	600	lbs
BHP required per engine for long-range cruise (e)		910	830	HP
Exhaust back pressure causes a loss per engine		9	6	HP
Additional power loss due to loss of exhaust jet thrust		0	40	HP
Total loss per engine		9	46	HP
Total loss to airplane		36	184	HP
Fuel weight, sfc = 0.45, 16 hours flight (f)		260	1325	lb
Total Weight	662	860	1925	lb

(a) Combustion heaters are mounted in the wings and tail. The engines are equipped with jet stacks.

(b) A collector ring is mounted on each engine, the exhaust gases manifold together and passed through a heat exchanger. The loss in jet thrust is not charged against anti-icing.

(c) Some of the exhaust gases are diverted to an exchanger.

(d) Supply of heat sufficient for one engine inoperative.

(e) Less HP is required if jet thrust available from engine exhaust.

(f) Two hours in icing in 16 hours flying.

The air temperature is limited by the allowable temperature (less than 300°F) of the aluminum alloys used in airfoil construction. The softening temperature of the plastic used in safety glass similarly limits the temperature in a windshield anti-icing system to less than 200°F.

Several proposals have been made to extract exhaust gases from the engine and to dilute them with fresh air. In a jet engine the relative purity of the exhaust gases and the moderate temperature make the system attractive. No announcements have been made of such systems in actual use.

Great care must be exercised in the design of the leading-edge construction of large wings. The thermal expansion at the leading edge may cause severe stresses. An early experimental Navy flying boat was reported to have had such a severe leading-edge expansion that the ailerons were locked in place as the trailing edge was compressed. More recently an experimental airplane was reported to have "popped its rivets" during a ground run-up.

Economical Aspects of Ice Protection

Most workers in the field of ice prevention like to feel that the equipment being designed will be used to enable the pilot to fly through an icing condition without affecting his schedule or course. This happy day has not yet dawned, however, and most ice protection equipment is still looked upon for emergency use only. Since neither the military nor the airlines reckon the value of a life in terms of dollars and cents, it is difficult to discuss the worth of the de-icing apparatus.

Nevertheless, some figures are available on the cost of operating anti-icing equipment in the airlines. Dave North and Dan Beard of American Airlines have made a critical comparison of the costs of operating the Douglas DC-6 (combustion heaters) and the Convairliner 240 (heat exchanger). Table II gives a summary of the data reported by North and Beard.[11]

Unfortunately these data represent "debugging" or breaking-in experience so that the cost figures must be considered as tentative. On the other hand, most airplanes have short lives so that the "debugging" period is an appreciable fraction of the life span.

In the field of military aircraft a careful "operational analysis" is required. The added weight of de-icing equipment detracts from the pay load or top speed which may therefore result in greater loss due to enemy action. This loss must be balanced against the probable loss by icing and the military advantages of being able to fly in ice.

The commercial airliner must balance the cost of the equipment against the loss in revenue from schedule delays and possible crashes.

These economical aspects of the de-icing problem have not been studied as thoroughly as have the scientific problems. Those few persons who have had

to face this problem have almost invariably concluded that what is needed is a removable anti-icing system, one which could be installed for special missions and left off for others.

Only the mechanical de-icer of the Goodrich type at present meets this removability requirement. Such a system also enjoys the advantage that a company may specialize in de-icer design and therefore prepare de-icers for several airplanes. The continued sale of rubber de-icers in the face of competition from other more effective systems (viz., thermal) is probably directly attributable to this latter advantage.

TABLE II

COMPARATIVE COSTS FOR TWO COMMERCIAL DE-ICING SYSTEMS

	Douglas DC-6	Convair 240
WING AND TAIL		
Heater replacement	$2400	$24,000
Heater maintenance	384	1,520
System maintenance	312	255
System replacements	328	225
Fuel cost	576	---
Fuel required to make up thrust loss	---	10,500
Subtotal for wings and tail	$4000	$16,000
PROPELLER		
Heated "shoes"	$1920	$ 2,880
Maintenance of "shoes"	320	240
Maintenance of system	160	120
System replacements	400	260
Subtotal for propellers	$2800	$ 3,500
WINDSHIELDS		
Electrically-heated glass, breakage	$----	$ 1,150
System maintenance	----	115
System replacements	----	135
Hot-air windshield costs	400	------
Subtotal for windshields	$ 400	$ 1,400

Based on a 4000-hour period, 6 per cent of flying time is in icing. The two systems are not strictly comparable. The Convairliner is lower to the ground (increased propeller abrasion) and has development problems in the relatively unconventional exhaust heater system.

REFERENCES

1. Langmuir, Irving, "Final Report on Icing Research up to July 1, 1945". G.E. Research Laboratory, Contract No. W33-038-AC-951 (14006) October 1945.

2. Boelter, L. M. K., Johnson, H. A., Sanders, V. D., and Rubesin, M. W., "Icing Report by the University of California, Fiscal Year 1946". AAF Tech. Rept. 5529, Sectionl, p. 4, July 1946.

3. Guibert, A. G., "Thermal Anti-Icing Survey on Mt. Washington". Trans. ASME, November 1947, p. 829 shows drawings of the water drops or rivulets on the surface of a cylinder.

4. Tribus, M., "A Review of Some German Developments in Airplane Anti-Icing". Trans. ASME, July 1947, p. 505.

5. Loughborough, D. L. and Haas, E. G., "Reduction of the Adhesion of Ice to De-Icer-Surfaces". Jour. Aero. Sec. vol. 13 (3) pp. 126-134, March 1946.

6. Smith-Johannsen, Robert, "Basic Icing Research by General Electric Company, Fiscal Year 1946". Section 9 "The Peel Off Mechanical Wing De-Icer", AAF Tech. Report 5539, June 1946.

7. Hardy, J. K., "Kinetic Temperature of Wet surfaces, A Method of Calculating the Amount of Alcohol Required to Prevent Ice and the Derivation of the Psychrometric Equation". NACA WR A-8, September 1945.

8. Theodorsen, Theodore and Clay, William C., "Ice Prevention on Aircraft by Means of Engine Exhaust Heat and a Technical Study of Heat Transmission from a Clark Y Airfoil". NACA Report 403, 1931.

9. Tribus, M. and Tessman, J., "Report on the Development and Application of Heated Wings". AAF TR 4972, Add L, January 9, 1946.

10. Jongeneel, T. W. and David, R. H., "Effects on Airplane Performance of Heat Anti-Icing by Exhaust Heat Exchanger as Compared to Combustion Heaters". Unpublished report, 1946.

11. Beard, M. G. and North, D., "Operational Results of Thermal Anti-Icing", SAE Jour., vol 58 (May 1950), p. 56.

12. Gardner, T. B., "Investigation of Runback". Air Materiel Command, Ice Research Base, Report IRB 46-36-IF, July 1946.

13. Lewis, J. P. and Gelder, T. F., "Comparison of Heat Transfer from Airfoil in Natural and Simulated Icing Conditions". NACA TN2480, September 1951.

CHAPTER IV

THE ENERGY TRANSFERS AT AN ICING SURFACE

(Analysis of the Separate Modes of Energy Transfer)

At a nonporous* surface exposed to the impingement of super-cooled water droplets seven modes of energy transfer are possible. These modes of energy transfer are depicted in Figure IV-1, where the arrows denote the direction of energy flow. (The radiation term is negligible at conventional flight speeds in icing.) If heat is supplied from behind the icing surface, a word equation for the heat balance is:

The heat flux from the ice side of the ice-to-air interface	equals	the heat loss to the air boundary layer by convection
	minus	the frictional heating by the air stream
	plus	the energy loss via evaporation or sublimation
	minus	the heat release due to fusion of ice
	plus	the heat loss due to sensible heating of the water
	minus	the gain from kinetic energy of the drops
	plus	radiation to the surroundings.

*D. M. Patterson has called attention to the porosity of some ice formations and suggested that leakage of air under and around an ice formation may be significant. Adequate observations are not yet available.

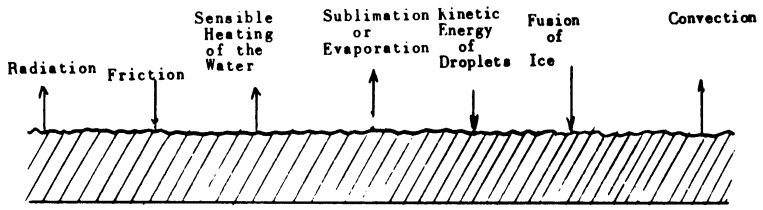

Figure IV-1

If the surface temperature is above 32°F the term involving the heat of fusion does not appear. (References 1, 2, 3, and 4 treat the heat loss from surfaces in icing where the temperature is above the freezing point.)

Below the freezing point the formation of ice liberates heat and the surface temperature is raised until the other modes of energy transfer are sufficient to offset the heat of fusion. Figures IV-2a, b, c are taken from NACA icing wind-tunnel measurements[5] and serve to illustrate the heat-of-fusion term in the energy balance. In each figure the curves represent records made of the time–temperature histories of propeller blades exposed to icing conditions. The curves are particularly interesting because in each case we see the temperature of the blade before and after the water sprays are turned on. The temperature rise is the greatest when the liquid-water content is large.

Energy flux when the surface temperature is below freezing is treated in References 6, 7, and 8.

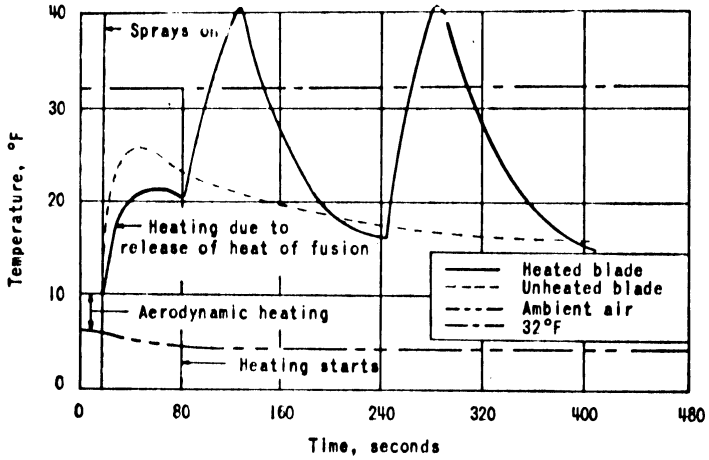

MEASUREMENTS BY LEWIS FOR INTERNALLY HEATED BLADE

Figure IV-2a. (Figure 10f, Ref. 5) 800 rpm, 5°F ambient, r/R = 0.33, 0.4 grams/meter^3. Heat of fusion causes 10°F temperature rise.

In References 1 through 8 the various modes of energy transfer have been treated as though they were independent of one another. Unfortunately the experimental difficulties have been too great to permit close checking upon the individual terms during icing. The best that can now be said is that the data available from the experiments conducted on surfaces above the freezing point do not contradict this view.

In this chapter we consider the separate terms in the energy balance. The treatment given here must of necessity be brief, for each mode of energy transfer is a subject worthy of study by itself. In the next chapter the terms will be put together.

The Heat Loss by Convection

The convective heat loss to the air is confined (by definition) to a boundary layer. This boundary layer begins at the stagnation region as a

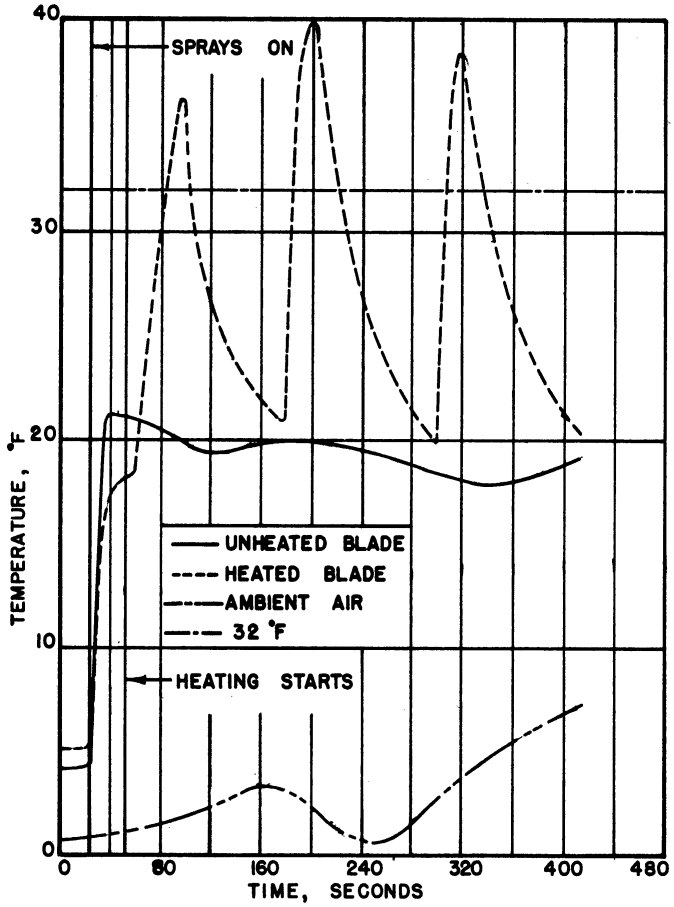

Figure IV-2b. Measurements by Lewis for internally heated blade. Liquid water content of air, 0.3 grams/meter^3.

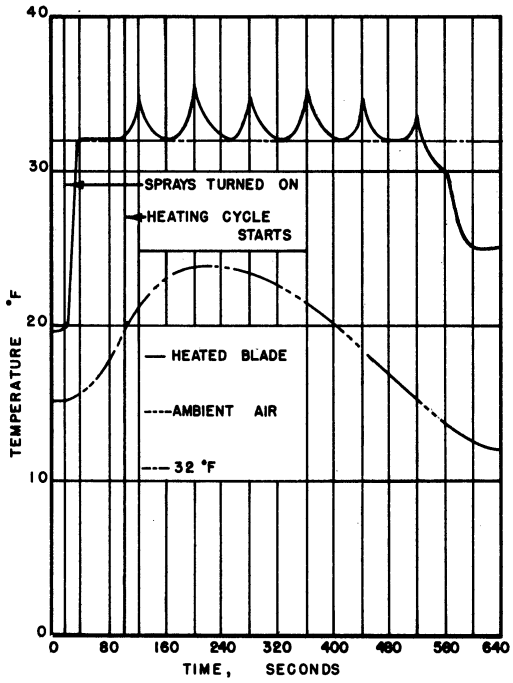

Figure IV-2c. Measurements by Lewis for internally heated blade. Liquid water content of air, 0.9 grams/meter^3.

relatively thin laminar flowing film which increases in thickness along the surface. At some point, or more likely, over a region of the surface, the laminar layer changes to a turbulent one. The blanket of warm air in the boundary layer retards the heat flux from the regions downstream of the heated leading edge.

For a surface heated to a uniform temperature the heat flux via convection is usually calculated from the equation

$$q_c = h_c A (t_s - \tau_1),$$

where

q_c = convective heat flux, BTU/hr
A = area of heat flux, ft^2
t_s = surface temperature, °F
τ_1 = air temperature outside the boundary layer, °F
h_c = unit thermal conductance, defined by above equation, BTU/hr ft^2 °F.

The unit thermal conductance for an isothermal surface depends on the velocity distribution in the boundary layer and on the fluid properties. For most systems the conductance is determined experimentally, though for certain simple shapes analytical methods are available. Eckert[9] gives a description of some of the simpler techniques. Seban[10] surveys the methods available for laminar flow when both the pressure and surface temperature are not constant. Martinelli[11] discusses turbulent flows and presents and empirical method which appears to be as accurate as any other available and considerably more rapid than most.

The case of laminar flow yields to analytical treatment more easily than does turbulent flow. For many systems, however, experimental methods are more suitable, particularly since the pressure distribution and the location of the transition point are not always known in advance. Giedt[12] has shown how artificially induced turbulence may change the heat transfer by more than 20 per cent. Lewis and Gelder[13] have shown how the turbulence from a spray bar 40 feet upstream moved the transition point on a wing model and increased the heat transfer. (We shall later see that under some circumstances this effect is not important.)

The unit thermal conductance may be measured for a particular body by conducting an experiment in which q, A, t_s, and τ_1 are measured simultaneously. The conductance is then calculated from

$$h_c = \frac{q}{A(t_s - \tau_1)} .$$

One technique for measuring h_c is to put an electrical heating element on the surface, properly insulated from the back side, and measure the power input, surface temperature, and free-air temperature. Such an arrangement is described on page 78 of Reference 1 and also in Reference 14. In each of these references a thin nichrome ribbon heater was laid over cork insulation wrapped around the leading edge.

First approximations to the heat transfer in the laminar boundary layer may be obtained by treating the leading-edge region as a cylinder and the afterbody as a flat plate.[11] (The method of Seban[10] should be used where more accuracy is needed.) A suitable empirical expression for the heat flux from an isothermal cylinder (± 15 per cent) is:

$$h_c = 0.194\ T_f^{\,0.49} \left(\frac{U_\infty \gamma}{D}\right)^{0.5} \left[1 - (\phi/90)^3\right]$$

h_c = "local" unit thermal conductance, BTU/hr ft^2 °F
T_f = "film" or average boundary layer temperature, °R
U_∞ = air velocity far from cylinder, ft/sec
γ = air density, lbs/ft^3
D = cylinder diameter, ft
ϕ = angle measured from stagnation point, degrees ($0 \leq \phi < 80°$).

For an isothermal flat plate in laminar flow an empirical equation is

$$h_c = 0.0562\ T_f^{\,0.5}\ (U_\infty \gamma)^{0.5}\ x^{-0.5}$$

x = distance from stagnation point, ft.

Chapman and Rubesin[15] have shown how the above equation may be seriously in error for nonuniform temperature systems if the flow is laminar. The criterion for the importance of the nonuniformity of the surface in the case where the surface temperature varies linearly with distance from the stagnation point is

$$x\ (dt/dx)/(t_s - \tau_1)_o \ ,$$

where

x = distance from stagnation point
dt/dx = temperature gradient (constant)
$(t_s - \tau_1)_o$ = surface to air temperature difference at x = 0.

Figure IV-3 shows the effect of nonuniformity of surface temperature as a function of the above parameter.[16]

For the case of turbulent flow Martinelli recommends that the equation for a flat plate be used except that the local velocity should be

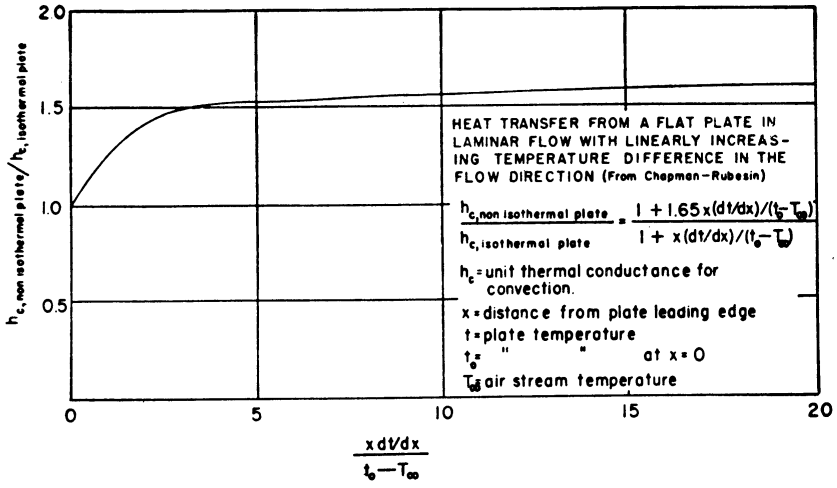

Figure IV-3. Heat transfer from a flat plate in laminar flow with linearly increasing temperature difference in the flow direction.

substituted for the (uniform) velocity over a flat plate. A suitable empirical expression for the unit thermal conductance over an isothermal flat plate is

$$h_c = 0.51\, T_f^{0.3}\, (U_1 \gamma)^{0.8}\, x^{-0.2}$$

T_f = "film" or average boundary layer temperature, °R
U_1 = velocity just outside boundary layer, ft/sec
γ = air density, lbs/ft^3
x = distance back from stagnation point, ft.

For the turbulent boundary layer over a nonisothermal flat plate Scesa[17] has shown how the corrections by Rubesin[18] may be used to predict heat transfer in the vicinity of an abrupt change in surface temperature.

A particular case of interest is one where the surface is unheated for a distance, S, and then the heating starts. Such a case arises during intermittent heating of separate wing sections. The Rubesin analysis yields a correction of the form

$$h_{c_{\text{nonisothermal}}} = h_{c_{\text{isothermal}}} \left[1 - (S/x)^{39/40}\right] - 7/39 \quad ,$$

where

x = distance from leading edge
S = length of unheated starting section.

Scesa[17] obtains excellent agreement between the above expression and a set of experimental data over a wide range of (S/x) and Reynolds modulus.

The Heat Gain Due to Frictional Heating

The growth of the boundary layer is brought about by the viscous nature of the fluid. As the laminations of air flow past one another, the viscosity causes a drag force to be exerted. This frictional drag is an irreversible working of the fluid elements and results in an increase in temperature. The heating in any one lamination is offset by the thermal conductivity of the fluid which conducts heat from the hotter to the colder laminations. In the case of air, the net result of these two opposing effects is an increase in the temperature near an insulated wall. The temperature rise of the fluid adjacent to the surface when there is no heat flux is described by

$$t_e - \tau_1 = r \frac{U_1^2}{2gJC_p} \quad ,$$

where

t_e = "equilibrium" surface temperature °F
τ_1 = air static temperature just outside boundary layer, °F
U_1 = air velocity just outside boundary layer, ft/sec
C_p = air heat capacity, BTU/lb °F
g = 32.2 ft/sec^2
J = 778 ft lb/BTU

Experimentally, for air, it has been found that the recovery, r, defined in the above equation is approximately 0.85 for laminar and 0.92 for turbulent boundary layers.

Where aerodynamic heating is important, it is customary to redefine the unit thermal conductance as follows:

$$q = h_c A (t_s - t_e) ,$$

or

$$q = h_c A \left(t_s - \tau_1 - r \frac{U_1^2}{2gJC_p}\right) .$$

The net effect of aerodynamic heating is therefore to supply a heat source of relative strength

$$q_{(\text{friction})} = h_c A r \frac{U_1^2}{2gJC_p} .$$

References 19 and 20 discuss aerodynamic heating in greater detail.

Sublimation or Evaporation

The evaporation or diffusion of water from a wetted or iced surface proceeds whenever the vapor pressure at the surface exceeds the vapor pressure in the surrounding air. The diffusion is hindered by the boundary layer of water vapor which grows as the air moves downstream along the surface. The mechanism for the water boundary layer growth and diffusion is similar to the mechanism whereby heat is convected; hence it is quite natural to define a conductance for mass transfer by the equation

$$g = h_m A (H_s - H_i) ,$$

where

g = mass flux, lbs H_2O/hr
A = area of evaporation, ft^2
H_s = humidity at surface, lbs H_2O/lb air
H_i = humidity outside boundary layer lbs H_2O/lb air.

These define h_m = unit mass conductance, lbs/hr ft^2. The above definition is not unique. The vapor pressure or water concentration could just as well have been chosen as potentials instead of humidity.

Experiments[21] have shown that, when defined as above, the unit mass conductance bears a simple relation to the unit thermal conductance for heat transfer, i.e., in the range of temperatures of interest in icing,

$$\frac{h_m C_{p_a}}{h_c} \simeq 1.0,$$

where C_{pa} = unit heat capacity of air BTU/lb °F.

Because the humidity is not a convenient parameter, the working equations usually use the equation

$$H_s - H_i = \frac{0.62}{B} (P_s - P_i),$$

where:

0.62 = ratio, molecular wt of water/mol. wt air
B = barometric pressure, "H_g
P_s = surface vapor pressure of water, "H_g
P_i = stream vapor pressure of water, "H_g.

Since each pound of water requires L BTU/lb during vaporization, the heat loss during evaporation is

$$q_e = \frac{0.62}{B} \frac{h_c L A}{C_{p_a}} (P_s - P_i) \quad ,$$

In the case where the surface temperature is nonuniform, the above relation becomes inaccurate.

Energy Transfer to or From the Impinging Water (Sensible heating and fusion)

Langmuir[22] has shown that the drops travel through the disturbed air so rapidly that they undergo negligible change in temperature during their transit time. If the rate of water impingement is R_w (lbs/hr ft^2) and the enthalpy of the water before and after impact is denoted by G_∞ and G_s (the usual symbols h or H for enthalpy were used in the previous sections for conductance and humidity, respectively), then the energy added to the water is

$$q_{water} = R_w A (G_s - G_\infty) .$$

If there is no change in phase (i.e., no ice formed) the change in enthalpy is

$$G_s - G = C_{p_w} (t_s - T_\infty),$$

where

C_{p_w} = heat capacity of water, BTU/lb °F.

The above equation applies for $t_s > 32°F$.

If ice forms,

$$G_s - G_\infty = C_{p_i} (t_s - 32) - 144 + C_{p_w} (32 - T_\infty),$$

where

C_{p_i} = heat capacity of ice, BTU/lb °F
144 = heat of fusion of ice at 32°F.

Thus we have two different equations depending upon whether the temperature is above or below the freezing point:

$$q_{\text{sensible}} = Rw\ A\ C_{p_w}\ (t_s - \tau_\infty) \qquad t_s > 32°F$$

$$q_{\text{sensible + fusion}} = RwA\left[-144 + 32\ (C_{p_w} - C_{p_i}) + C_{p_i} t_s - C_{p_w}\right] \qquad t < 32°F\ .$$

This last equation is separated into two parts, as follows:

$$q_{\text{sensible}} = RwA\ C_{p_w}\ (t_s - \tau_\infty) \qquad \text{all } t_s$$

$$q_{\text{fusion}} = RwA\left[-144 + (32 - t_s)\ (C_{p_w} - C_{p_i})\right] \qquad t_s < 32°F\ .$$

The discussion of the appropriate equation when $t_s = 32°F$ will be deferred until the complete energy balance is taken up.

The term in R_w is taken from the trajectory data.

Kinetic Energy of the Drops

The drops arrive with velocity V and therefore have a kinetic energy

$$\frac{V^2}{2g\ J}$$

with respect to the surface. The energy added to the surface thus is

$$q_{KE} = R_w\ A\ \frac{V^2}{2g\ J}$$

The velocity possessed by the drops at impact may be calculated from the trajectory data. The contribution of this last term is small compared to the others, but not entirely negligible in the heat balance at high speeds. In most design work V may be taken equal to U_∞. In research work V may be taken from a calculation such as represented in Figure II-7.

REFERENCES

1. Tribus, M., and Tessman, J., "Report on the Development and Application of Heated Wings". AAF Technical Report 4972 Add 1, January 9, 1946.

2. Neel, Carr. B., "The Calculation of the Heat Required for Wing Thermal Ice Prevention in Specified Icing Conditions." Paper presented before SAE, October 4, 1947.

3. Bergrun, Norman R., "General Results of NACA Flight Research in Natural Icing Conditions During the Winters of 1945 and 1946". Aero. Eng. Rev., January 1948, p. 20.

4. Hardy, J. K., "An Analysis of the Dissipation of Heat in Conditions of Icing from a Section of the Wing of a C-46 Airplane". NACA Report 831, 1945.

5. Lewis, James P., and Stevens, H. C., Jr., "Icing and De-Icing of a Propeller with Internal Electric Blade Heaters". NACA TN 1691, August 1948.

6. Tribus, M., "Intermittent Heating for Aircraft Ice Protection with Application to Propellers and Jet Engines". Trans ASME, November 1951.

7. Weiner, F., "Further Remarks on Intermittent Heating for Aircraft Ice Protection". Trans ASME, November 1951.

8. Messinger, Bernard L., "Equilibrium Temperature of an Unheated Icing Surface as a Function of Airspeed." IAS paper Sherman M. Fairchild Fund (IAS Preprint 342), June 1951.

9. Eckert, E. R. G., Introduction to the Transfer of Heat and Mass. McGraw-Hill Book Company, 1950, p. 59.

10. Seban, R. A., "Calculation Method for Two-Dimensional Laminar Boundary Layers with Arbitrary Free Stream Velocity Variation and Arbitrary Wall Temperature Variation", Inst. of Eng. Res., Report 12, Series 2, University of California, Berkeley.

11. Martinelli, R. C., et. al., "An Investigation of Aircraft Heaters: VIII, A Simplified Method for the Calculation of the Unit Thermal Conductance over Wings". NACA ARR, March 1943.

12. Giedt, W. H., "Effect of Turbulence Level of Incident Air Stream on Local Heat Transfer and Skin Friction on a Cylinder". Jour. Aero. Sci., November 1951, p. 725.

13. Lewis, J. P., and Gelder, T. F., "Comparison of Heat Transfer from Airfoil in Natural and Simulated Icing Conditions". NACA TN 2480, September 1951.

14. Walker, K., Decker, M. S., and Weller, D. W., "External Heat Transfer Coefficient of Wing Leading Edge Determined by Flight Test". Report No. R78-053, Fairchild Aircraft, December 1944.

15. Chapman, D., and Rubesin, M. W., "Temperature and Velocity Profiles in the Compressible Boundary Layer with Arbitrary Distribution of the Surface Temperature". Jour. Aero. Sci., vol 1-6, No. 9 (1949).

16. Tribus, M. Comments on paper by Seban and Shimizaki, Trans. ASME., August 1951, p. 807.

17. Scesa, Steve, "Experimental Investigation of Convective Heat Transfer to Air From a Flat Plate with a Stepwise Discontinuous Surface Temperature". MS Thesis, University of California, Berkeley, 1951.

18. Rubesin, M. W., "An Analytic Investigation of the Heat Transfer between a Fluid and a Flat Plate Parallel to the Direction of Flow Having a Stepwise Discontinuous Surface Temperature". MS Thesis, University of California, Berkeley, 1946.

19. Johnson, H. A., Rubesin, M. W., Sauer, F. M., Slack, E. G., Possner, L., "A Design Manual for Determining the Thermal Characteristics of High Speed Aircraft", AAF Tech. Rept. 5632, September 10, 1947.

20. Johnson, H. A., Rubesin, M. W., Sauer, F. M., Slack, E. G., Possner, L., Bibliography of Aerodynamic Heating and Related Subjects". AAF Tech. Rept. 5633, September 10, 1947.

21. Boelter, L. M. K., Cherry, V. H., Johnson, H. A., Martinelli, R. C., Heat Transfer Notes, University of California Press, 1948. Chapt. XVI.

22. Langmuir, I., "The Cooling of Cylinders by Fog Moving at High Velocities". Research Laboratory Report, General Electric Company, March 1945.

CHAPTER V

THE ENERGY TRANSFERS AT AN ICING SURFACE

(The Complete Energy Balance and Some Applications)

Messinger[1] has distinguished the three important regimes of heating, as follows:

$$\begin{array}{lll} A & t_s > 32°F \\ B & t_s = 32°F \\ C & t_s < 32°F. \end{array}$$

In the treatment which follows we shall follow the notation used by Messinger and consider each regime separately.

A. Surface Above 32°F

The heat-balance equation is

$$q = q_{convection} + q_{evaporation} + q_{sensible} - q_{friction} - q_{kinetic}$$

or, from Chapter IV,

$$q/A = h_c (t_s - T_\infty) \quad 2.9L/B (P_s - P_\infty) + R_w (t_s - T_\infty) - h_c r \frac{U_\infty^2}{2gJC_{pa}} - R_w \frac{U_\infty^2}{2g J} .$$

The above equation is awkward to handle, hence certain new groupings of the above variables are made which simplify (but do not clarify) calculations.

A parameter b is defined

$$b = \frac{R_w \, C_{p_w}}{h_c}$$

and the three functions

$$\theta_1'' = t_s \, (1 + b) + \frac{2.9L}{B} \, P_s$$

$$\theta_2'' = \mathcal{T}_\infty \, (1 + b) + \frac{2.9L}{B} \, P_\infty$$

$$\theta_3 = (r/C_{p_a} + b) \, (U_\infty^2/2gJ),$$

where

t_s = surface temperature, °F
$\mathcal{T}_\infty$ = air temperature, °F
L = heat of vaporization of water, BTU/lb
P_s = saturation pressure of water at t_s, "H_g
P_∞ = saturation pressure of water at $\mathcal{T}_\infty$, "H_g
B = barometric pressure, "H_g
r = "recovery factor"
U_∞ = free stream velocity ft/sec.

The heat flux equation is

$$(q/A) = h_c \, (\theta_1'' - \theta_2'' - \theta_3) \quad .$$

Note that θ_1'' depends primarily upon t_s, θ_2'' upon $\mathcal{T}_\infty$ and θ_3 upon U_∞, with b as a parameter. Graphs of these functions are given in Figures V-1, V-2, and V-3. (The above equation is restricted to the case where t_s is uniform and above 32°F.)

Hardy[2] has suggested a different grouping of these variables

$$q = q_{convection} \left(1 + \frac{q_{evaporation}}{q_{convection}}\right) - q_{friction} + q_{sensible}$$

The ratio $(q_{evaporation}/q_{convection})$ is given the symbol X. From Chapter IV,

$$X = \frac{0.62L}{B \, C_{p_a}} \left[\frac{P_s - P_\infty}{t_s - \mathcal{T}_\infty}\right].$$

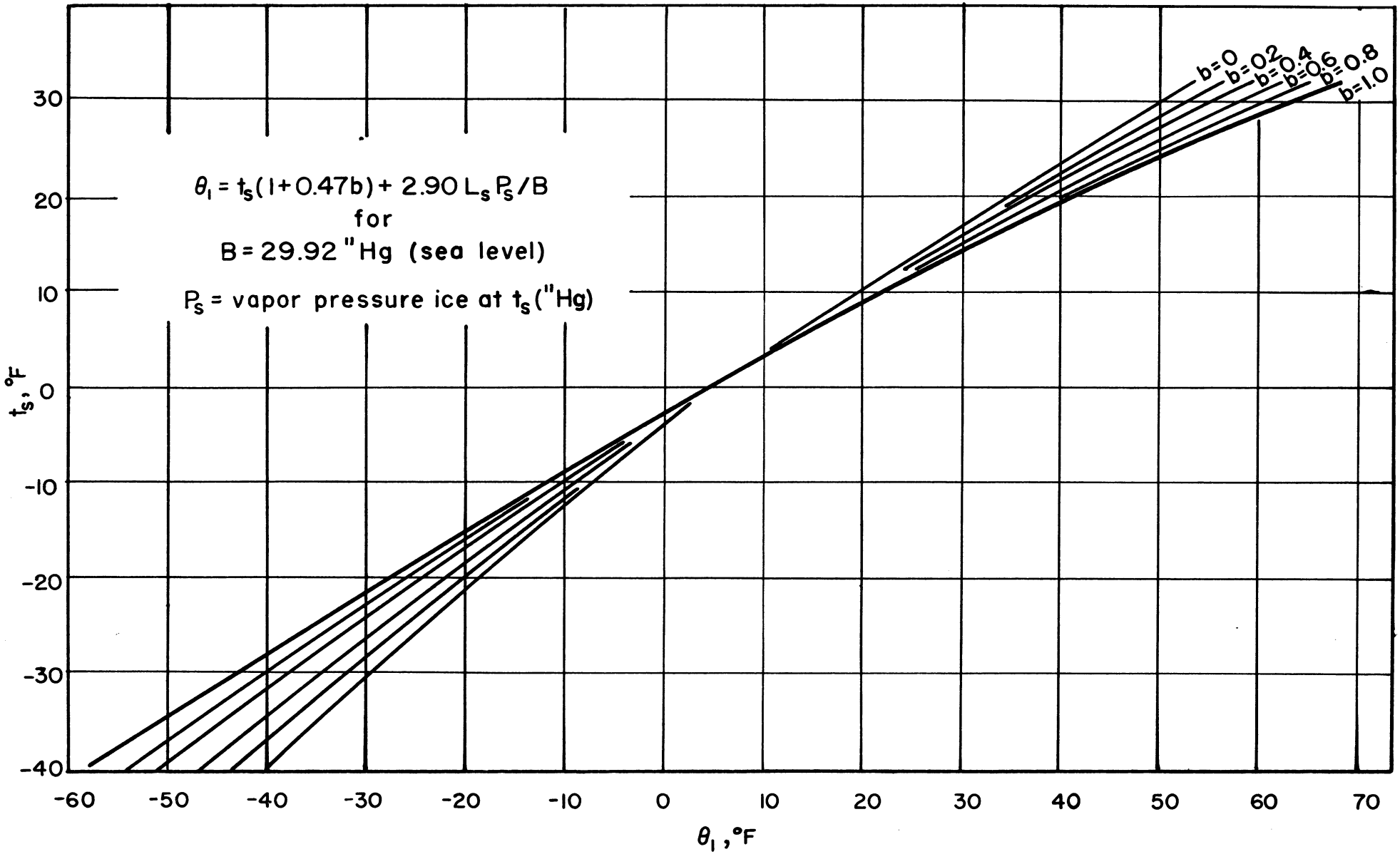
$\theta_1 = t_s(1+0.47b) + 2.90\, L_s P_s / B$
for
B = 29.92 "Hg (sea level)
P_s = vapor pressure ice at t_s ("Hg)
b=0
b=0.2
b=0.4
b=0.6
b=0.8
b=1.0
t_s, °F
θ_1, °F
30
20
10
0
-10
-20
-30
-40
-60
-50
-40
-30
-20
-10
0
10
20
30
40
50
60
70

Figure V-1a

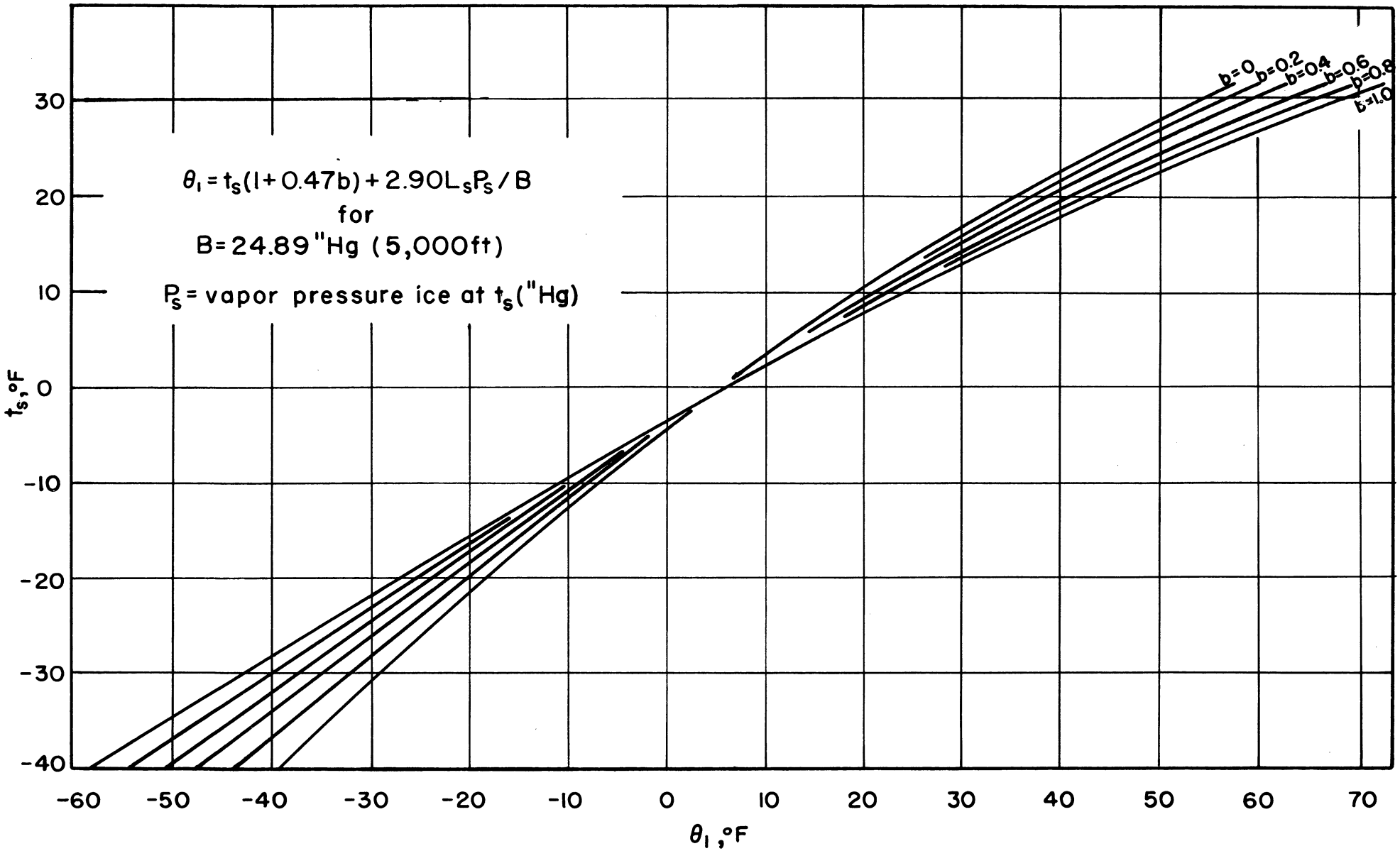
$\theta_1 = t_s(1+0.47b) + 2.90L_sP_s/B$
for
B=24.89"Hg (5,000ft)
P_s = vapor pressure ice at t_s("Hg)
b=0
b=0.2
b=0.4
b=0.6
b=0.8
b=1.0
t_s, °F
θ_1, °F
30
20
10
0
-10
-20
-30
-40
-60
-50
-40
-30
-20
-10
0
10
20
30
40
50
60
70

Figure V-1b

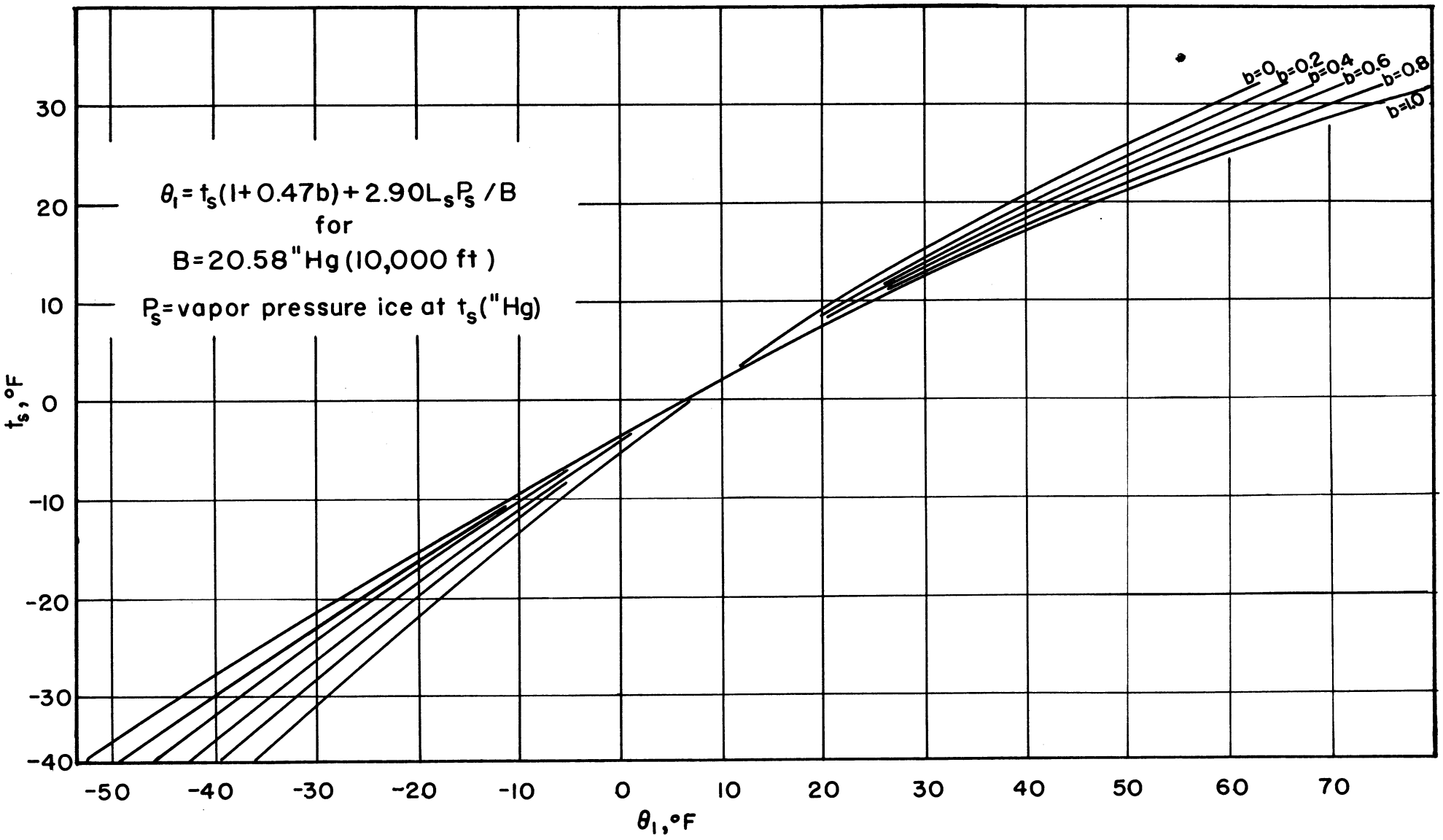
$\theta_1 = t_s(1+0.47b) + 2.90 L_s P_s / B$
for
B=20.58"Hg (10,000 ft)
P_s=vapor pressure ice at t_s("Hg)
b=0
b=0.2
b=0.4
b=0.6
b=0.8
b=1.0
t_s, °F
θ_1, °F
30
20
10
0
-10
-20
-30
-40
-50
-40
-30
-20
-10
0
10
20
30
40
50
60
70

Figure V-1c

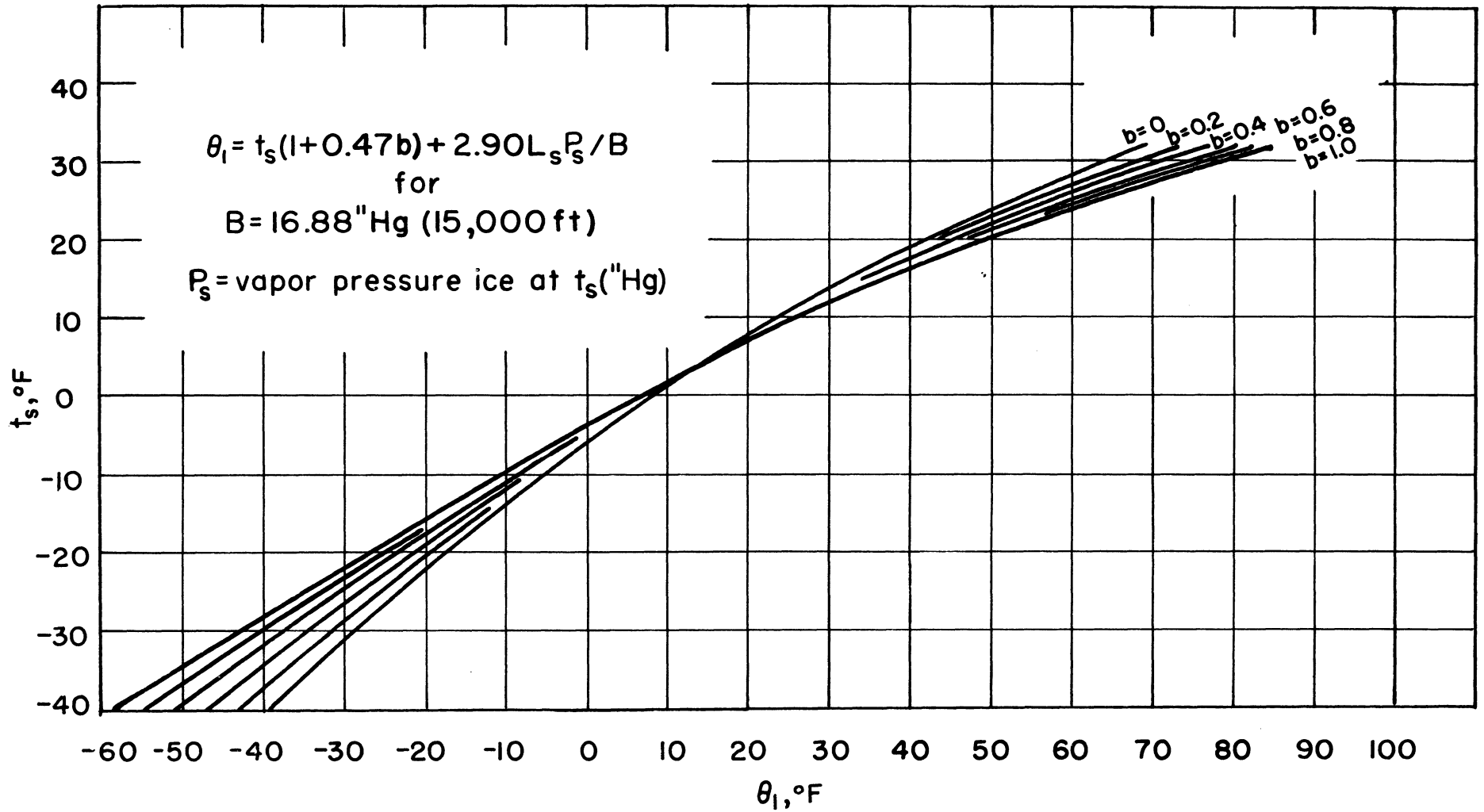
$\theta_1 = t_s(1+0.47b) + 2.90 L_s P_s/B$
for
B = 16.88"Hg (15,000 ft)
P_s = vapor pressure ice at t_s("Hg)
b=0
b=0.2
b=0.4
b=0.6
b=0.8
b=1.0
t_s, °F
40
30
20
10
0
-10
-20
-30
-40
-60 -50 -40 -30 -20 -10 0 10 20 30 40 50 60 70 80 90 100
θ_1, °F

Figure V-1d

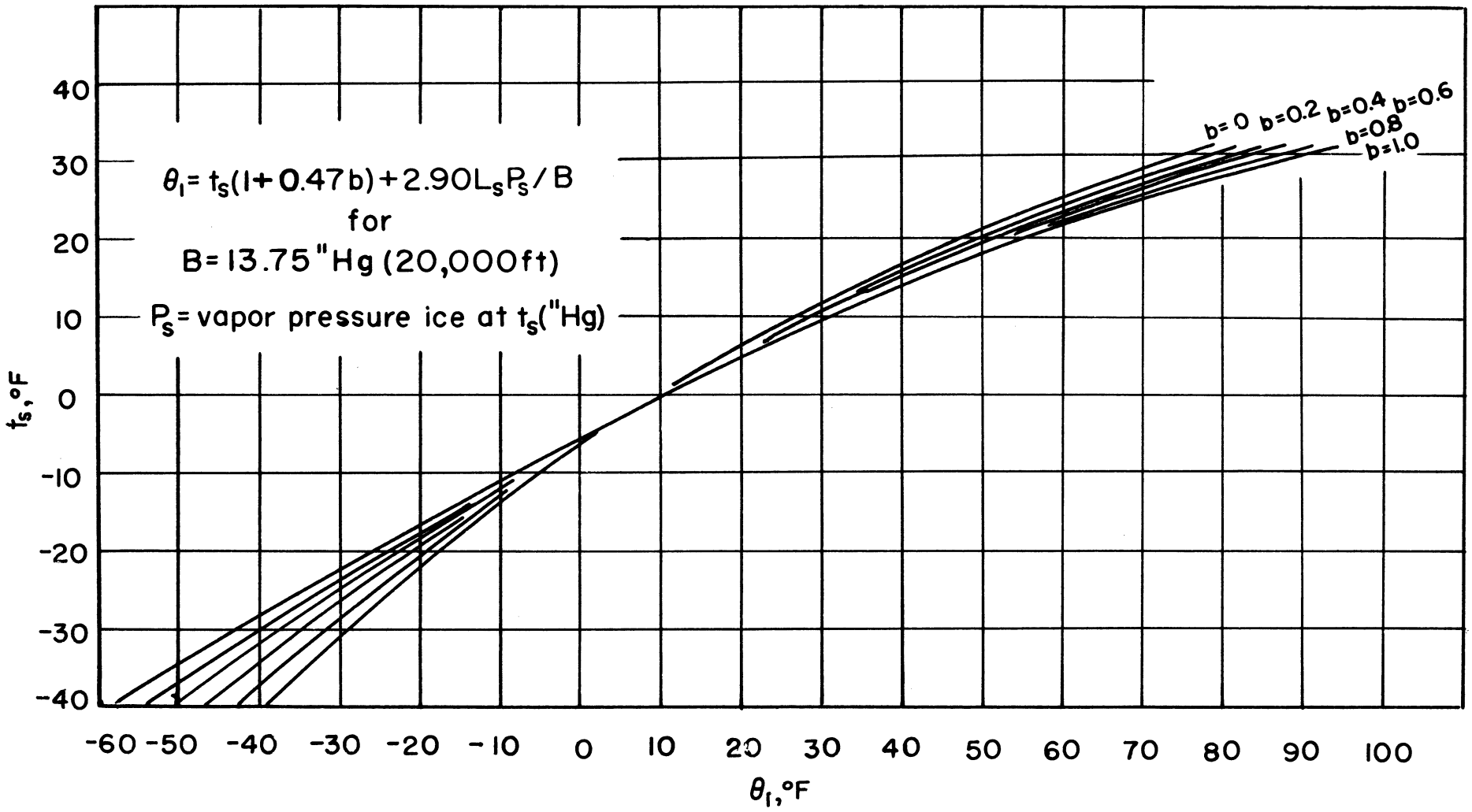
$\theta_1 = t_s(1+0.47b)+2.90L_sP_s/B$
for
B = 13.75 "Hg (20,000ft)
P_s = vapor pressure ice at t_s ("Hg)
b= 0
b=0.2
b=0.4
b=0.6
b=0.8
b=1.0
t_s, °F
θ_1, °F
40
30
20
10
0
-10
-20
-30
-40
-60 -50 -40 -30 -20 -10 0 10 20 30 40 50 60 70 80 90 100

Figure V-1e

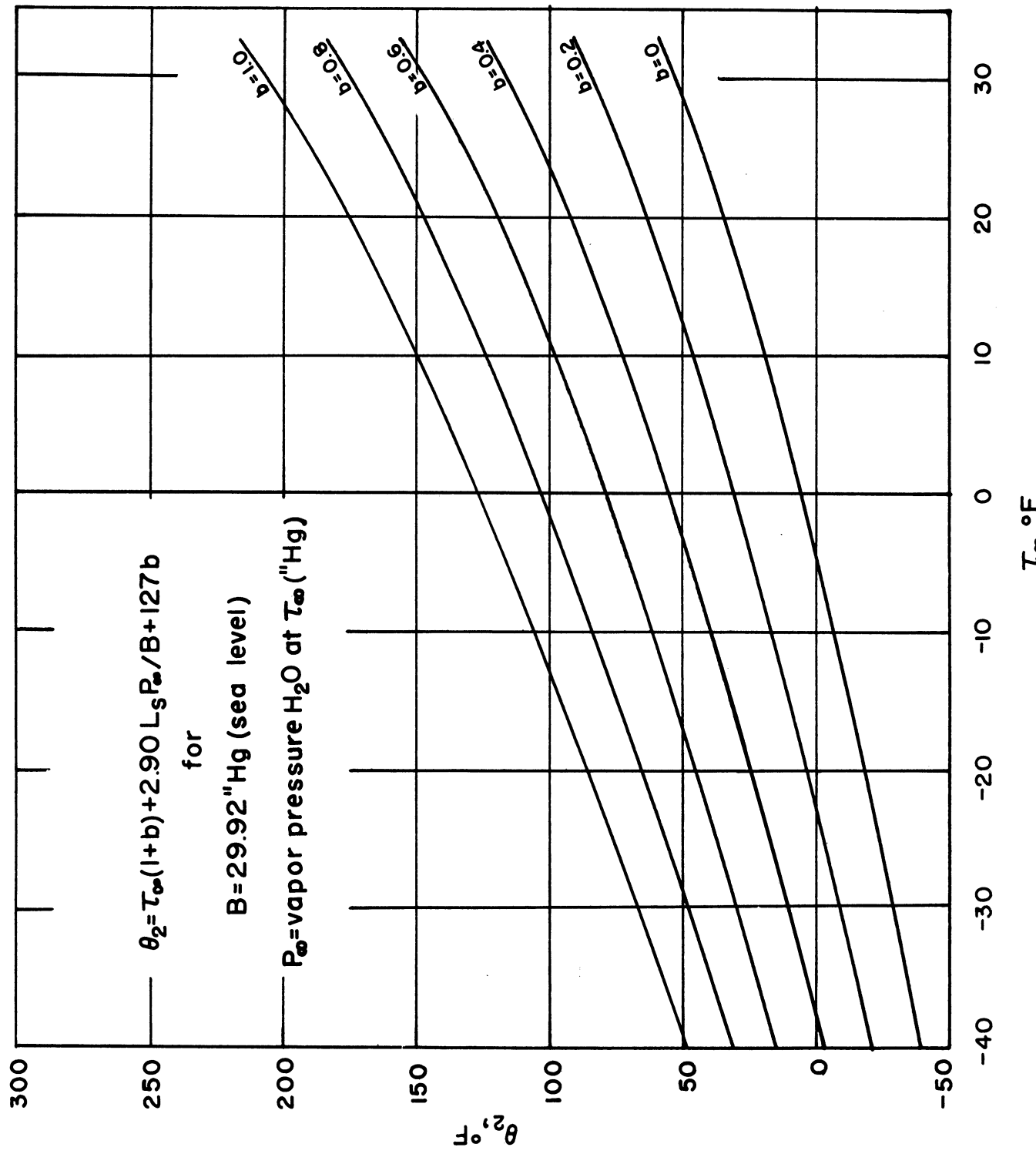
$\theta_2 = T_\infty(1+b) + 2.90\, L_s P_\infty / B + 127b$
for
B=29.92"Hg (sea level)
P_∞=vapor pressure H_2O at T_∞("Hg)
b=0
b=0.2
b=0.4
b=0.6
b=0.8
b=1.0
θ_2,°F
300
250
200
150
100
50
0
-50
T_∞,°F
-40
-30
-20
-10
0
10
20
30

Figure V-2a

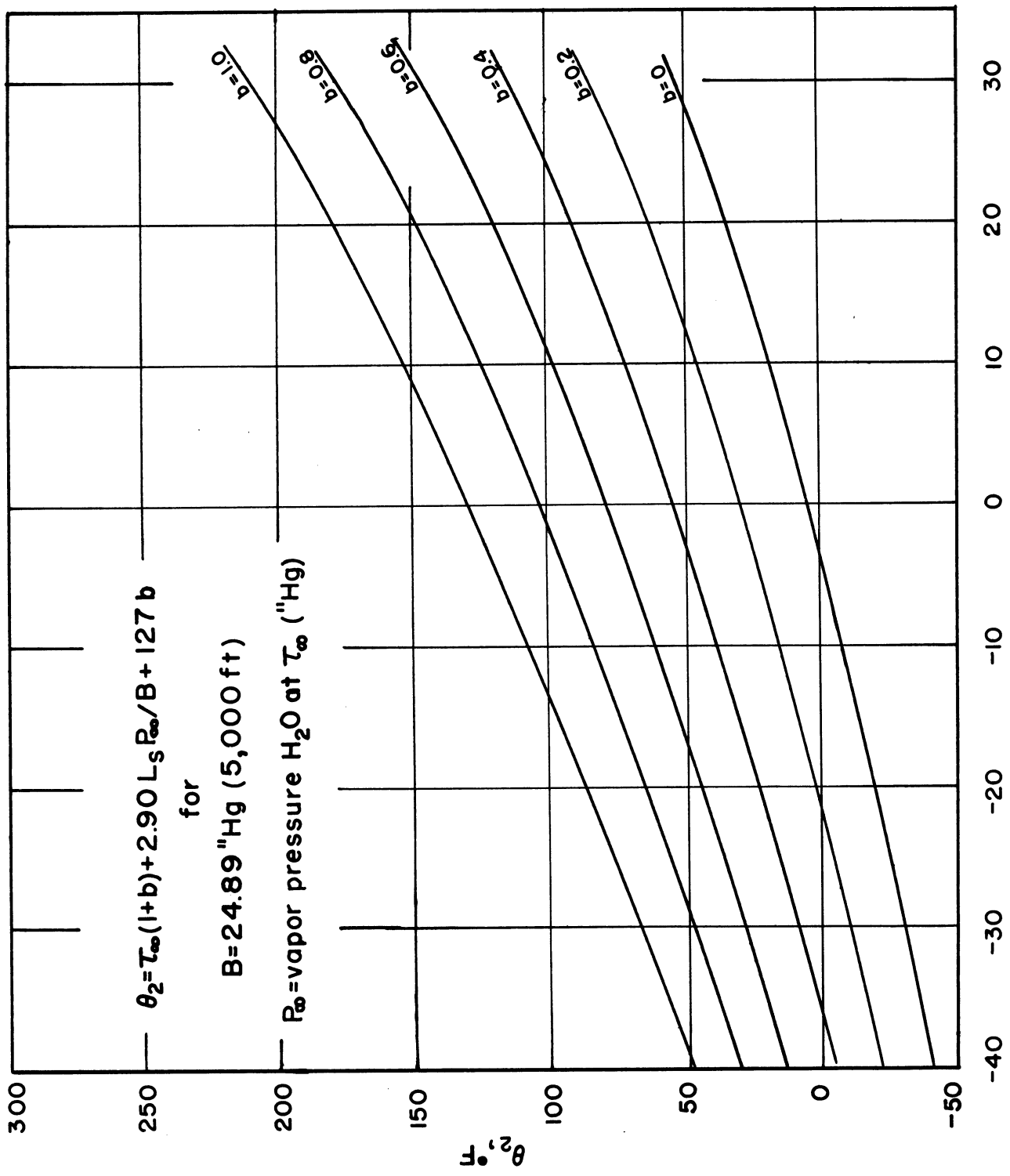
$\theta_2 = T_\infty(1+b) + 2.90\, L_s P_\infty / B + 127\, b$
for
B=24.89 "Hg (5,000 ft)
P_∞ = vapor pressure H_2O at T_∞ ("Hg)
b=0.1
b=0.8
b=0.6
b=0.4
b=0.2
b=0
θ_2, °F
T_∞, °F
300
250
200
150
100
50
0
-50
-40
-30
-20
-10
0
10
20
30

Figure V-2b

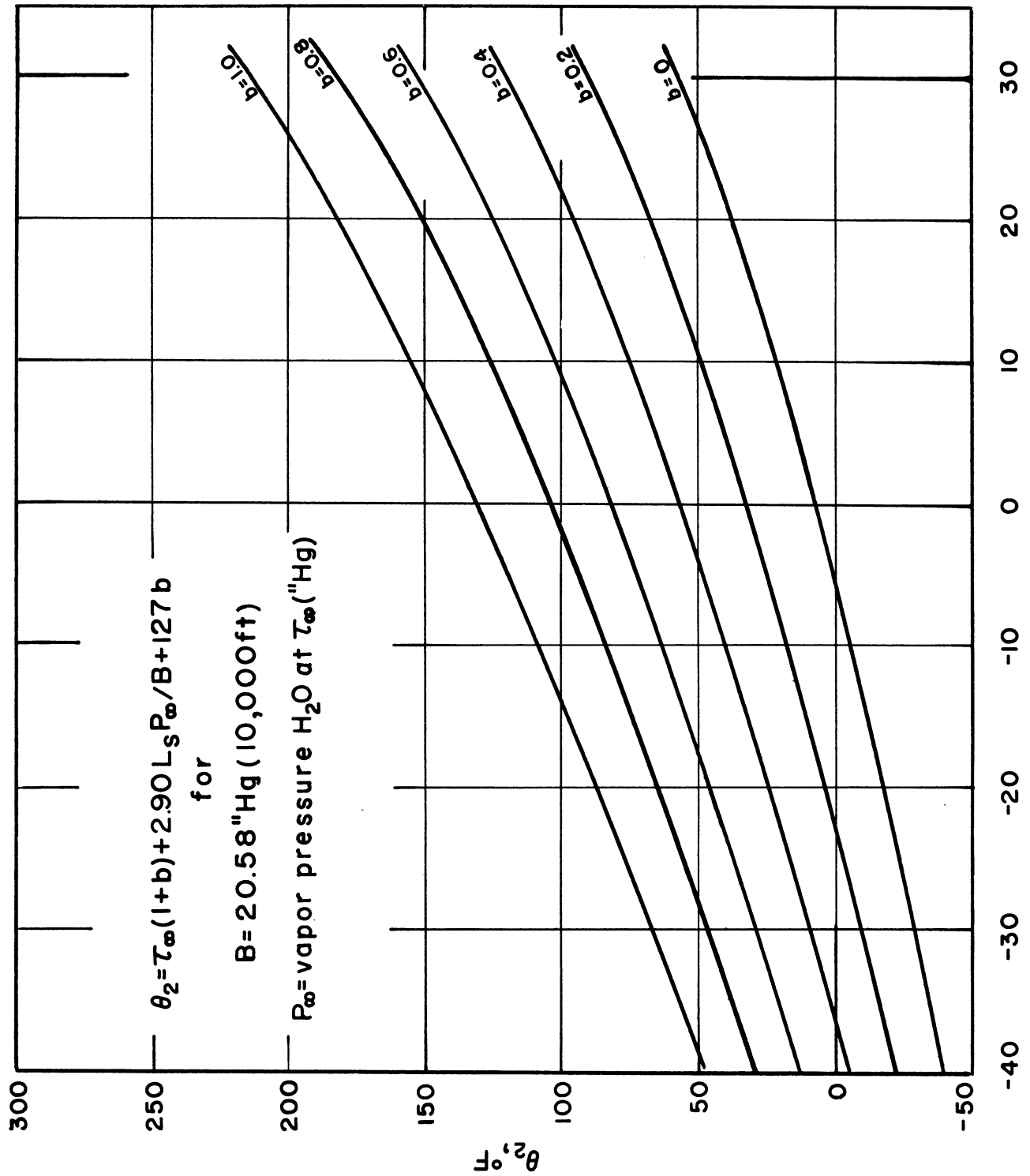
$\theta_2 = T_\infty(1+b) + 2.90 L_s P_\infty / B + 127\, b$
for
B = 20.58" Hg (10,000 ft)
P_∞ = vapor pressure H_2O at T_∞ ("Hg)
b=1.0
b=0.8
b=0.6
b=0.4
b=0.2
b=0
θ_2, °F
T_∞, °F
300
250
200
150
100
50
0
-50
30
20
10
0
-10
-20
-30
-40

Figure V-2c

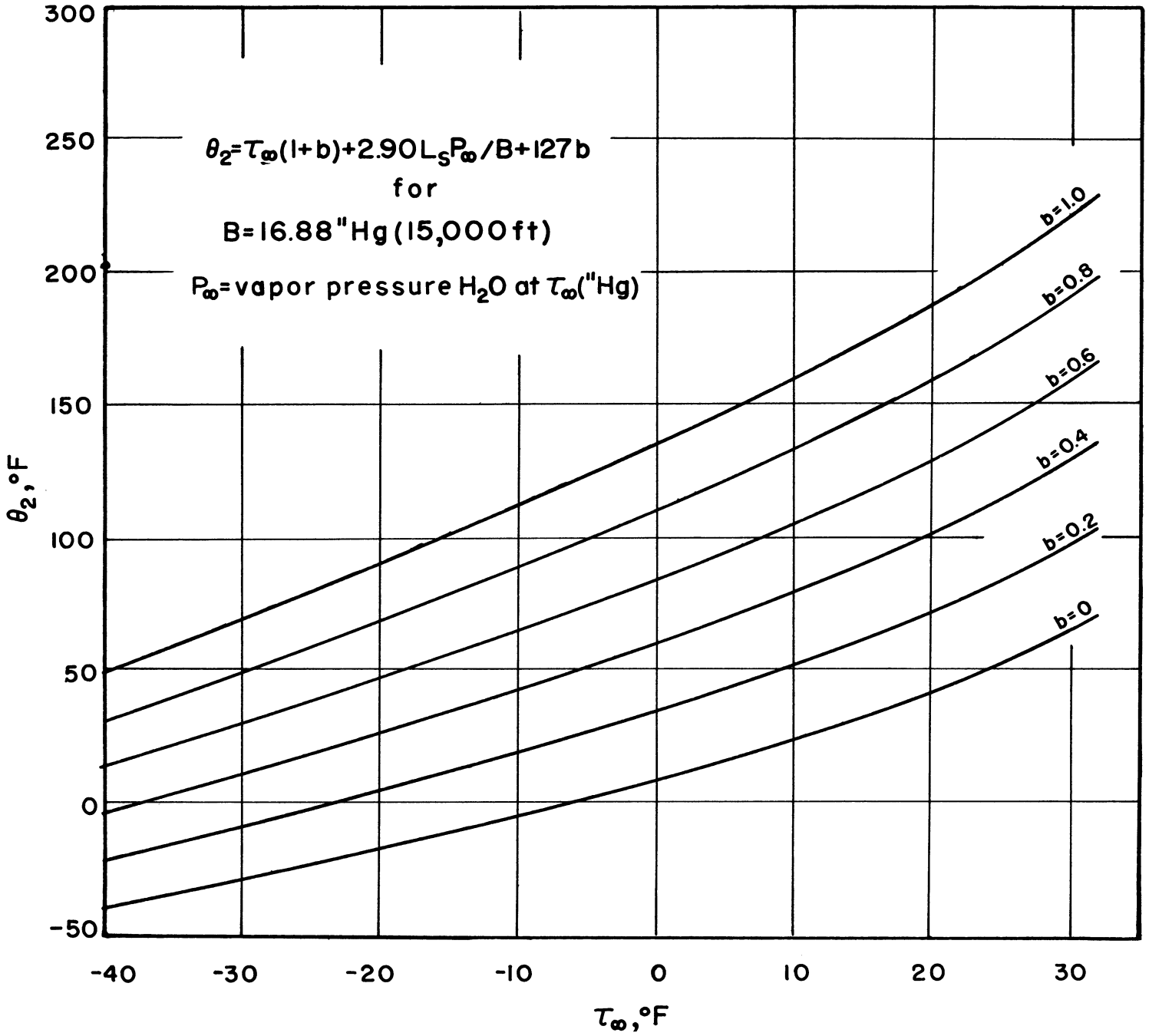
$\theta_2=\tau_\infty(1+b)+2.90L_sP_\infty/B+127b$
for
B=16.88"Hg (15,000 ft)
P_∞=vapor pressure H_2O at τ_∞("Hg)
b=1.0
b=0.8
b=0.6
b=0.4
b=0.2
b=0
300
250
200
150
100
50
0
-50
θ_2, °F
-40
-30
-20
-10
0
10
20
30
τ_∞, °F

Figure V-2d

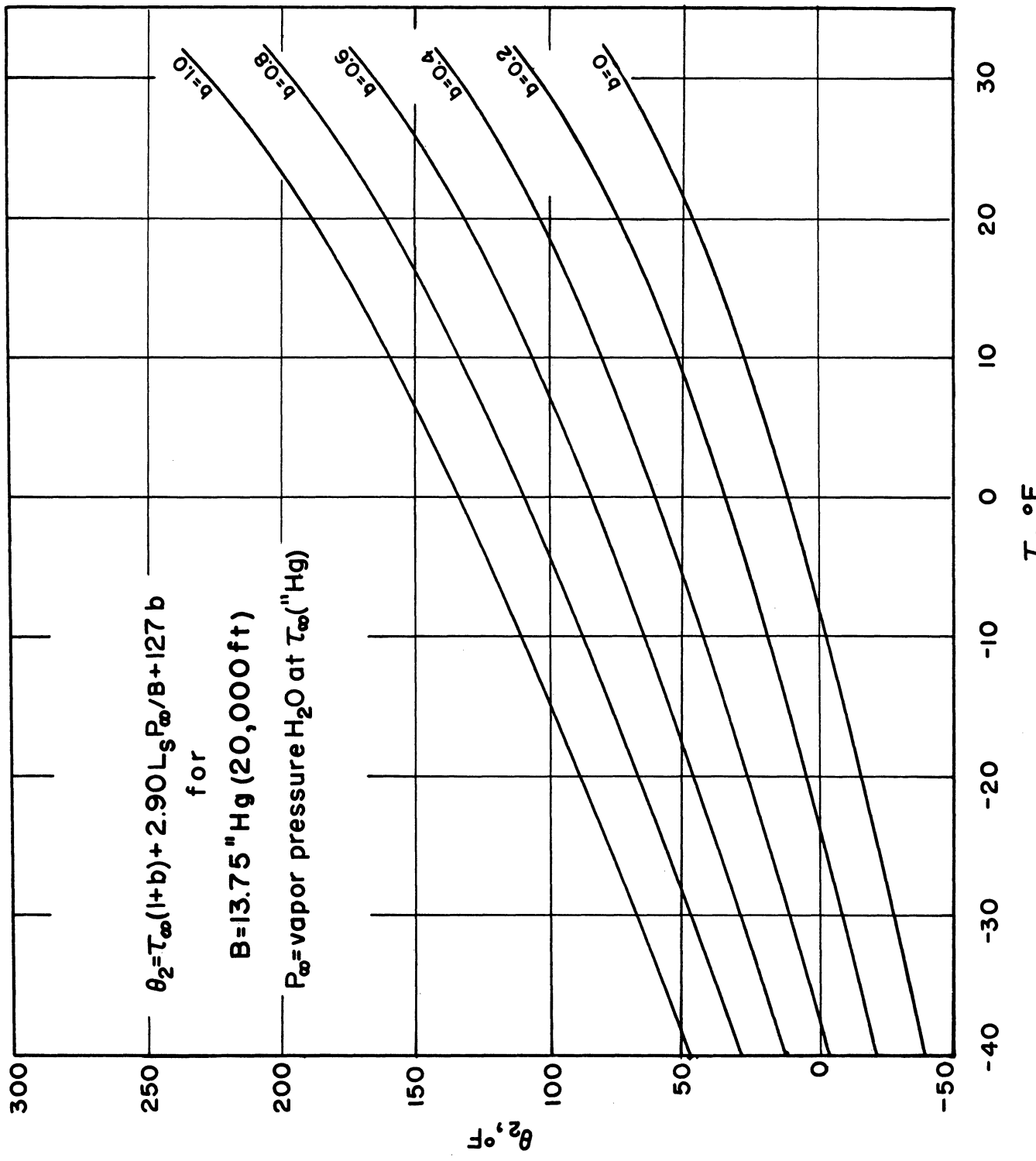
$\theta_2 = T_\infty(1+b) + 2.90 L_s P_\infty / B + 127\,b$
for
B=13.75" Hg (20,000 ft)
P_∞ = vapor pressure H_2O at T_∞ ("Hg)
b=0
b=0.2
b=0.4
b=0.6
b=0.8
b=1.0
θ_2, °F
T_∞, °F
300
250
200
150
100
50
0
-50
-40
-30
-20
-10
0
10
20
30

Figure V-2e

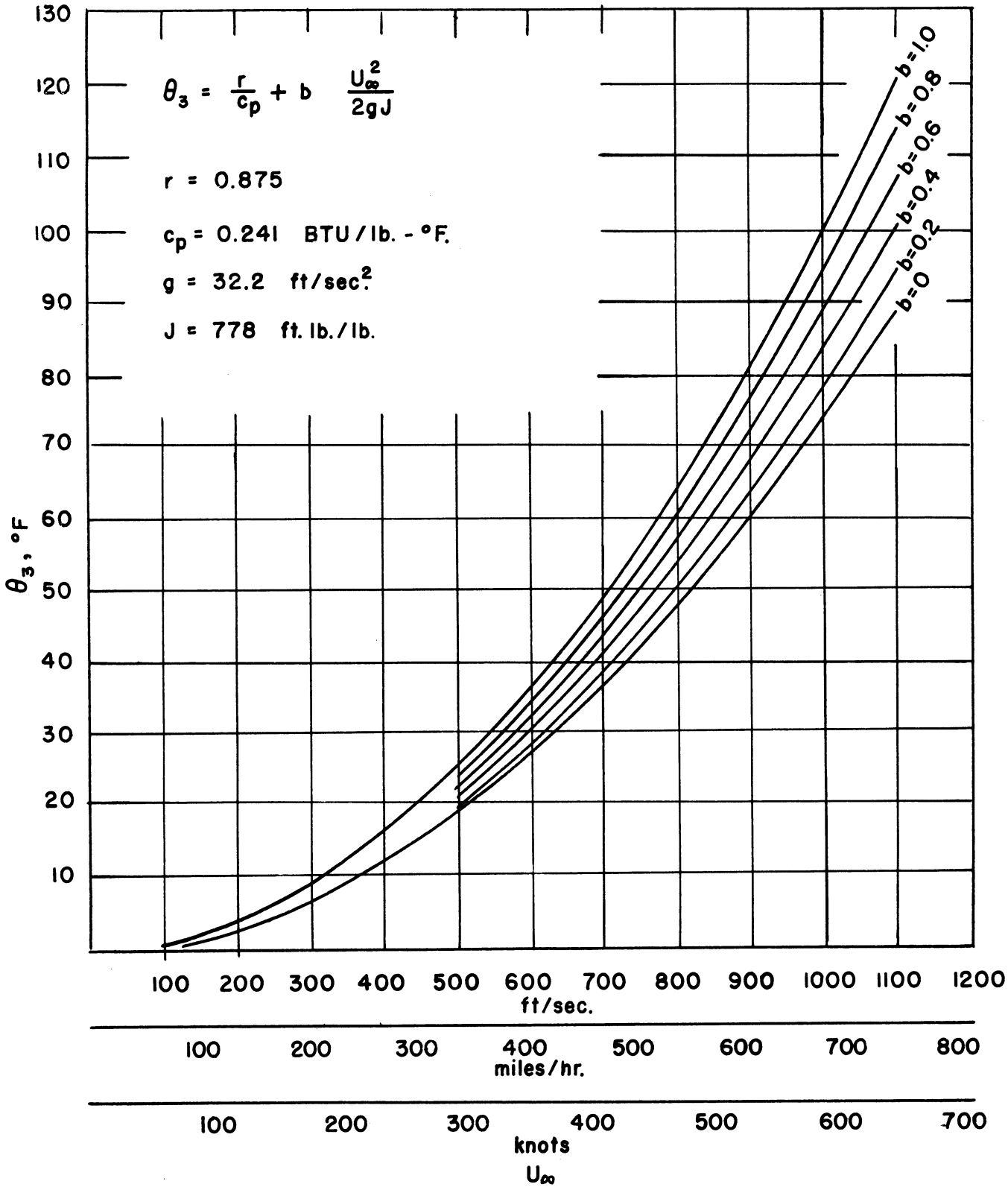
$\theta_3 = \frac{r}{c_p} + b \frac{U_\infty^2}{2gJ}$
r = 0.875
c_p = 0.241 BTU / lb. - °F.
g = 32.2 ft/sec.²
J = 778 ft. lb. / lb.
b=1.0
b=0.8
b=0.6
b=0.4
b=0.2
b=0
θ_3, °F
130
120
110
100
90
80
70
60
50
40
30
20
10
100 200 300 400 500 600 700 800 900 1000 1100 1200
ft/sec.
100 200 300 400 500 600 700 800
miles/hr.
100 200 300 400 500 600 700
knots
U_∞

Figure V-3

At low speeds (such as takeoff or landing approach) and neglecting sensible heating, the heat-flux equation is simply

$$(q/A) = h_c\ (t_s - T_\infty)\ (1 + X).$$

The term (1 + X) is thus a multiplier which shows how much greater the heat loss in wet air is as compared to dry air (if h_c is unchanged).

Tables of X are presented in Reference 3.

The term X/(1 + X) represents the heat loss which is actually used to evaporate water. Since X increases with temperature, it follows that a thermally efficient heated anti-icer has a high surface temperature.

B. Surface Below 32°F

The heat balance when $t_s < 32°F$ is:

$$q = q_{convection} + q_{sublimation} + q_{sensible} - q_{fusion} - q_{friction} - q_{kinetic}$$

From Chapter IV,

$$(q/A) = h_c\ (t_s - T_\infty) + \frac{2.9 L_s\ h_c\ (P_s - P_\infty)}{B} + R_w\ (t_s - T_\infty)$$

$$- R_w \left[144 - (32 - t_s)\ (C_{p_w} - C_{pi})\right] - h_c\ r\ \frac{U_\infty^2}{2gJC_{pa}} - R_w\ \frac{U_\infty^2}{2gJ}\ .$$

Again, define the Θ functions

$$\Theta_1 = t_s\ (1 + 0.47b) + 2.90 L_s\ P_s/B$$

$$\Theta_2 = T_\infty\ (1 + b) + 2.90 L_s\ P_\infty/B + 127b,$$

where

t_s = surface temperature, °F
T_∞ = air temperature, °F
L_s = heat of sublimation of ice, BTU/lb
P_s = vapor pressure of ice at t_s, "H_g
P_∞ = vapor pressure of supercooled water at T_∞ "H_g
B = barometric pressure, "H_g.

The heat flux equation is therefore

$$q/A = h_c\ (\Theta_1 - \Theta_2 - \Theta_3)$$

Graphs of θ_1 and θ_2 are given in Figures V-4 and V-5.

C. Surface at 32°F

When t_s = 32°F, there is present a two-phase system of ice and water, and an additional parameter is required to describe the nature of the surface conditions. Messinger[1] introduced the "freezing fraction", n. When n = 1, all the water is frozen and the surface runs dry. When n = 0, no ice is formed. For $0 < n < 1$, the surface is coated with ice and water.

The energy balance is written

$$q = q_{convection} + q_{evaporation} + q_{sensible} - q_{fusion} - q_{friction} - q_{kinetic},$$

or

$$(q/A) = h_c (32 - \mathcal{T}_\infty) + \frac{2.9L\ h_c}{B} (0.180 - P_\infty) + R_w (32 - \mathcal{T}_\infty) - n R_w 144 - h_c r \frac{U_\infty^2}{2gJ C_{p_a}} - R_w \frac{U_\infty^2}{2g J}$$

Define now the θ' functions

$$\theta_1' = 32 (1 + b) + \frac{2.9L P_s}{B}$$

$$\theta_2' = \mathcal{T}_\infty (1 + b) + \frac{2.9L P_\infty}{B} + 144 n b,$$

where

$\mathcal{T}_\infty$ = free stream temperature, °F
L = heat of vaporization of water at 32°F
P_s = vapor pressure of water at 32°F, "H_g
P_∞ = vapor pressure of water at 32°F, "H_g
B = barometric pressure, "H_g.

The heat flux is thus

$$(q/A) = h_c (\theta_1' - \theta_2' - \theta_3).$$

The θ_1' and θ_2' functions are presented in Figures V-6 and V-7. Figures V-1 through V-7 follow the scheme of Reference 1 but are for all altitudes of interest.

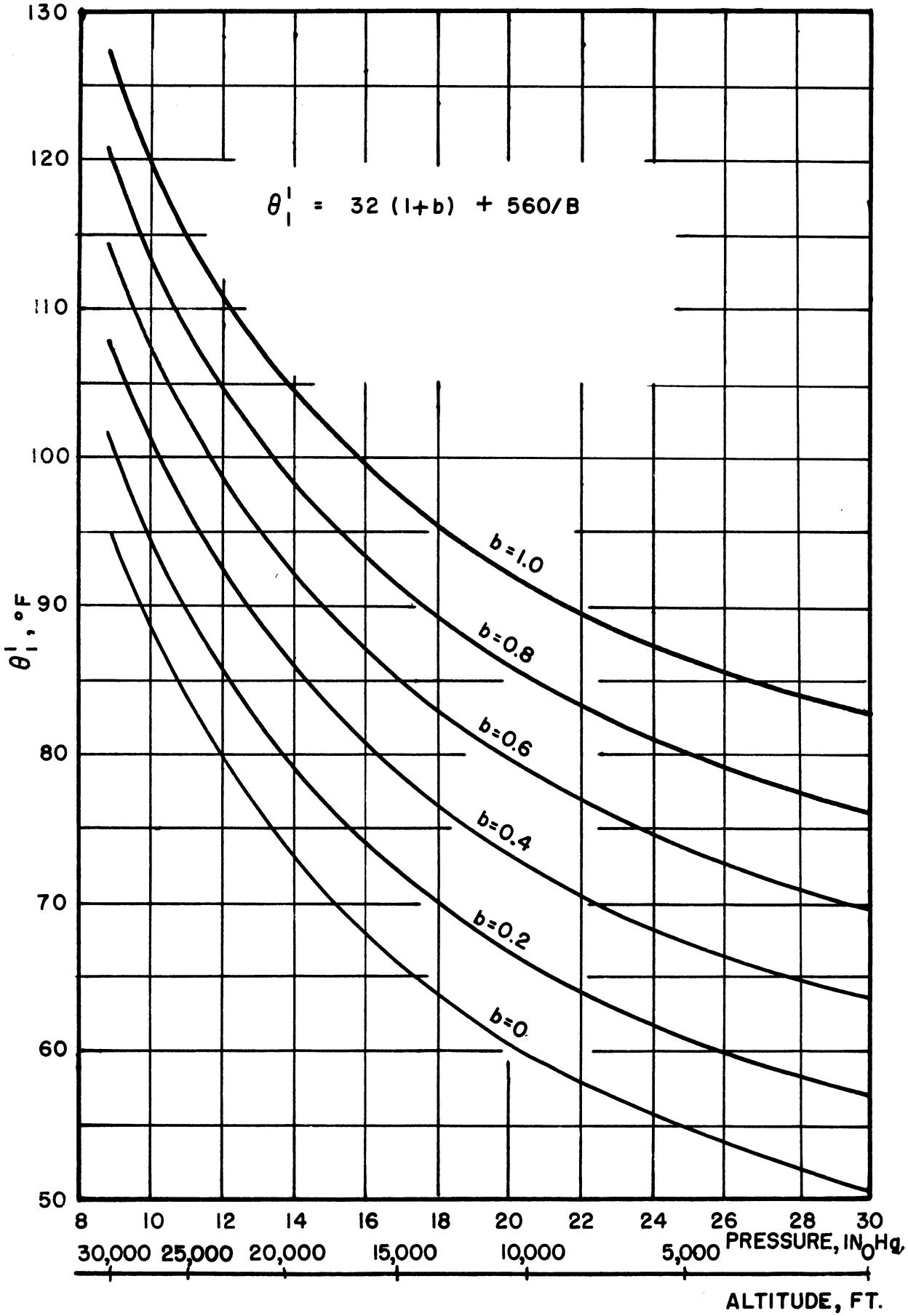
$\theta_1^1 = 32\,(1+b) + 560/B$
b=1.0
b=0.8
b=0.6
b=0.4
b=0.2
b=0
θ_1^1, °F
130
120
110
100
90
80
70
60
50
8
10
12
14
16
18
20
22
24
26
28
30
PRESSURE, IN. Hg.
30,000
25,000
20,000
15,000
10,000
5,000
ALTITUDE, FT.

Figure V-4

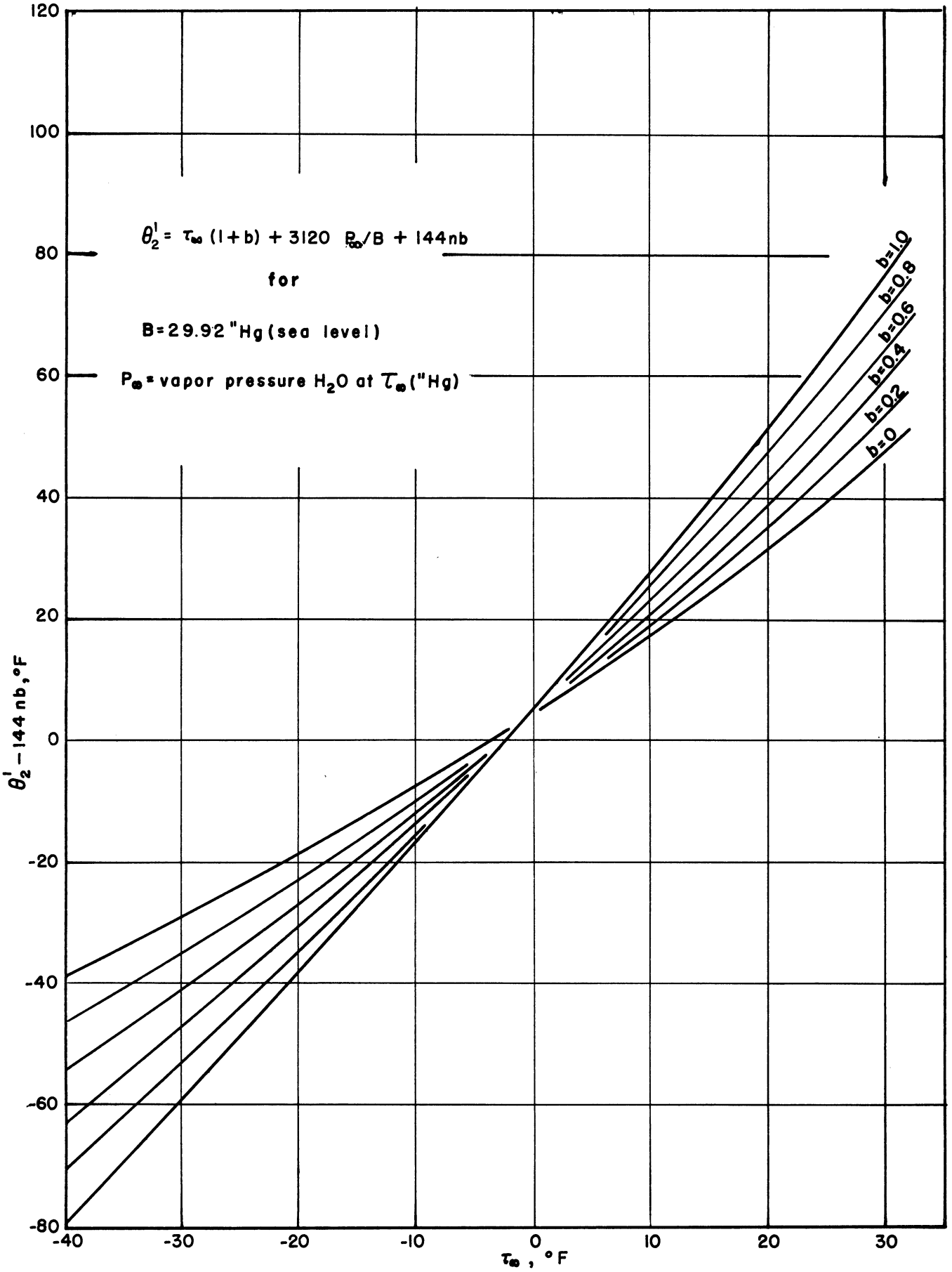
$\theta_2' = \tau_\infty (1+b) + 3120\ P_\infty/B + 144nb$
for
B = 29.92 "Hg (sea level)
P_∞ = vapor pressure H_2O at τ_∞ ("Hg)
b=1.0
b=0.8
b=0.6
b=0.4
b=0.2
b=0
$\theta_2' - 144\,nb$, °F
τ_∞, °F
120
100
80
60
40
20
0
-20
-40
-60
-80
-40
-30
-20
-10
0
10
20
30

Figure V-5a

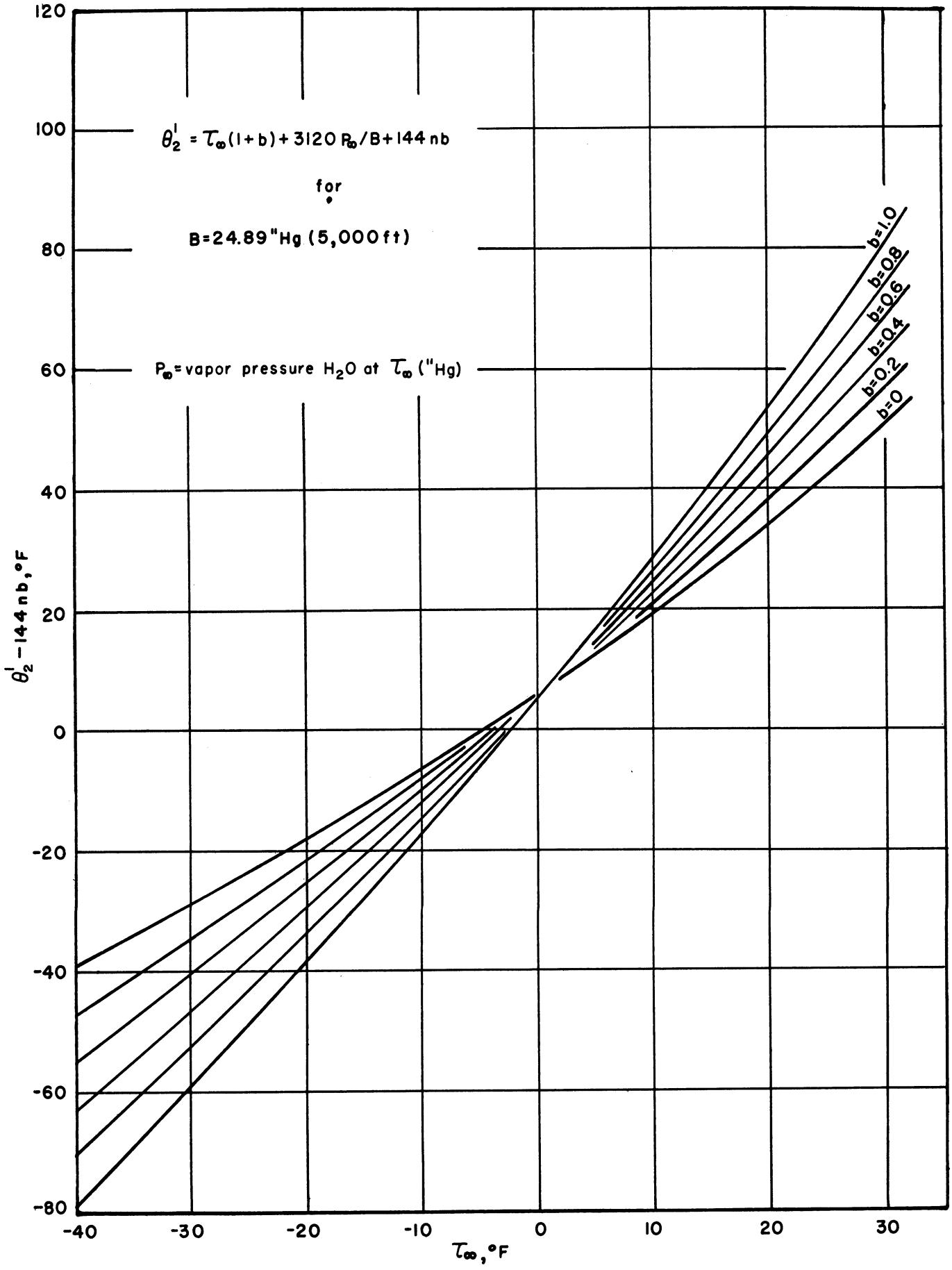
$\theta_2' = \tau_\infty(1+b) + 3120\, P_\infty/B + 144\, nb$
for
B=24.89"Hg (5,000 ft)
P_∞=vapor pressure H_2O at τ_∞ ("Hg)
b=1.0
b=0.8
b=0.6
b=0.4
b=0.2
b=0
$\theta_2' - 144\, nb$, °F
τ_∞, °F
120
100
80
60
40
20
0
-20
-40
-60
-80
-40
-30
-20
-10
0
10
20
30

Figure V-5b

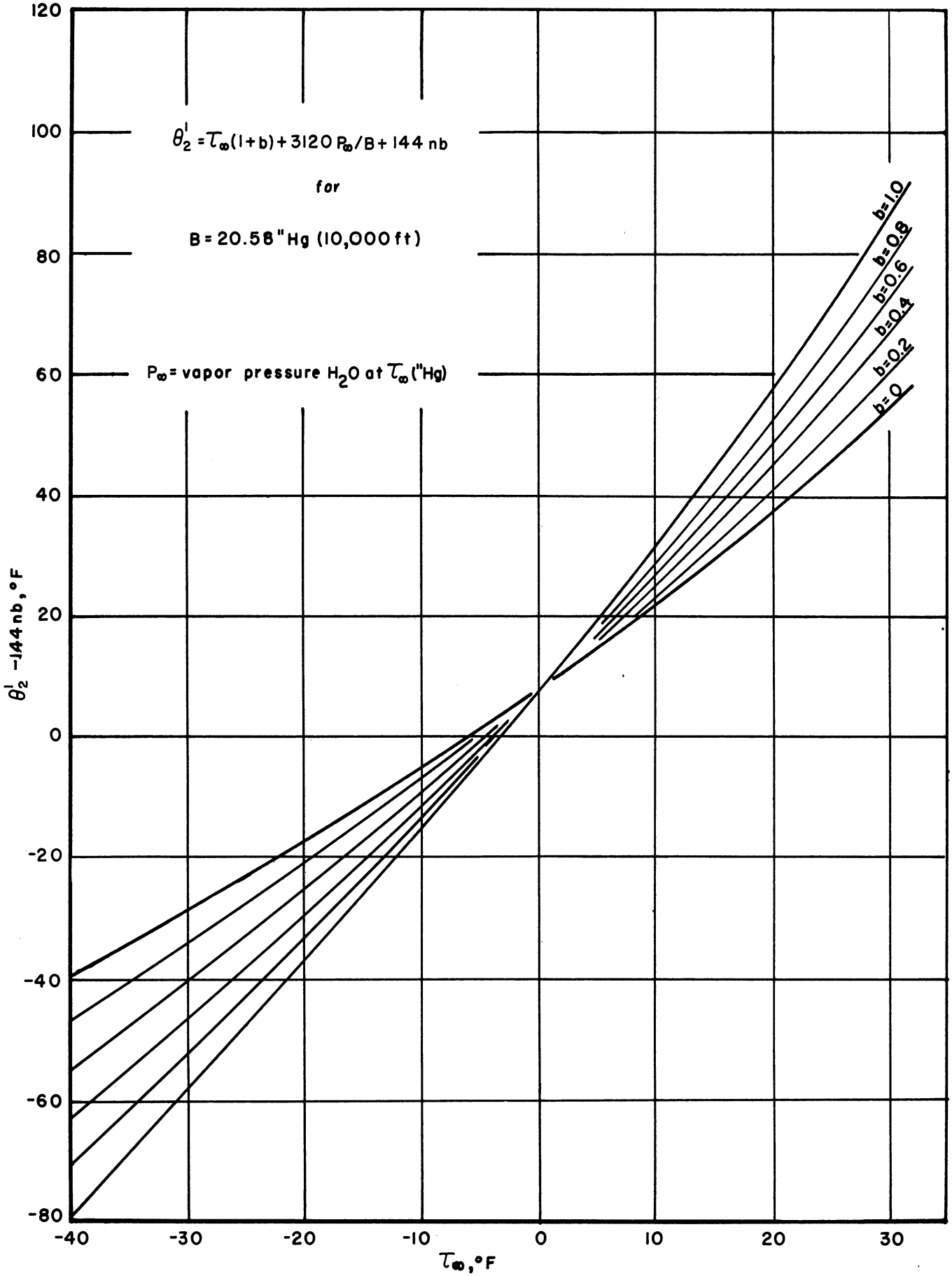
$\theta_2' = \tau_\infty(1+b) + 3120\,P_\infty/B + 144\,nb$
for
B = 20.58 "Hg (10,000 ft)
P_∞ = vapor pressure H_2O at τ_∞ ("Hg)
b=1.0
b=0.8
b=0.6
b=0.4
b=0.2
b=0
$\theta_2' - 144\,nb$, °F
τ_∞, °F
120
100
80
60
40
20
0
-20
-40
-60
-80
-40
-30
-20
-10
0
10
20
30

Figure V-5c

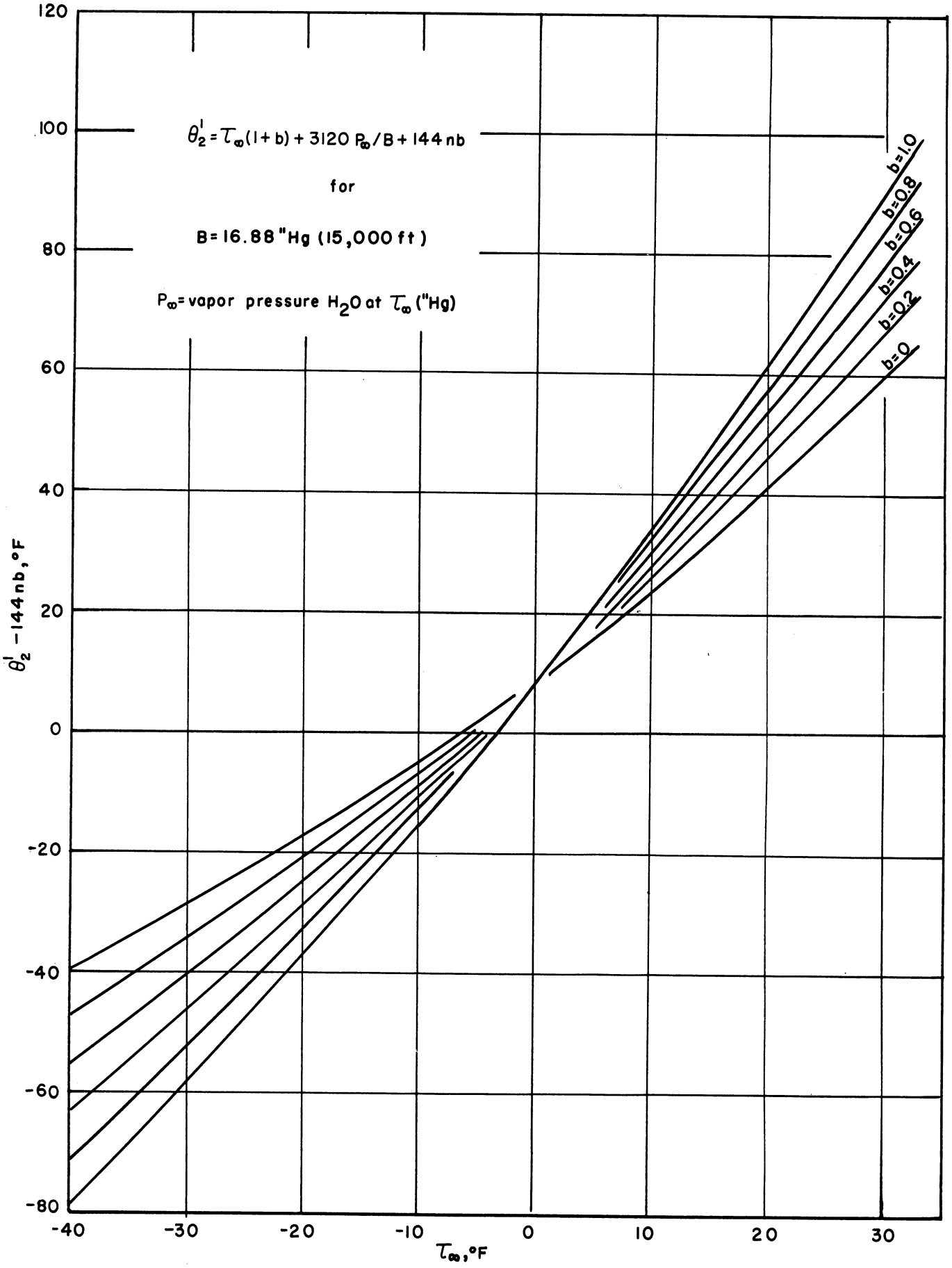
$\theta_2' = T_\infty(1+b) + 3120\, P_\infty/B + 144\, nb$
for
B = 16.88 "Hg (15,000 ft)
P_∞ = vapor pressure H_2O at T_∞ ("Hg)
b=1.0
b=0.8
b=0.6
b=0.4
b=0.2
b=0
$\theta_2' - 144\, nb$, °F
T_∞, °F
120
100
80
60
40
20
0
-20
-40
-60
-80
-40
-30
-20
-10
0
10
20
30

Figure V-5d

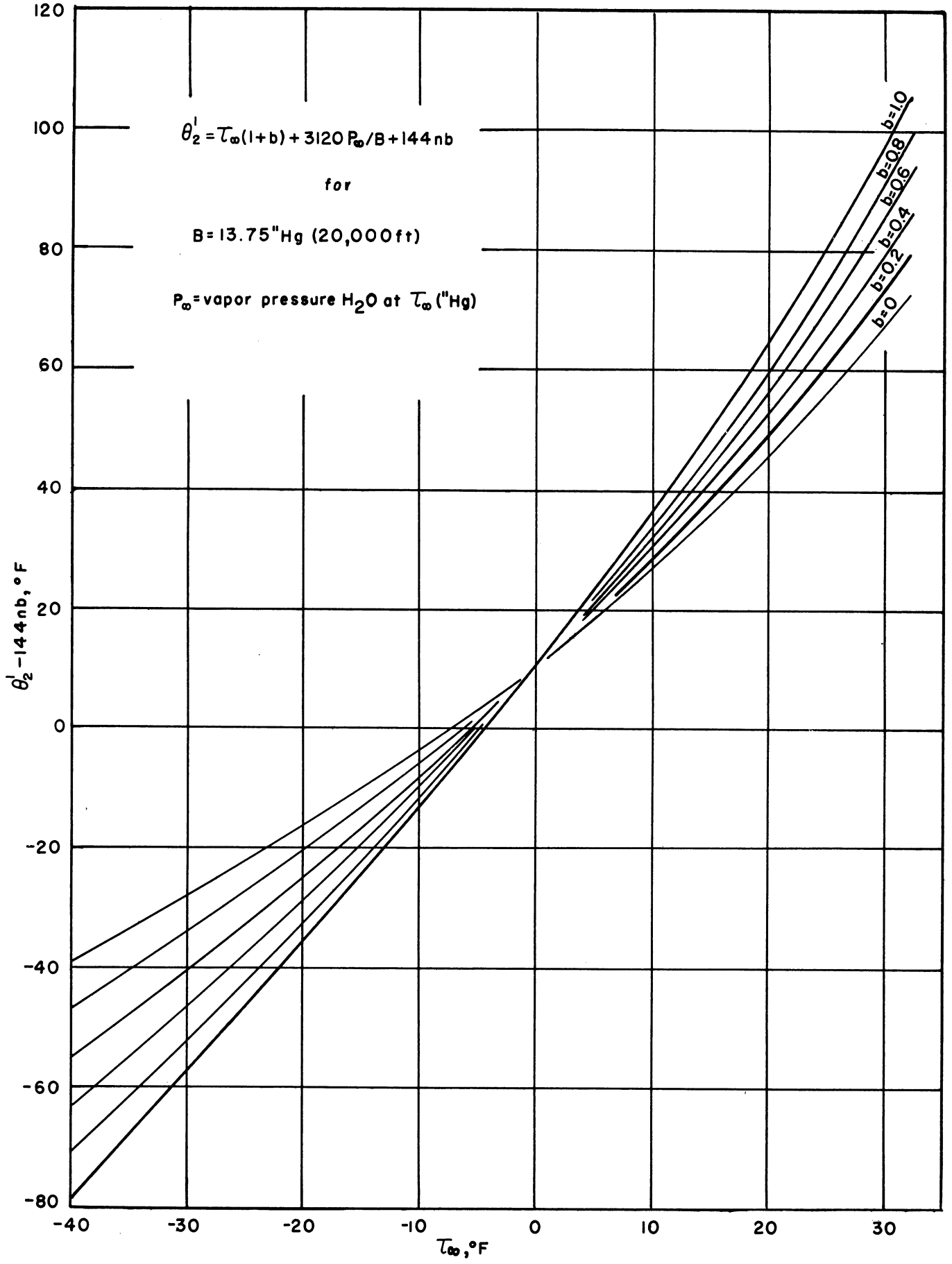
$\theta_2' = \tau_\infty(1+b) + 3120\,P_\infty/B + 144nb$
for
B = 13.75"Hg (20,000 ft)
P_∞ = vapor pressure H_2O at τ_∞ ("Hg)
b=1.0
b=0.8
b=0.6
b=0.4
b=0.2
b=0
$\theta_2' - 144nb$, °F
τ_∞, °F
120
100
80
60
40
20
0
-20
-40
-60
-80
-40
-30
-20
-10
0
10
20
30

Figure V-5e

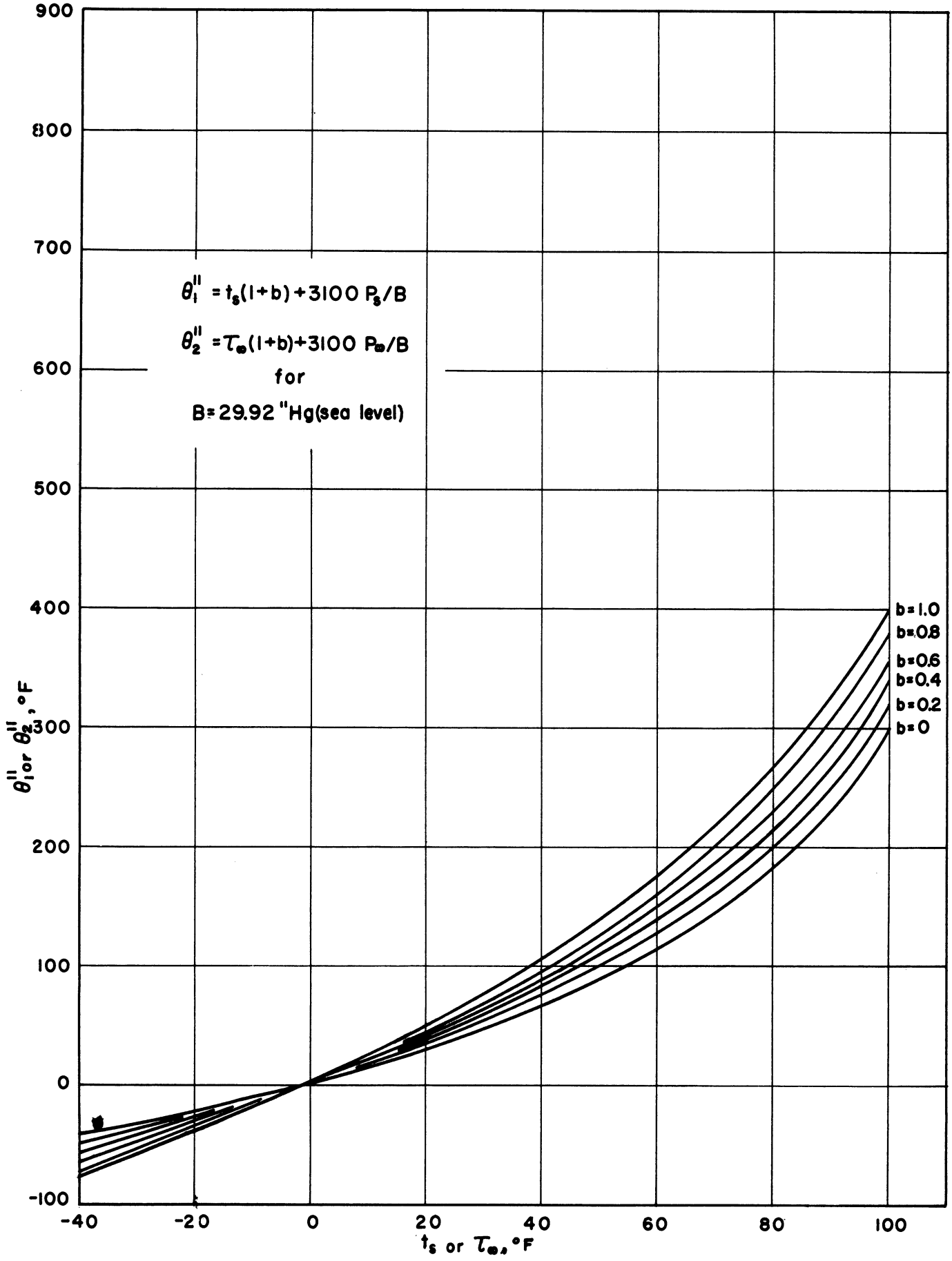
$\theta_1'' = t_s(1+b)+3100\ P_s/B$
$\theta_2'' = \tau_\infty(1+b)+3100\ P_\infty/B$
for
B = 29.92 "Hg(sea level)
b = 1.0
b = 0.8
b = 0.6
b = 0.4
b = 0.2
b = 0
θ_1'' or θ_2'', °F
t_s or τ_∞, °F
900
800
700
600
500
400
300
200
100
0
-100
-40
-20
0
20
40
60
80
100

Figure V-6a

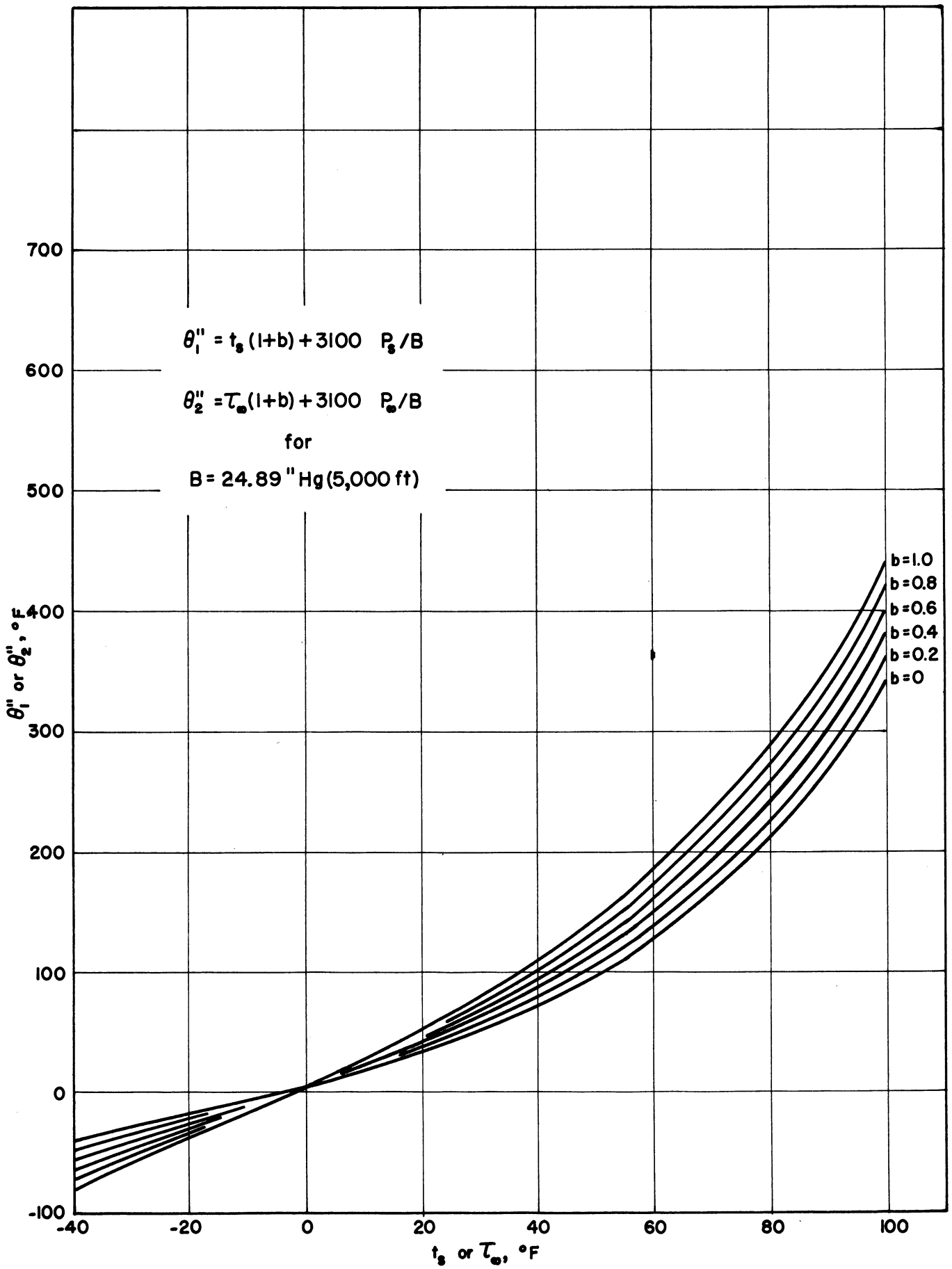
$\theta_1'' = t_s(1+b) + 3100\ P_s/B$
$\theta_2'' = \tau_\infty(1+b) + 3100\ P_\infty/B$
for
B = 24.89 "Hg (5,000 ft)
b=1.0
b=0.8
b=0.6
b=0.4
b=0.2
b=0
θ_1'' or θ_2'', °F
t_s or τ_∞, °F
700
600
500
400
300
200
100
0
-100
-40
-20
0
20
40
60
80
100

Figure V-6b

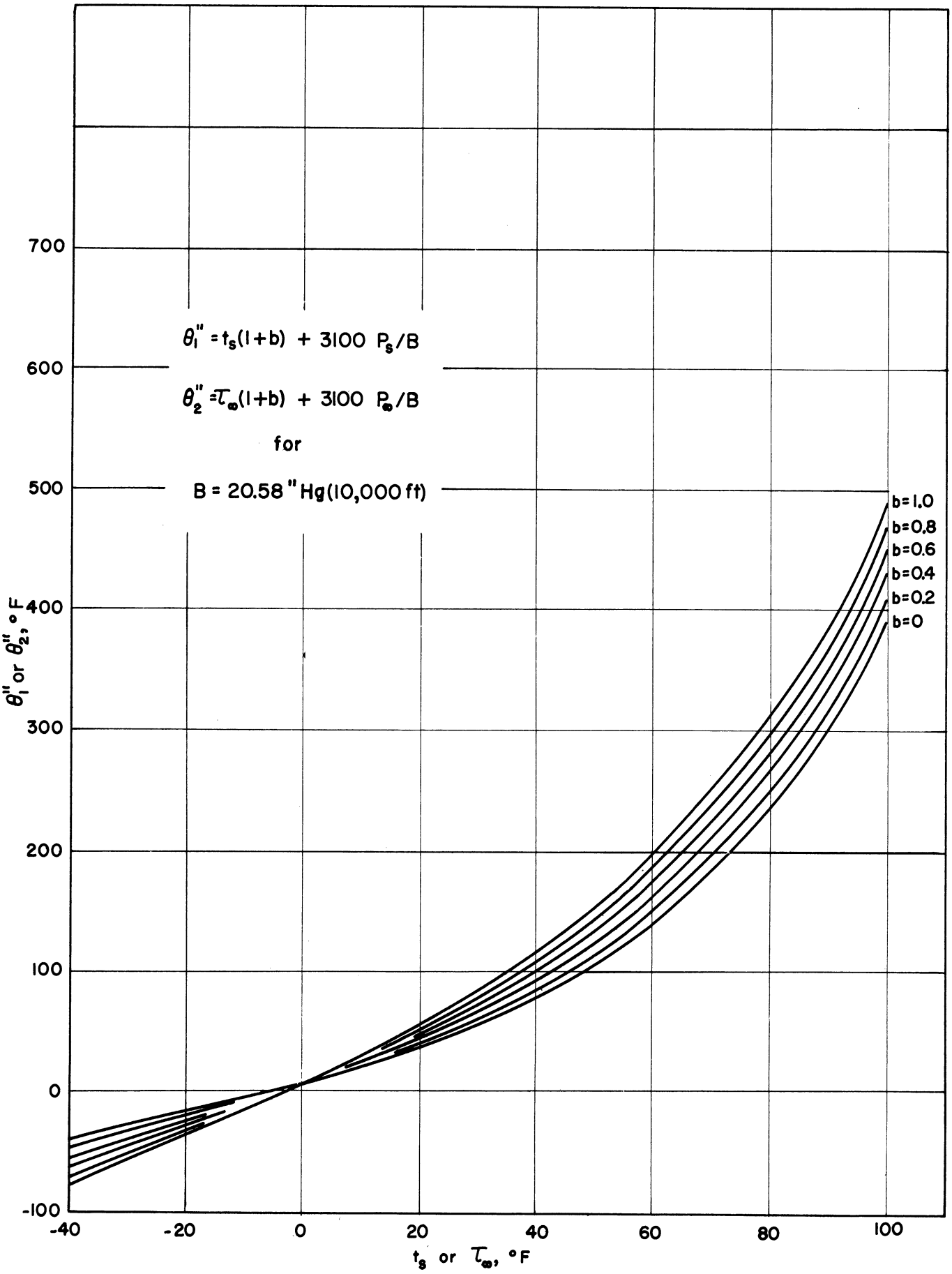
$\theta_1'' = t_s(1+b) + 3100\ P_s/B$
$\theta_2'' = \tau_\infty(1+b) + 3100\ P_\infty/B$
for
B = 20.58 " Hg(10,000 ft)
b=1.0
b=0.8
b=0.6
b=0.4
b=0.2
b=0
θ_1'' or θ_2'', °F
t_s or τ_∞, °F
700
600
500
400
300
200
100
0
-100
-40
-20
0
20
40
60
80
100

Figure V-6c

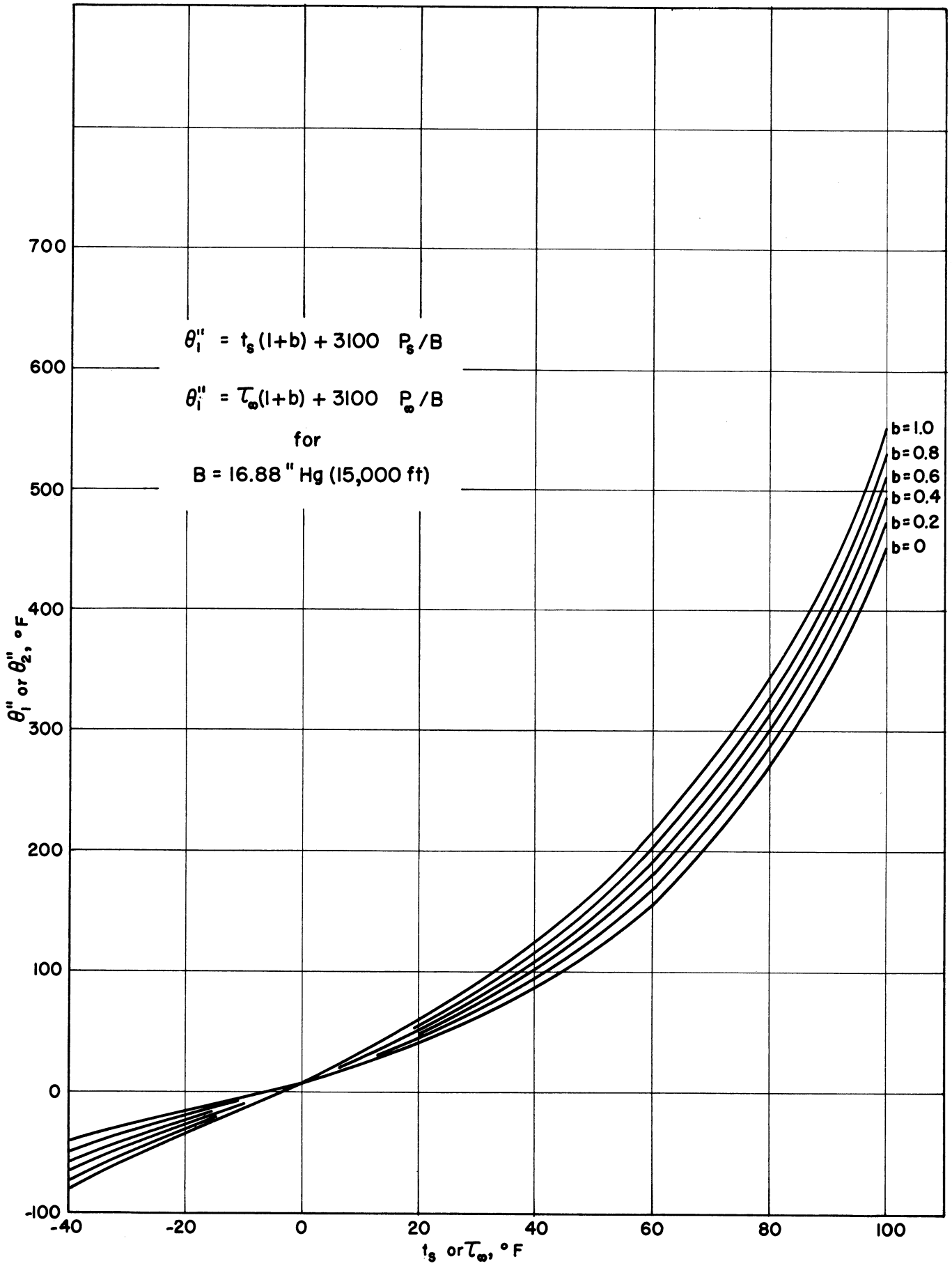
$\theta_1'' = t_s(1+b) + 3100\ P_s/B$
$\theta_1'' = \tau_\omega(1+b) + 3100\ P_\omega/B$
for
B = 16.88 " Hg (15,000 ft)
b=1.0
b=0.8
b=0.6
b=0.4
b=0.2
b=0
700
600
500
400
300
200
100
0
-100
-40
-20
0
20
40
60
80
100
θ_1'' or θ_2'', °F
t_s or τ_ω, °F

Figure V-6d

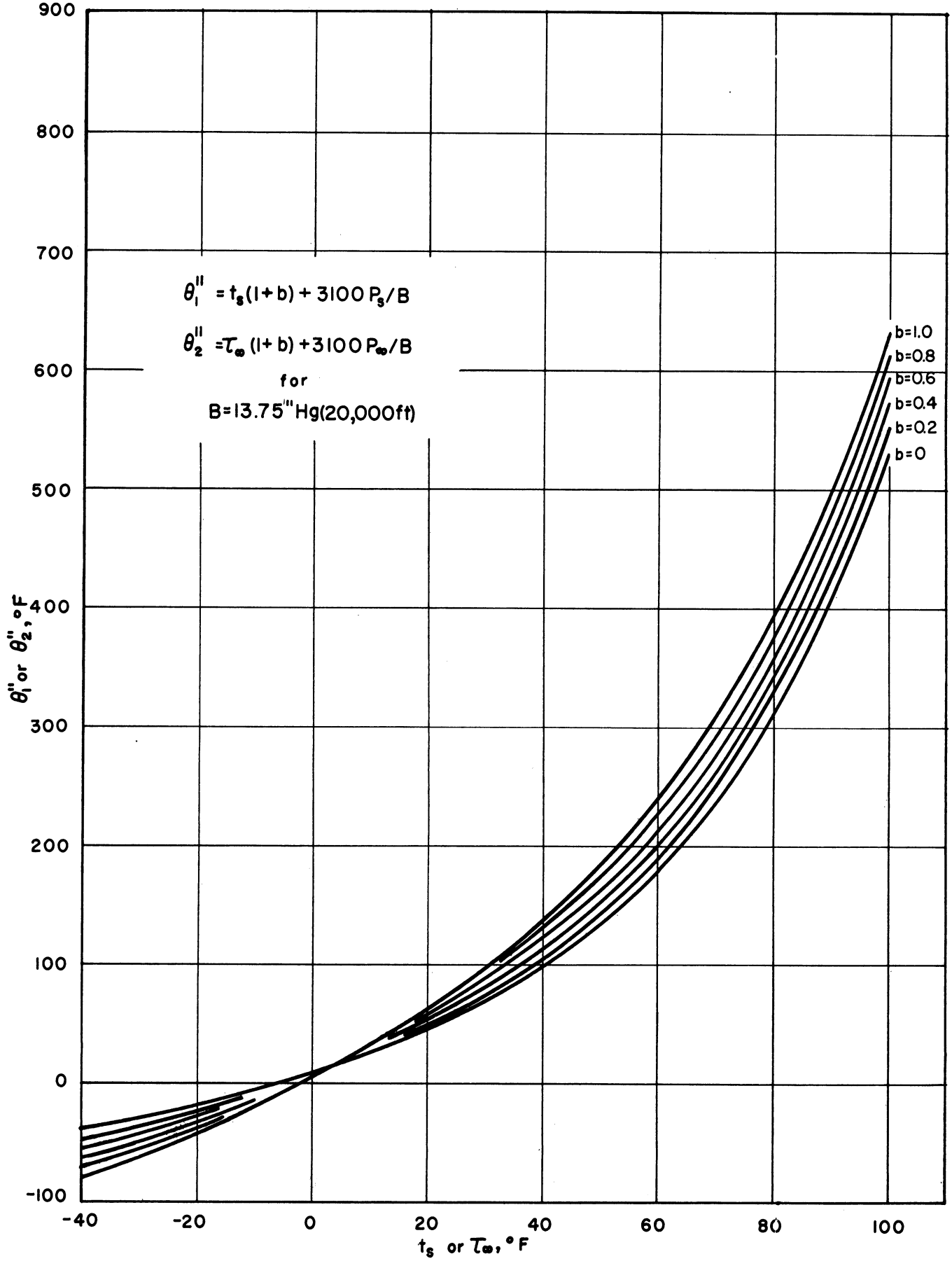
900
800
700
600
500
400
300
200
100
0
-100
-40
-20
0
20
40
60
80
100
θ_1'' or θ_2'', °F
t_s or τ_∞, °F
$\theta_1'' = t_s(1+b) + 3100\,P_s/B$
$\theta_2'' = \tau_\infty(1+b) + 3100\,P_\infty/B$
for
B=13.75" Hg(20,000ft)
b=1.0
b=0.8
b=0.6
b=0.4
b=0.2
b=0

Figure V-6e

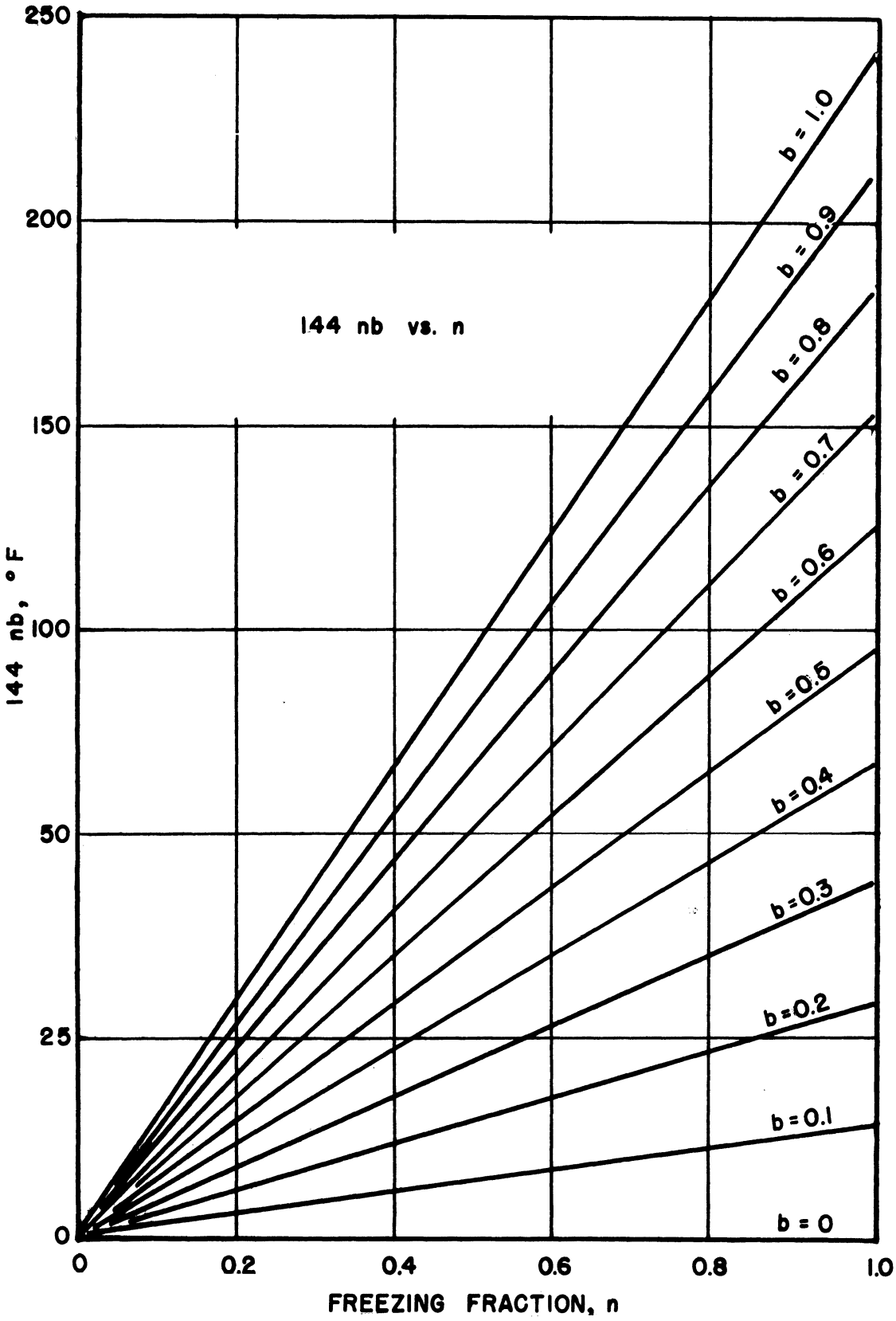
144 nb vs. n
144 nb, °F
FREEZING FRACTION, n
250
200
150
100
50
25
0
0
0.2
0.4
0.6
0.8
1.0
b = 1.0
b = 0.9
b = 0.8
b = 0.7
b = 0.6
b = 0.5
b = 0.4
b = 0.3
b = 0.2
b = 0.1
b = 0

Figure V-7

Recapitulation

For

$$t_s < 32°F \qquad q/A = h_c\,(\theta_1 - \theta_2 - \theta_3)$$

$$t_s = 32°F \qquad q/A = h_c\,(\theta_1' - \theta_2' - \theta_3)$$

$$t_s > 32°F \qquad q/A = h_c\,(\theta_1'' - \theta_2'' - \theta_3'').$$

Evaporation rate:

$$g = 2.9\, h_c\, A\, (P_s - P_\infty)\, B^{-1} \quad \text{lbs/hr.}$$

First Application: The Temperature of an Unheated Surface. If we set $(q/A) = 0$, we have from the equations above

$$\theta_1 = \theta_2 + \theta_3$$

$$\theta_1' = \theta_2' + \theta_3'$$

$$\theta_1'' = \theta_2'' + \theta_3''$$

For a given value of airplane speed, altitude-free air temperature, liquid-water content and effective droplet size, we may calculate the unit thermal conductance (h_c), the water catch rate (R_w), and, therefore, the dimensionless parameter b. We then enter the graphs of θ_2'' and θ_3. The sum is equal to θ_1'', and the graph of θ_1'' is used to find t_s. If $t_s < 32$ we must use the θ functions. Using the θ_2 and θ_3, functions we obtain θ_1, and if the resultant is above the graph we known that $t_s = 32°F$. Finally, using the θ' functions we determine n, the "freezing fraction".

These three cases will be illustrated using data from the NACA icing wind tunnel. Figure V-8 shows a sketch of the NACA experimental setup. Figure V-9 shows a typical set of data reported by Lewis[4].

Our interest centers in the temperature just before the heating cycle. Table I below gives three sets of data taken from Reference 4.

TABLE I

case	T_∞	W	radius	rpm	x*	t_s measured	Figures in Reference 4
d	11	0.46	1.98	925	1.8	32,32,33,34,31	25b, 26b, 27b 30b, 31b,
f	2	0.20	3.02	925	1.2	19, 21, 16	24a, 24b, 29b
p	11	0.50	1.15	925	1.2	28, 30, 32, 28	26b, 27b, 30b, 31b
	°F	g/m^3	ft.		in.	°F	

*distance from airfoil nose.

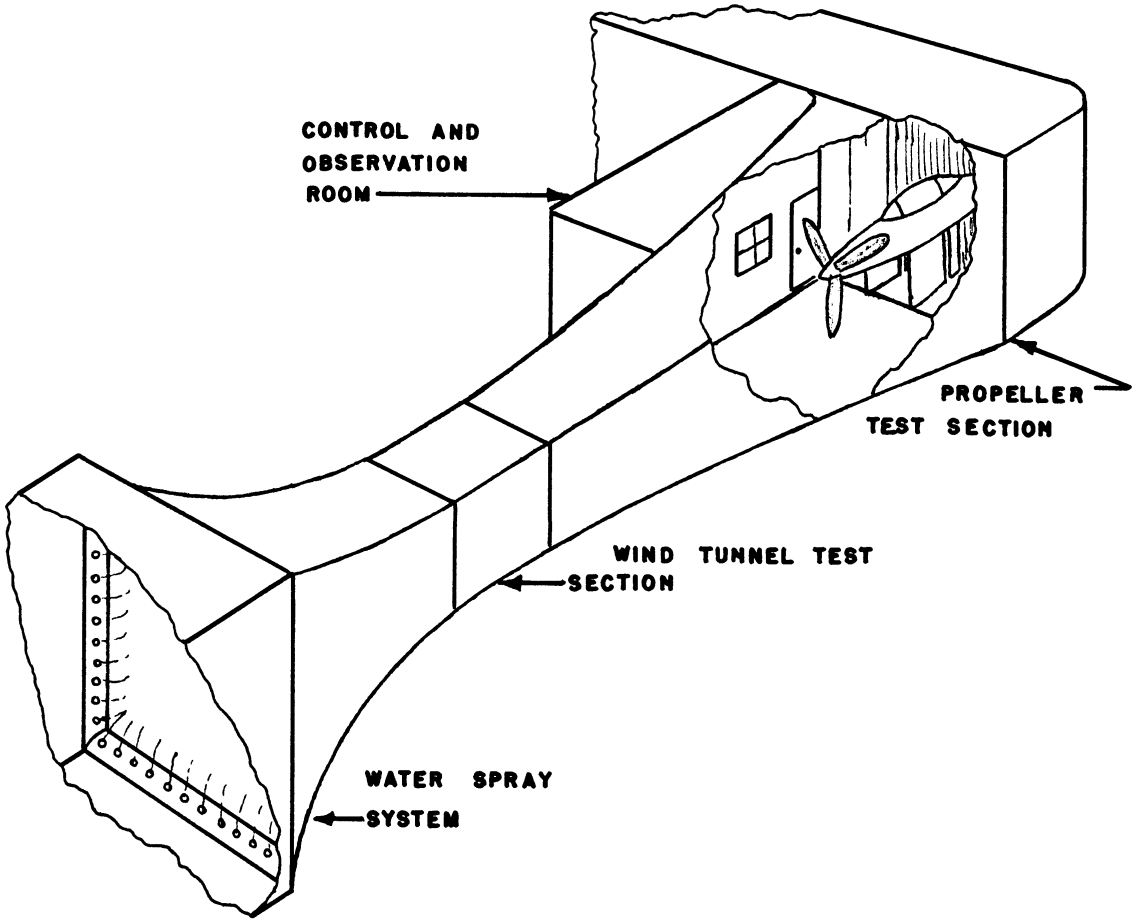

Figure V-8. Sketch of test setup used by Lewis. Since the throat of the tunnel could not accommodate the propeller, the diffuser was used.

The catch rate in the vicinity of the measuring point (x inches from the leading edge) was calculated by using the trajectory date of Reference 5. The mean drop size reported by Lewis was 50 microns. The relative velocity between propeller and air was found by adding vectorially the tunnel air speed to the propeller station tangential velocity.

Table II shows the computed data preparatory to entering the charts.

TABLE II

Case	U_∞	Ψ	R_u	E_M	$\Delta E/E_M$	h_c	$\Delta s/c$	t/c	b
d	290	101	395	0.80	0.30	21.3	0.20	0.24	0.44
f	363	112	495	0.80	0.28	25.0	0.15	0.12	0.105
p	246	54	333	0.85	0.04	17.5	0.10	0.75	0.44
	ft/sec					$\frac{BTU}{hr\ ft}$			

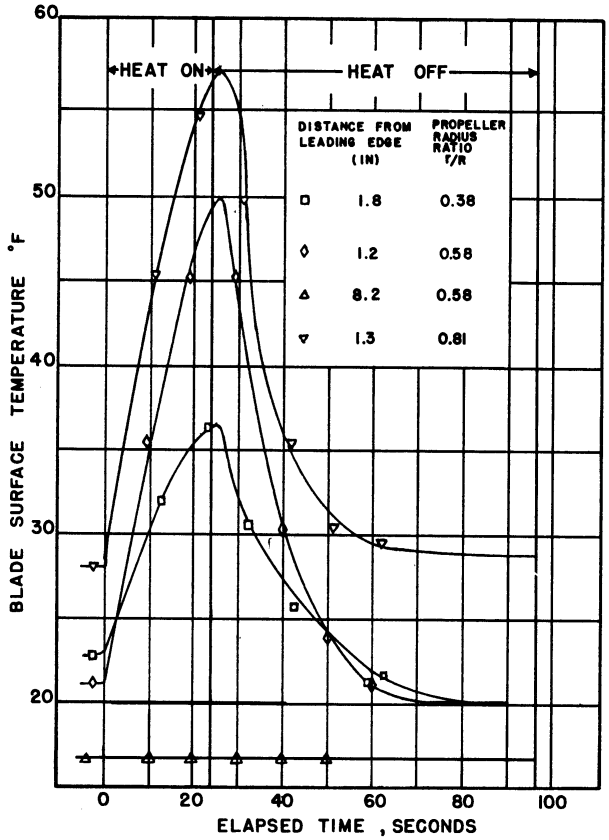

Figure V-9. Typical data reported by Lewis for the time-temperature variations on an intermittently heated propeller blade. In this test the cycle time was 96 seconds, tunnel temperature 2F, 925 rpm. The heating intensity was 9 watts per square inch on the nose and 8 watts per square inch on the first four inches of the camber face, 8 watts per square inch for the first inch on the thrust face.

For example, in case d, we enter Figure V-3 and read $\theta_3 = 5°F$. Then we enter Figure V-6a (the tunnel operated at seal level) and read $\theta_2'' = 20$ opposite $\gamma_\infty = 11°F$. The sum is $\theta_1'' = 25°F$, which in Figure V-6a corresponds to below 32°F. Therefore, the surface temperature is at or below freezing. We next enter Figure V-2a and read $\theta_2 = 80$. The sum of 80 and 5 is 85 ($= \theta_1$). We then read in Figure V-1a and find $t_s > 32°F$. Thus we know that $t_s = 32°F$. The freezing fraction is next found from the θ' functions. In Figure V-4 we find $\theta_1' = 66$. Then, since $\theta_2' = \theta_1' - \theta_3' = 66 - 5 = 61$, from Figure V-5a, we find $\theta_2' - 144nb = 24$. Therefore, $144\ nb = 37$, and since $b = 0.44$, from Figure V-7, $n = 0.45$.

We predict therefore that at this station the temperature is 32°F and that the surface of the ice is running wet with water which flows back and freezes along the aft surface. Sixty-five per cent of the water freezes as it strikes.

Table III shows a summary of the results of calculations for these cases

TABLE III

Case	θ_3	θ_2"	θ_1"	θ_2	θ_1	θ_1'	(θ_2'-144nb)	n	t_s predicted	t_s measured
d	5	20	25≠	80	85*	66	24	0.65	32	31 to 34
f	10	5	15≠	20	30	--	--	1.0	18	16 to 21
p	5	18	23≠	80	85*	66	24	0.65	32	28 to 32

≠ Below 32°F
* Above 32°F

Messinger has used these functions to prepare graphs showing the effects of speed on wing temperatures. Figure V-10 is taken from Messinger's paper and shows the free stream velocity required to prevent freezing at various free air temperatures. The required speed increases with increasing altitude.

Figure V-11, also taken from Messinger's paper, shows the variations in surface temperature as a function of airspeed. Although b is shown as an independent parameter, b is also a function of airspeed. In laminar regions b varies almost as the square root of velocity. In turbulent regions b varies more nearly with the 0.2 power of velocity. When ice is forming the value of b changes due to the effect of the distortion of the streamlines. Both the water catch and unit thermal conductance will thus be changed in an unpredictable fashion.

A Second Application. Energy Requirements for Heating Small Cylinders. Using the three equations for the three regimes, we may graph the heat required as a function of surface temperature. Figure V-12 shows such a graph. From Figure V-12 we see that the heat flux varies with b differently above and below the freezing point.

Below 32°F increasing b requires decreasing q. Above 32°F the reverse is true, but the dependence upon b is not so strong.

It is of interest to calculate the energy required to keep a surface warm and dry during an icing condition. Under these circumstances the impinging moisture must be evaporated as soon as it arrives. If the rate of water catch is known and if the unit thermal conductance is known, the mass-transfer equation may be used to predict the required surface temperature for evaporation. Then the heat flux equation may be used to predict the heat loss.

Schaefer[6] has presented data on the energy required to keep a small "calrod" dry during exposure to an icing condition. Reference 7 presents an

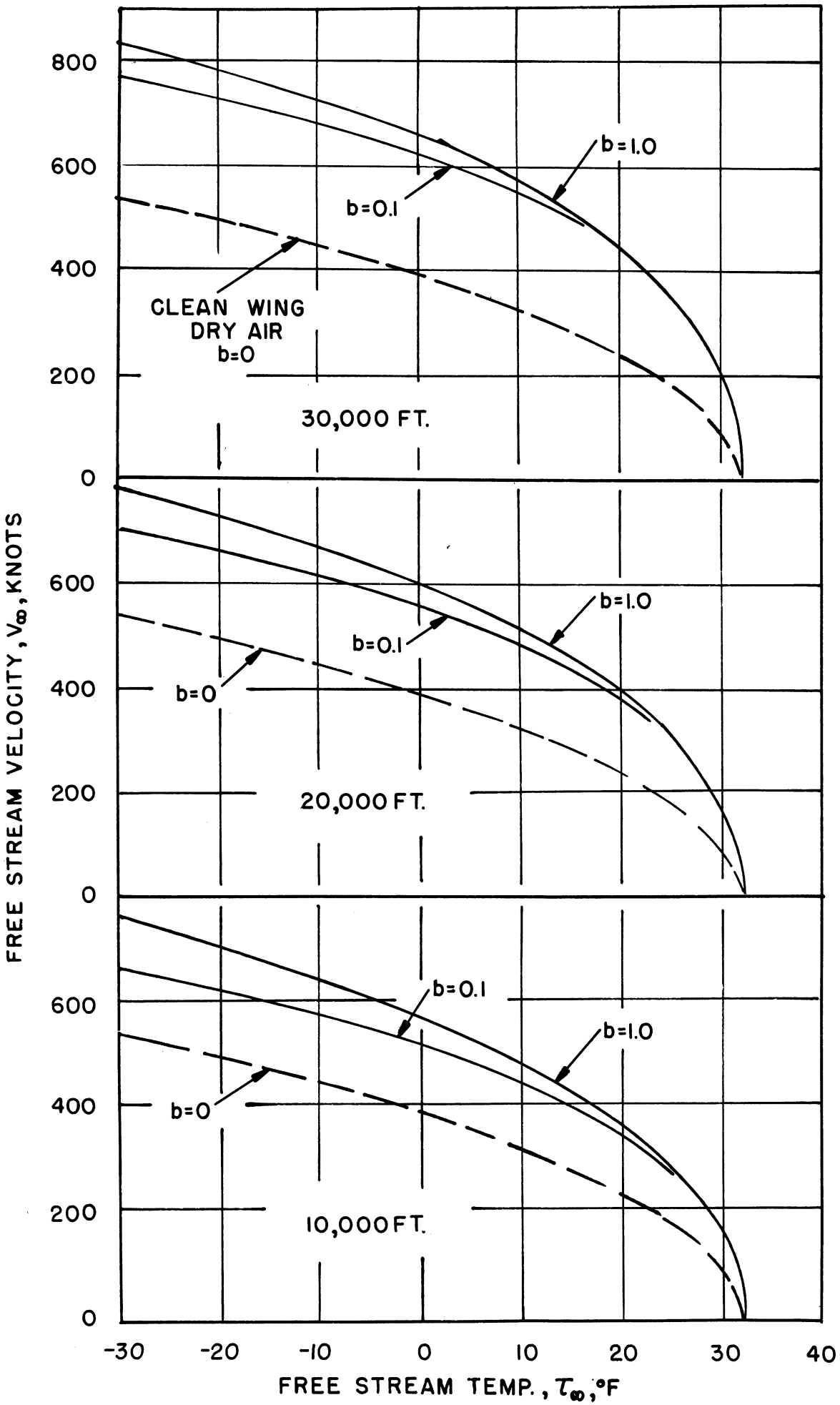
FREE STREAM VELOCITY, V_∞, KNOTS
800
600
400
200
0
b=1.0
b=0.1
CLEAN WING
DRY AIR
b=0
30,000 FT.
b=1.0
b=0.1
b=0
20,000 FT.
b=0.1
b=1.0
b=0
10,000 FT.
-30
-20
-10
0
10
20
30
40
FREE STREAM TEMP., T_∞, °F

Figure V-10

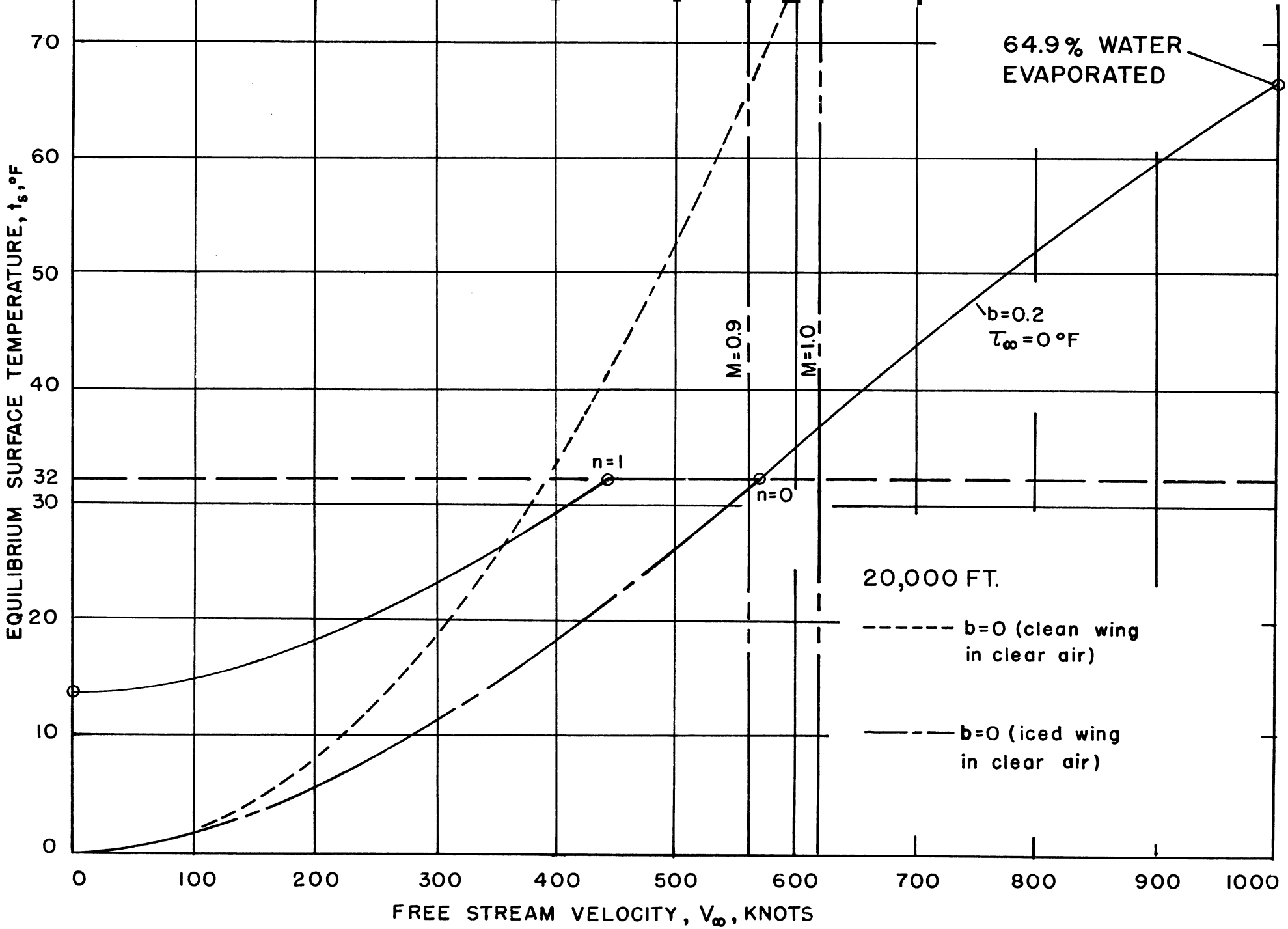
EQUILIBRIUM SURFACE TEMPERATURE, t_s, °F
0
10
20
30
32
40
50
60
70
0
100
200
300
400
500
600
700
800
900
1000
FREE STREAM VELOCITY, V_∞, KNOTS
64.9% WATER EVAPORATED
b=0.2
τ_∞ = 0 °F
M=0.9
M=1.0
n=1
n=0
20,000 FT.
b=0 (clean wing in clear air)
b=0 (iced wing in clear air)

Figure V-11

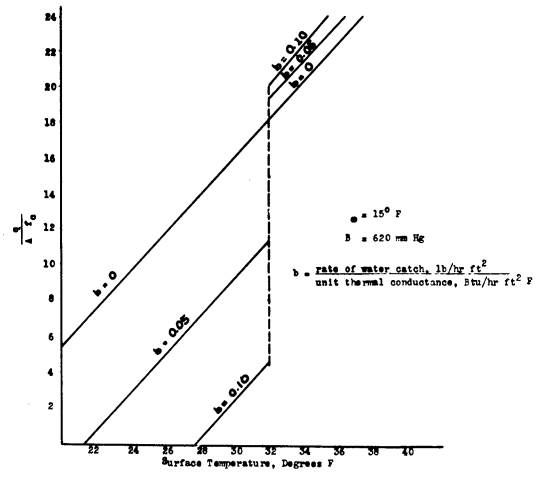

Figure V-12. Heat flux versus t_s with parameter b.

analysis of Schaefer's data. Table IV presents a summary of comparisons between Schaefer's data and computed data. The data gathered by Schaefer represent observations of the heat required to keep the calrod dry and also heat required to permit the leading edge to appear slightly moist. Most of the computed heat fluxes are bracketed by Schaefer's data.

A Third Qualitative Illustration

The physical nature of the ice formation in its initial stages may be predicted from the previous equations. When the surface temperature is low (either low value of T_∞ or low value of b), the drops are expected to freeze upon impact. The ice accretion should resemble a graph of the local catch rate. The ice should be rather porous, for the solid phase is being formed in much the same fashion as a porous sintered metal is made of small particles joined by melting.

TABLE IV

COMPARISON OF EXPERIMENTS AND COMPUTED DATA

	Measured						Computed										
					Heat Loss							Heat Lost/Frontal Area, Btu/hr ft^2					
Run	Drop Diam. Micron	Liq.Wat. Content g/m^3	Air Temp °F	Air Speed mph	Dry	Moist	E_M	β_o	$h_{c,o}$	t_s °F	$h_{c,av}$	Convect.	Evap'n	Radiant	Sensible	Total Watts/cm^2	Comment
1	5.8	0.29	7	41	1.7	1.3	0.14	0.70	50.0	60	27.4	4570	577	167	28	1.68	Light Snow
2	6.6	0.38	7	64	2.2	1.9	0.30	0.48	62.2	62	36.1	6350	2450	176	137	2.86	Very Light Snow
3	6.9	0.31	- 2	62	2.8	2.2	0.33	0.51	61.2	57	35.6	6600	2170	185	121	2.91	Light Snow
4	7.6	0.37	- 2	56	3.1	2.8	0.36	0.53	58.2	63	33.1	6760	2590	204	166	3.05	Very Light Snow
5	7.6	0.37	- 6	59	3.3	3.0	0.36	0.55	60.0	64	34.4	7570	2690	220	178	3.34	Very Light Snow
6	8.2	0.38	3	70	3.7	3.2	0.44	0.60	65.1	70	38.0	8010	4020	211	255	3.92	Trace of Snow
7	8.2	0.39	8.5	60	3.2	2.6	0.41	0.57	60.2	66	34.8	6290	3340	180	182	3.14	Light to Moderate Snow
8	8.6	0.28	- 6	77	3.3	2.8	0.47	0.62	68.5	64	40.4	9050	3520	220	246	4.10	Light Snow
9	8.9	0.25	- 0	64	3.1	2.5	0.44	0.60	62.2	56	36.2	6360	2450	176	130	2.87	Heavy Snow
10	10.2	0.38	3	64	4.0	3.4	0.52	0.66	62.2	71	36.2	7740	4350	214	280	3.94	Trace of Snow
11	10.2	0.44	1	67	4.6	3.9	0.53	0.66	63.6	76	37.1	8750	5390	236	383	4.64	Light Snow
12	12.7	0.13	0	56	4.7	4.1	0.60	0.72	58.2	43	33.4	4620	1520	284	67	2.03	Moderate Snow
13	8.3	0.32	3	80	5.5	5.2	0.47	0.62	69.9	68	41.3	8560	4180	208	280	4.18	Very Light Snow
14	9.0	0.50	14	61	5.4	5.0	0.45	0.60	61.1	76	35.2	6960	4770	198	290	3.85	Heavy Snow
15	9.6	0.42	7	76	7.5	4.3	0.53	0.66	68.0	77	40.1	8810	5880	219	390	4.80	Very Light Snow
16	11.7	0.62	12	80	7.0	6.9	0.62	0.74	69.8	93	41.3	10500	10700	279	820	7.00	Light to Moderate Snow
17	15.0	0.43	1	88	5.8	6.5	0.73	0.83	73.1	89	43.6	11900	9700	273	850	7.14	No Snow
18	17.1	0.75	12	57	5.2	4.5	0.72	0.82	58.8	98	33.7	9000	10700	267	910	6.55	Light Snow
19	16.3	0.65	30	62	5.8	5.1	0.71	0.81	61.2	94	35.6	7160	9940	201	572	5.60	Light Snow
20	17.7	1.12	25	48	5.6	5.1	0.71	0.81	54.0	109	30.4	7650	13200	251	1050	6.95	No Snow
21	5.7	0.12	28	71	0.7	0.4	0.24	0.43	65.8	43	38.6	2170	710	57	30	0.93	No Snow
22	8.8	0.10	-18	75	3.6	2.1	0.26	0.77	67.5	40	39.8	7250	677	182	37	2.55	Light Snow
					Watt/Cm^2								Btu/hr, ft^2			Watt/cm^2	

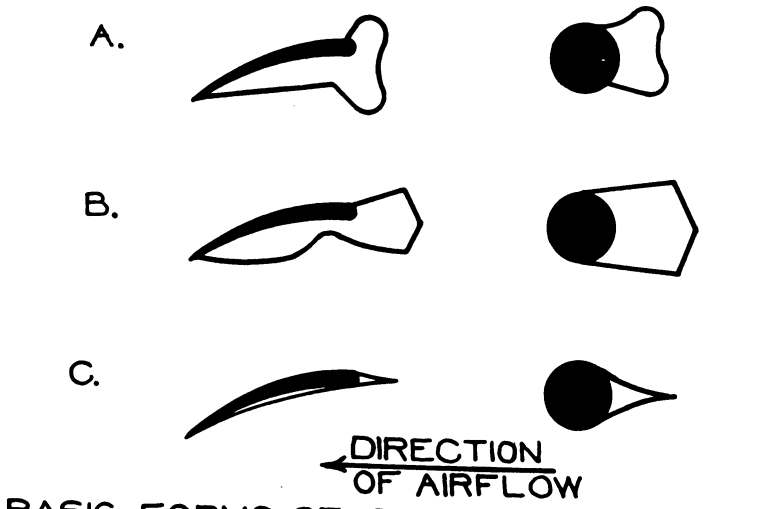

Figure V-13

When τ_∞ or b are large, the surface of the ice should run wet. However, at the "edge" of the catch zone, the value of b will drop to zero. We expect then, that the ice accretion will be flattened, since near the stagnation point there will be excess water which freezes near either side. Now, a flat surface catches ice near the edges, hence, the ice buildup will shift to produce the familiar "horned" shape.

Bartlett and Dickey[8] have observed and classified ice formations on jet-engine guide vanes. Their classifications and observations are shown in Figures V-13 and V-14 and support the above description.

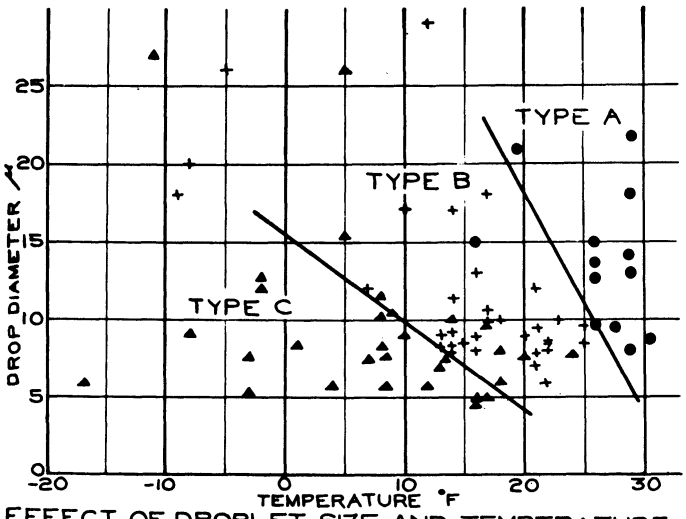

EFFECT OF DROPLET SIZE AND TEMPERATURE ON THE FORM OF ICE ACCRETION

Figure V-14

REFERENCES

1. Messinger, B. L., "Equilibrium Temperature of an Unheated Icing Surface as a Function of Airspeed". IAS Paper, S.M.F. Fund (IAS Preprint 342).

2. Hardy, J. K., "An Analysis of the Dissipation of Heat in Conditions of Icing from a Section of the Wing of a C-46 Airplane". NACA report 831, 1945.

3. Tribus, M. and Tessman, J., "Report on the Development and Application of Heated Wings," AAF TR 4972, Add. 1, January 9, 1946.

4. Lewis, J. P., "De-Icing Effectiveness of External Electric Heaters for Propeller Blades". NACA TN 1520, February 1948.

5. Guibert, et. al., "Impingement of Waterdrops on Various Airfoils from Trajectories obtained on Differential Analyzer", NACA RM 9A05, February 16, 1949.

6. Schaefer, Vincent J., "Heat Requirements for Instruments and Airfoils During Icing Storms on Mt. Washington", General Electric Co., Research Laboratory Report, April 1946.

7. Tribus, M., Young, G. B. W., and Boelter, L. M. K., "Analysis of Heat Transfer over a Small Cylinder in Icing Conditions on Mt. Washington". Trans. ASME, November 1948, p. 971.

8. Bartlett, P. M., and Dickey, T. A., "Gas Turbine Icing Tests at Mt. Washington, New Hampshire", SAE paper presented in Los Angeles, September 28-30, 1950.

CHAPTER VI

THE DESIGN OF A CONTINUOUSLY ANTI-ICED AIR-HEATED WING

Considerable analytical and experimental work on air-heated wing anti-icing systems has been accomplished by the NACA and the U. S. Air Force, as well as by the airplane companies. In principle, at least, the design of an air-heated wing is straightforward. Some design information remains yet to be gathered, particularly in regard to trajectory data on new airfoils at high speeds, and there are numerous practical difficulties in attempting to meet the heat requirements and yet remain within the weight limits currently considered acceptable. Nevertheless, the laying-out of a basic design can proceed today with considerable assurance based on the research efforts mentioned above.[1-4]

In this chapter the simplest and most straightforward design method will be presented in order that the important characteristics may be more clearly seen. After the general performance features have been surveyed, the calculation methods used for more accurate design will be considered.

Figures I-8 and I-9 show the general layout of a conventional air-heated wing. The basic problem in such a design is the determination of the air temperature and weight rate required to anti-ice successfully the wing under a given set of meteorological conditions. We shall defer to a later chapter the discussion of the appropriate meteorological conditions to be used for design purposes.

The preliminary design of an air-heated wing requires the simultaneous solution of three sets of equations. The first equations relate the heat transfer from the wing surface to the surrounding air stream (via convection, evaporation, etc.). The second set of equations describes the heat conduction in the wing metal, and the third describes heat transfer from the air in the double-skin gap. Once the air rate and inlet air temperature have been decided, the pressure necessary to pump the air must be calculated.

In low-speed aircraft the wing outer skin is generally as thin as possible. The chordwise conduction of heat is then small, and there is no need to solve the equation of heat conduction in the outer skin. Only two equations need be solved simultaneously. Neel[5] and Neel, Bergrun, Jukoff, and Schlaff[3] demonstrate a technique to be used for this case.

In high-speed aircraft the outer skin on the wing is quite thick, and the chordwise heat conduction tends to provide an isothermal surface. Under the restriction that the wing is isothermal, the simultaneous solution of the heat-flow equations is considerably simplified. For purposes of clarity this simpler system will be considered here and the more complex systems taken up later. In the analysis which follows, the wing surface is taken as isothermal.

The Heat Flux from the Heated Air to the Wing Surface

Consider now the typical heated-wing construction with double skin. Figures VI-1 and VI-2 show the heat flow paths from the air. The aluminum

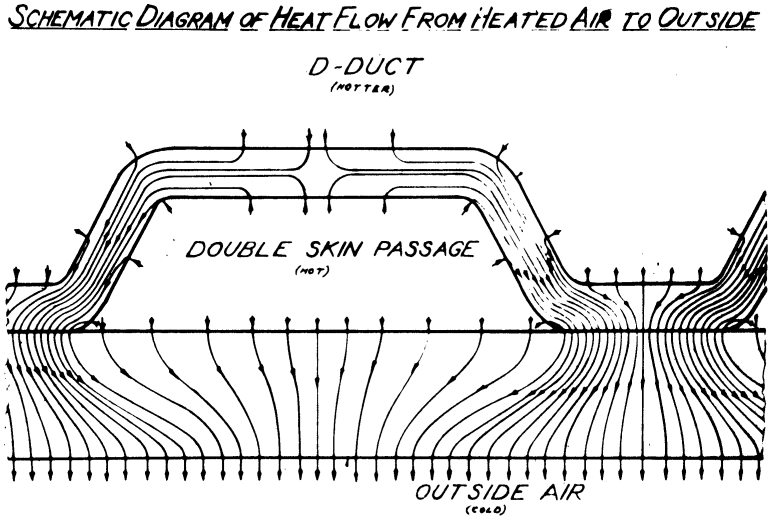

Figure VI-1. Schematic diagram of heat flow from heated air to outside.

used to form the double skin is a good conductor of heat, and, since it is usually well bonded to the outer skin, there is considerable heat transfer from the air in the "D" duct even before it enters the double skin.

The heat transfer from air to the walls of a conduit is described by the equation

$$q = h_i A (t_a - t_s),$$

where

q = heat flux, BTU/hr
A = surface area, ft^2
t_a = "mixed mean" air temperature at any section, °F
t_s = surface temperature, °F.

The above equation serves to define h_i, the unit thermal conductance for the heat transfer from the interior of the conduit.

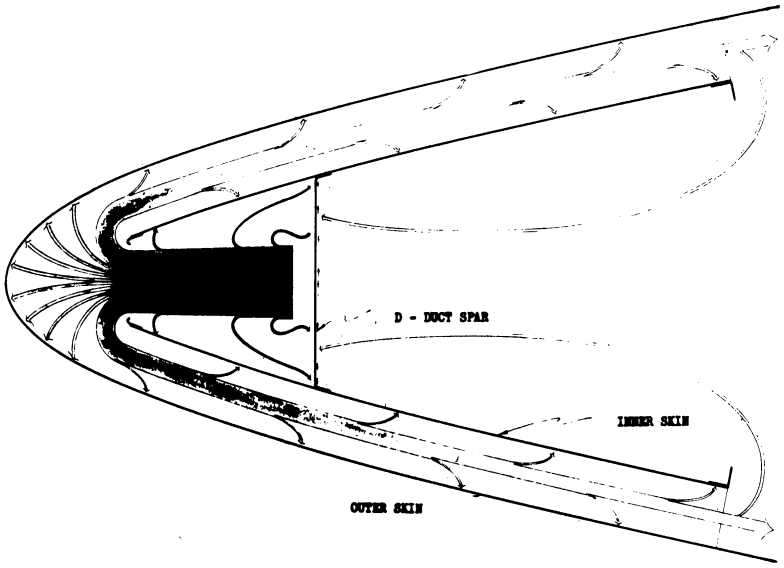

Figure VI-2. Schematic diagram of heat loss from heated air to inner ducting of leading edge system.

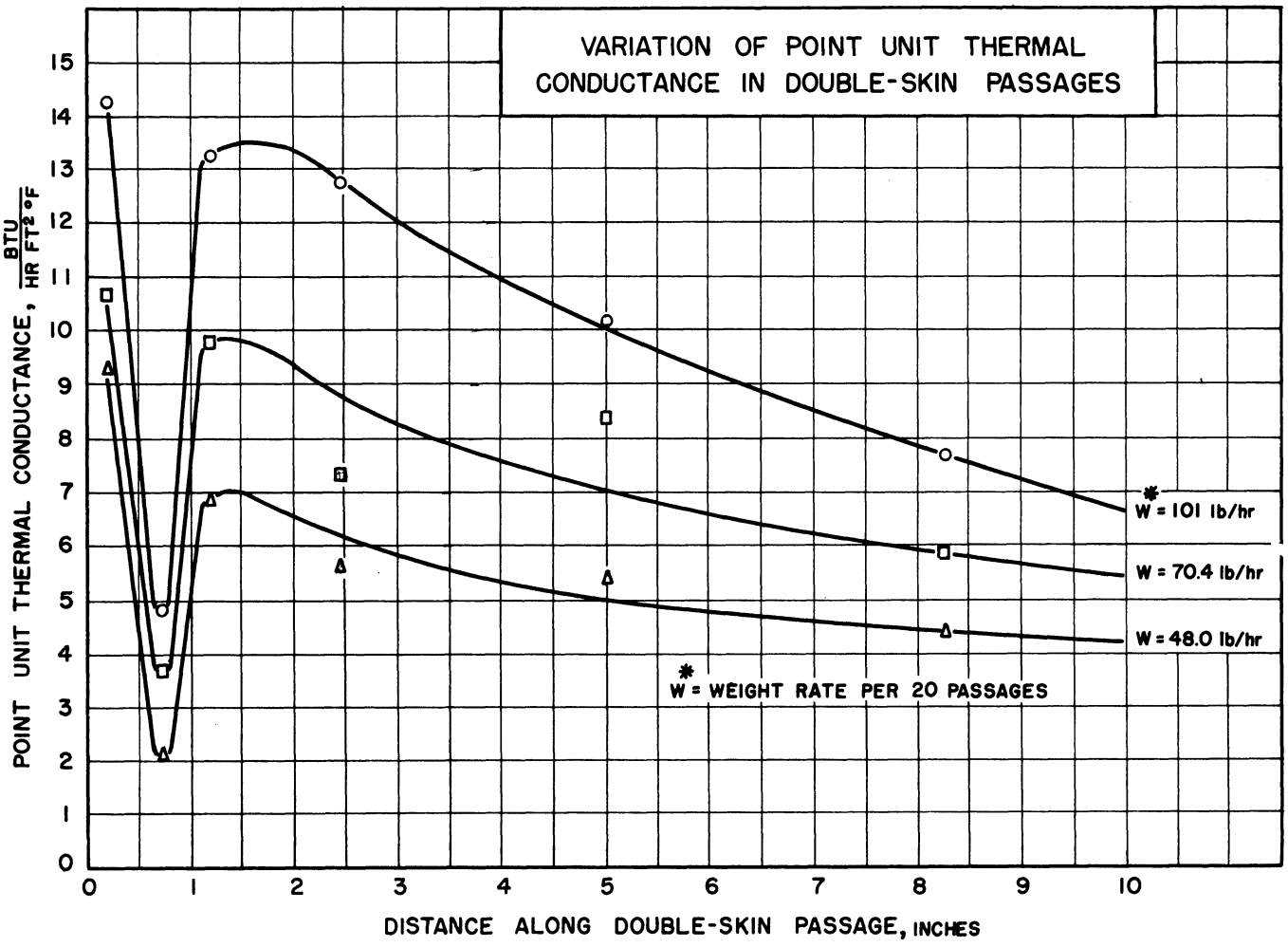

Figure VI-3

Figure VI-3 shows a typical variation in h_i along the double-skin passage. As the air turns and enters the air gap, the unit thermal conductance drops from a high to a low value. About an inch from the inlet, the flow becomes turbulent and the conductance rises abruptly. The conductance then falls slowly with distance along the duct.

A typical laboratory apparatus for measuring heat transfer within the double skin construction is shown in Figures VI-4 to VI-7. Figure VI-4 shows the inner skin. Figure VI-5 shows steam-condensation partitions installed on what would normally be the airfoil outer skin. Figure VI-6 shows the complete test unit with instrumentation on the interior and the steam jacket over the outside. Figure VI-7 shows the laboratory set up with the various steam condensate tubes visible below the steam jacket. The weight of steam collected in each tube is a measure of the heat transferred locally, since the heat of condensation is known. Average conductances may be obtained from the point values of Figure VI-3 by integration and may be used when the surface temperature is uniform.

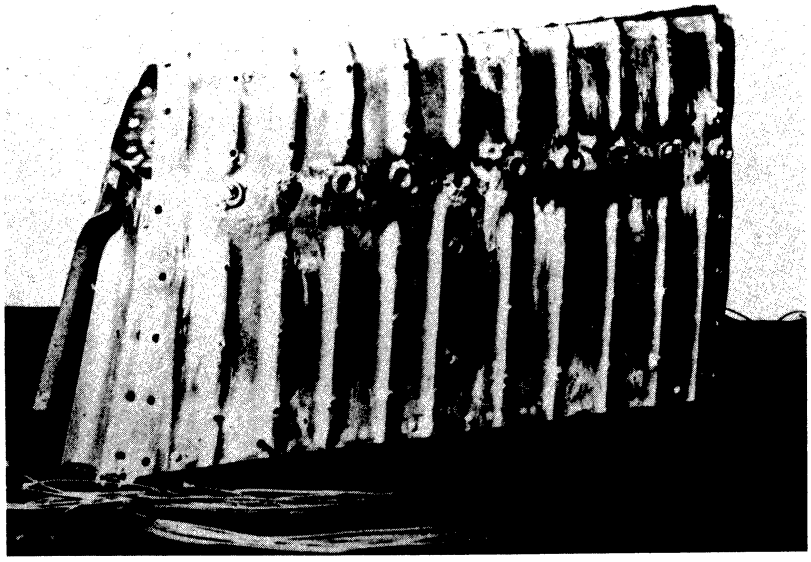

Figure VI-4

If one considers an air-heated wing system where the surface temperature is constant over the heated region and the conductance, h_i, is also constant at its average value, the following heat-balance equation may be applied:

$$dq = h_i (t_a - t_s)\, dA = - W C_p\, dt_a,$$

where

W = air rate, lbs/hr
C_p = air unit heat capacity, BTU/lb °F.

Since h_i, t_s, W, and C_p are considered constant, the above equation may be integrated to yield

$$\frac{t_{a2} - t_{az}}{t_{ai} - t_s} = 1 - e^{-\frac{h_i A}{W C_p}} .$$

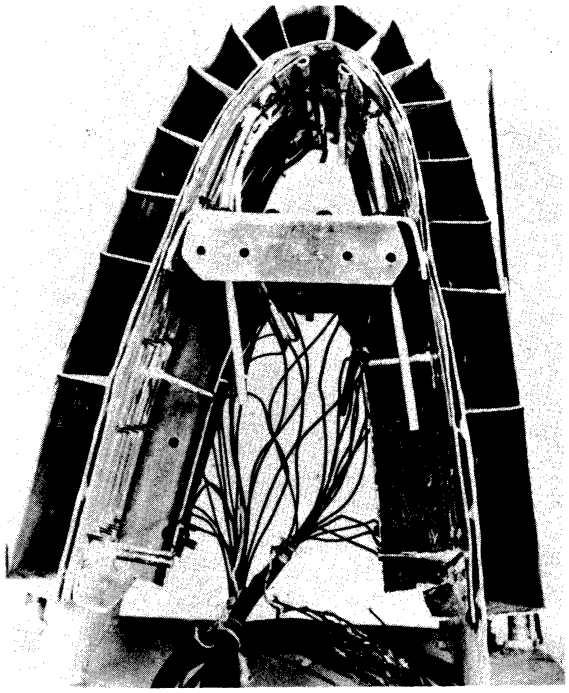

Figure VI-5

The total heat flux for the air may then be computed from

$$Q = WC_p\,(t_{ai} - t_{a2}') = WC_p\,(t_{ai} - t_{sa})\left\{1 - \exp\,(-\,hA/WC_p)\right\}.$$

The above equation may be used in several ways. For example, for a given surface temperature and heat flux, the required inlet air temperature may be computed as a function of air rate.

Matching the Interior Airflow to the Heat Requirements

As an example of the design of a heated-wing air system*, consider Figure 8, which shows the water catch rate on several airfoils (treated as

*D. M. Patterson has prepared a handy set of nomographs for use in rapidly carrying out the design of air-heated wings. The use of the nomographs obscures some of the variables, hence the calculations here are carried out in greater detail (See Reference 6).

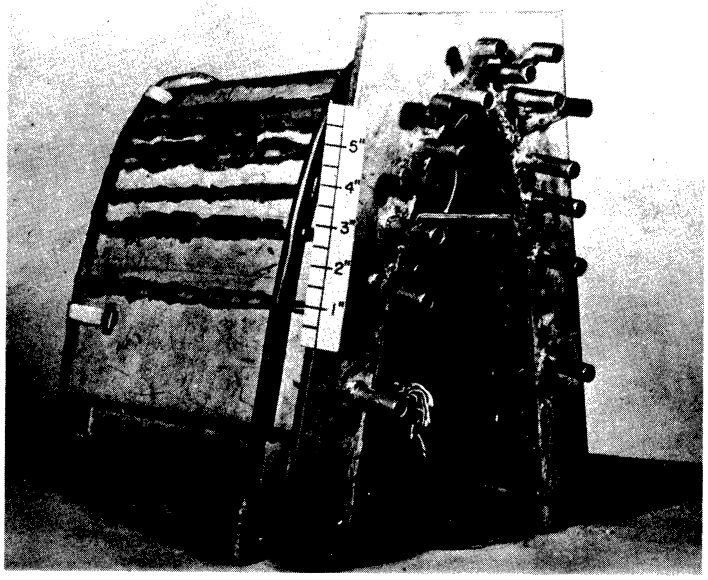

Figure VI-6

though they were cylinders).* The designer chooses the particular configuration and condition corresponding to his airfoil and prepares a table such as shown in Table I. Items 1 to 11 in Table I are self-evident entries. Item 9 may be taken from water droplet trajectory data.*

Item 12 is computed as follows:

(Consider 225 mph, sea level, 15°F, drops of 15 micron diameter, liquid water concentration of 1.0 grams/meter^3)

The evaporation rate is given by $g = h_m A (H_s - H_\infty)$ (see Chapter IV), which may be rearranged to yield

* The use of a cylinder as an approximation to an airfoil as suggested in Reference 2 does not yield accurate results. The data and References of Chapter II should be consulted.

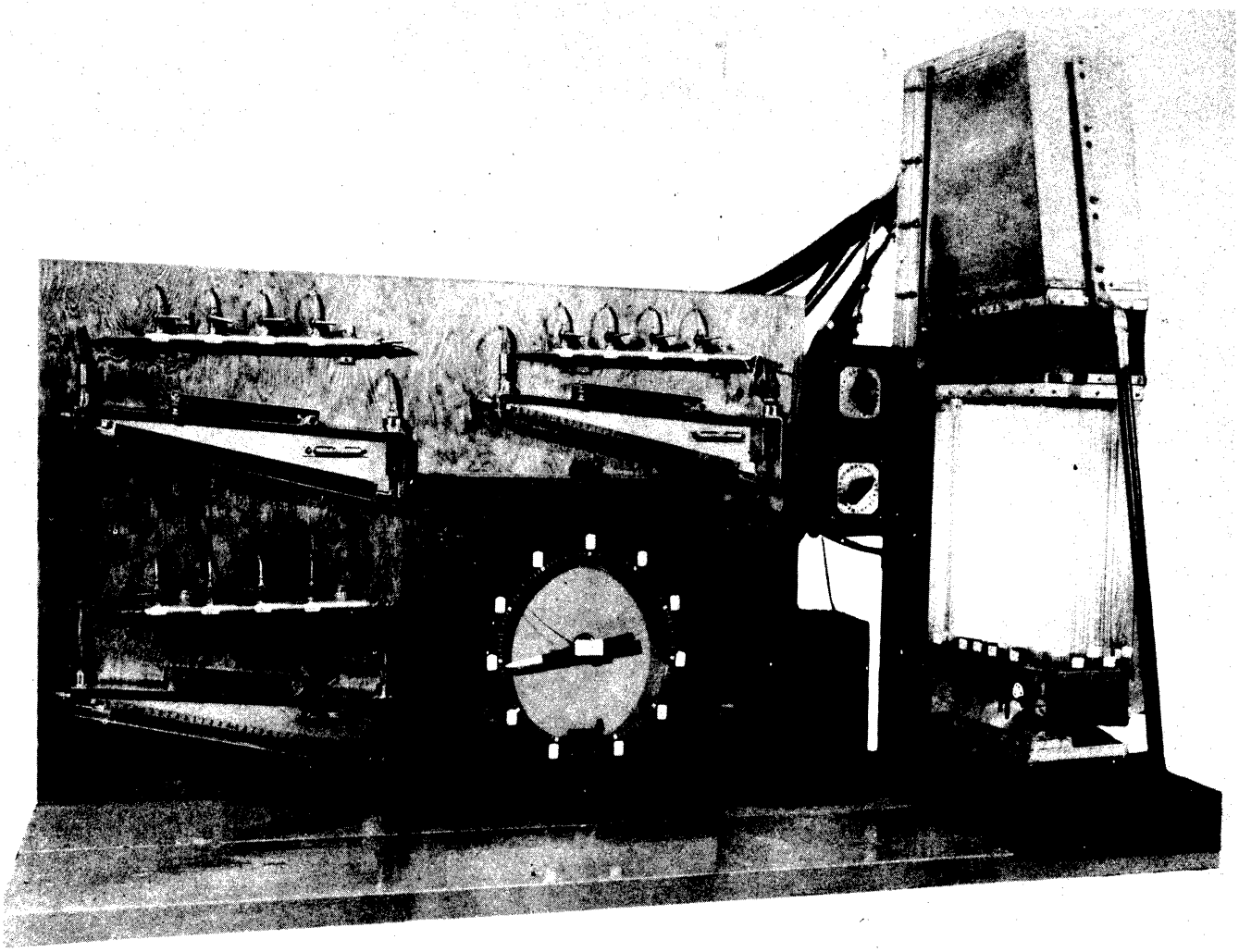

Figure VI-7. Test stand used for determination of internal heat transfer coefficients and pressure drops.

$$g = h_c/C_p \, A \, (0.62) \, (P_s - P_\infty)/B \text{ (see Chapter IV).}$$

For this case,

$$g = 3.03 \text{ lbs water/hr}$$
$$A = 6.0 \text{ ft}^2$$

(Top and bottom surfaces heated directly for 2 feet; one foot aft heated indirectly by conduction, see Reference 2).

$$B = 29.9 \text{ inches } H_g$$
$$C_p = 0.241 \text{ BTU/lb } ^\circ\text{F.}$$

The unit thermal conductance, h, may be approximated by treating the leading-edge region as a cylinder and the afterbody as a flat plate. (Much better approximations are available, but their application would cloud this

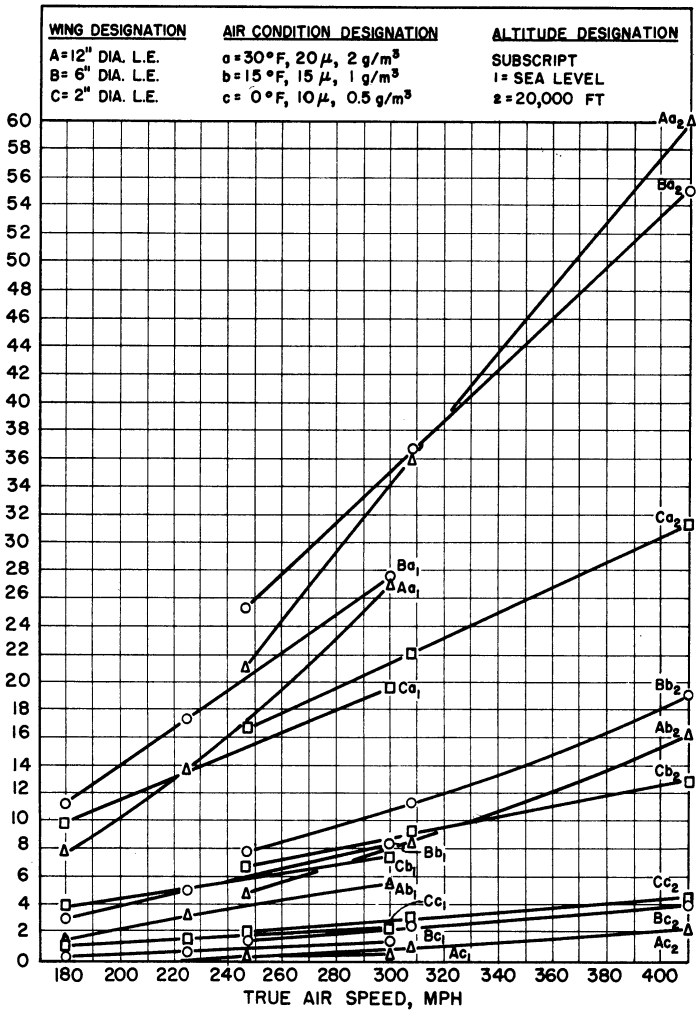

RATE OF WATER CATCH VS TRUE AIR SPEED

Figure VI-8

discussion). Figure VI-9 shows the nature of this idealization. Experiments with cylinders and airfoils have been predicted well by the following empirical equations:

A. For the cylinder:

$$h_\phi = 0.194\ T_f^{0.49} \left(\frac{U_\infty \gamma}{D}\right)^{0.5} \left[1 - (\phi/90)^3\right],$$

where

h_ϕ = local conductance at angle ϕ BTU/hr ft^2 °F
T_f = "film temperature", average between surface and free stream, °R
U_∞ = free stream velocity, ft/sec
γ = air density, lbs/ft^3
D = cylinder diameter, ft
ϕ = angle measured from a stagnation line, degrees.

TABLE I

Wing Characteristics:
12-inch diameter leading edge
Laminar 1.5 feet - turbulent rest of airfoil
2.0 feet heated length

No.	Item	Units	Value															
1	Altitude		Sea Level			Sea Level			Sea Level			20,000 ft.			20,000 ft.			20,000 ft.		
2	Ambient Air Temperature	°F	30			15			0			30			15			0		
3	Water Drop Size	Microns	20			15			10			20			15			10		
4	Liquid Water Content	Grams/(Meter)^3	2.0			1.0			0.5			2.0			1.0			0.5		
5	Air Viscosity	(lb)(sec)/(ft)^2	360 x 10^{-9}			350 x 10^{-9}			340 x 10^{-9}			360 x 10^{-9}			350 x 10^{-9}			340 x 10^{-9}		
6	Air Density	lbs/(ft)^3	0.0806			0.0835			0.0863			0.0407			0.0422			0.0437		
7	Indicated Air Speed	Miles/Hour	180	225	300	180	225	300	180	225	300	180	225	300	180	225	300	180	225	300
8	True Air Speed	Miles/Hour	180	225	300	180	225	300	180	225	300	247	308	411	247	308	411	247	308	411
9	Efficiency of Water Catch		0.065	0.093	0.137	0.025	0.041	0.057	0.002	0.004	0.013	0.130	0.178	0.222	0.061	0.084	0.120	0.010	0.017	0.030
10	Rate of Water Catch	lbs/hr	7.69	13.8	27.0	1.48	3.03	5.61	0.0591	0.148	0.640	21.1	36.0	60.0	4.94	8.46	16.2	0.405	0.860	2.03
11	Effective Ambient Air Temperature	°F	34.9	37.7	43.8	20.0	22.7	28.8	4.95	7.72	13.8	39.3	44.5	55.8	24.3	29.5	40.8	9.33	14.5	25.8
12	Required Wing Temperature for Evap.	°F	74	84	98	37	46	55	32	32	32	86	96	105	49	56	67	32	32	32
13	Heat to Raise Water Temperature	BTU/hr	338	746	1840	33	94	224	2	5	21	1180	2380	4500	168	348	842	13	26	65
14	Dry Heat Loss	BTU/hr	5320	7390	10,700	2330	3720	5170	3690	3860	3590	4930	6380	7520	2610	4520	4000	2400	2180	948
15	Heat to Evaporate Water	BTU/hr	8090	14,400	28,000	1590	3150	5960	64	159	689	22,000	31,400	62,100	5270	9000	17,100	437	926	2190
16	Total Heat Loss	BTU/hr	13,700	22,500	40,500	3950	6960	11,400	3760	4040	4300	28,100	46,200	74,000	8050	13,900	21,900	2850	3130	3200
17	Total Heat Loss Per Unit Area	BTU/(hr)(ft)^2	2280	3750	6750	662	1150	1900	627	673	717	4670	7700	12,300	1340	2320	3650	475	522	533
18	Heat to Raise Water Temperature	Per Cent	2.5	3.3	4.5	0.8	1.4	2.0	0.0	0.1	0.5	4.2	5.1	6.1	2.1	2.5	3.8	0.5	0.9	2.0
19	Dry Heat Loss	Per Cent	38.8	32.8	26.4	59.0	53.8	45.3	98.2	96.0	83.4	17.6	13.8	10.2	32.4	32.5	14.9	84.3	70.0	29.6
20	Heat to Evaporate Water	Per Cent	58.5	63.9	69.1	40.2	45.8	52.7	1.8	3.9	16.1	78.2	81.1	63.7	65.5	65.0	78.3	15.2	16.6	68.4
21	Heating Air Weight Rate*	lb/hr				82	166		76	82	90				182			55	82	163
22	Nonicing Wing Temperature	°F				65	90		50	56	52				115			51	67	61

Note: All items above are for one foot of span.
*Based on inlet air temperature of 250°F.

B. For laminar flow over a flat plate:

$$h = 0.0562\ T_f^{0.5}\ (U_\infty \gamma)^{0.5}\ x^{-0.5}\ ,$$

where x = distance from beginning of boundary layer, ft.

C. For turbulent flow over a flat plate:

$$h = 0.51\ T_f^{0.3}\ (U_\infty \gamma)^{0.8}\ x^{-0.2}\ .$$

For the case at hand, the individual conductances are plotted for the three regimes and the average conductance obtained by graphical integration. (The charts and equations by Patterson[6] enables one to find $h_{average}$ rapidly).

For the case at hand the average conductance is found to be h = 25. The required vapor pressure difference to evaporate the moisture is taken from

$$g = h/C_p\ A\ (0.62)\ (P_s - P_\infty)/B$$

$$P_s - P_\infty = \frac{g\ C_p\ B}{h\ A\ (0.62)} = \frac{3.03 \times 0.241 \times 29.9}{25 \times 6 \times 0.62} = 0.231\ .$$

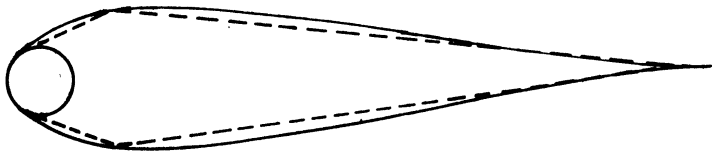

Airfoil idealized as a cylinder and series of flat plates.

Figure VI-9. Airfoil idealized as a cylinder and series of flat plates.

At 15°F the vapor pressure of water is 0.08 inches of mercury. From the steam tables we find that at P_s = 0.31 "H_g, that the temperature t_s = 46°F.

Entries 13 to 15 in Table I are computed as follows:

Item 13. Sensible heating of the water

$$Q = .3.03 \times (46 - 15) = 94 \text{ BTU/hr};$$

Item 14. Dry heat loss (convection minus frictional gain)

$$\text{Convection} = h A (t_s - T_\infty) = 25 \times 6 \times 31 = 4{,}650 \text{ BTU/hr},$$

$$\text{Frictional gain} = h A r \frac{U_\infty^2}{2 g_c J C_p} = 25 \times 6 \times 7.7 = 1{,}150 \text{ BTU/hr},$$

$$\text{Net} = 4{,}650 - 1{,}150 = 3{,}500;$$

Item 15. Heat to evaporate the water:

$$Q = 3.03 \times 1{,}065 = 3{,}200 \text{ BTU/hr} .$$

The remaining entries of Table I are self-evident with the exception of the last entry, which will be considered shortly.

The required inlet air temperature may now be computed as a function of the air rate, since both q and t_s are known. For example at 100 lbs/hr per ft of span (10 passages top plus 10 passages bottom, Figure VI-3) the average value of $h_i = 10.0$ for the interior. From the equation

$$Q = W\, C_p\, (t_{ai} - t_s)\, (1 - e^{-h\, A/W\, C_p})$$

$$6960 = 100 \times 0.24\, (t_{ai} - t_s)\, (1 - e^{-10x4/100x0.24}).$$

(Note A = 4 feet, since 2 feet are indirectly heated.)

$$t_{ai} - 46 = 35°F$$
$$t_{ai} = 403°F$$

On the other hand, if t_{ai} is restricted to 250°F, the required air weight flow is 166 lbs/hr as shown in Table I.

We may compute the "dry air" wing temperature as follows:

If the surface is such a good conductor that t_s = constant, then the heat flux from the wing to the air is

$$Q = h_o\, A\, (t_s - t_c).$$

The heat flux from the interior air is

$$Q = W\, C_{pa}\, (t_{ai} - t_s)\, (1 - e^{-h_i\, A/W\, C_p}).$$

Given W = 100 lbs/hr t_{ai} = 400°F A_i = 4 ft^2 inside C_p = 0.241 BTU/16°F

h_i = 10 BTU/hr ft^2 °F t_e = 22.7 °F h_o = 25 BTU/hr ft^2 °F A_o = 6 ft^2, outside

The above equations are solved to yield t_s = 70°F

In Table I some of the entries on lines 11 and 12 have been left blank. Under severe icing conditions it was found impossible to blow the required

amounts of air through the structure with the available pressures. Pressure drop considerations are not treated here since they are not peculiar to heated-wing design. See for example Reference 2, 12 and especially 13 for discussion of pressure drop.*

More Accurate Design Methods

The principal parameters which enter the design are:

h_o the unit thermal conductance from the wing exterior to the ambient air,

h_i the unit thermal conductance from the air inside of the wing,

R_w the local rate of water catch,

and, the wettedness, i.e., the ratio of the area wetted by water to the surface area for heat transfer.

References 9, 10, 11, 12, and 13 of Chapter V discuss the calculation of the exterior conductance.

The unit thermal conductance in the interior of the wing may be approximated by treating the flow to be similar to the inlet region of a conduit. Poppendiek[7] has reviewed the available literature on inlet effects. For the oddly shaped inlets which occur in conventional heated wings, experimental measurements are usually superior to analytical techniques.

The local rate of water catch is calculable from the type of data in Chapter II.

The Wettedness

NACA measurements[3,4,5,8] as well as experiments by Guibert[9] and Gardner[10] have shown that aft of the area of primary impingement ($\pm \Theta_M$, see Chapter II), the water does not usually flow in a sheet but flows in rivulets (see Figures III-1 and III-2). Guibert tried using wetting and nonwetting agents with erratic results. Gardner[10] and later Neel, et. al.,[3] reported that the rivulet pattern was not too sensitive to the rate at which the water flowed back, provided some minimum flow was maintained.

*Reference 12 does not calculate heat requirements in the more modern fashion.

Guibert[9] has suggested that aft of the area of primary water impingement the evaporation term in the heat balance be multiplied by the ratio, A_w/A_s, the fractional wettedness. Neel, et. al.,[3] used the traces (Figure III2a) of the rivulets to calculate the wettedness and reported values ranging from 15 to 35 per cent. Guibert[9] reported wettedness from 0.08 to 1.46, basing his result on heat-transfer considerations. The data showing A_w/A_s greater than 1.0 are obviously in error. The NACA scheme of wrapping a water sensitive tape about the surface should give a more accurate time average result provided the tape surface is not too different from the wing surface under study.

Accuracy of Design

In view of the uncertainties which surround each of the important parameters which enter the design of an anti-icing system, one may well question the accuracy with which the completed system's behavior may be predicted. The present state of the art certainly leaves much to be desired, but some of the uncertainties are not as bad as they may seem.

Messinger[11] has shown that the design of an air-heated anti-icing system is not too greatly affected by the magnitude of the exterior unit thermal conductance. (This effect is also discussed in Reference 2).

The reason for this peculiar result is that for a given airflow and air temperature inside the wing, an increased exterior conductance results in a lower wing surface temperature, thus increasing the effectiveness with which the heat supply from the heaters may be used. The exponential variation of the vapor pressure with temperature tends to stabilize the evaporative system. A large value of the conductance combined with a low-vapor-pressure difference may evaporate as much water as a low conductance combined with a high vapor-pressure difference. The size of air ducting and heaters may well be the same in the two cases, though the detailed behavior (surface temperatures, air outlet temperatures) may be radically different.

REFERENCES

1. Hardy, J. K., "An Analysis of the Dissipation of Heat in Conditions of Icing from a Section of the Wing of a C-46 Airplane". NACA Report 831, 1945.

2. Tribus, M., and Tessman, J., "Report on the Development and Application of Heated Wings". AAF TR 4972, ADD. I, January 9, 1946.

3. Neel, C. B., Bergrun, N. R., Jukoff, D., and Schlaff, B. A., "The Calculation of the Heat Required for Wing Thermal Ice Prevention in Specified Icing Conditions". NACA TN 1479, December 1947.

4. Bergrun, N. R., "General Results of NACA Flight Research in Natural Icing Conditions During the Winters of 1945 and 1946". Aero. Eng. Rev., January 1948, p. 20.

5. Neel, C. B., "The Calculation of the Heat Required for Wing Thermal Ice Prevention in Specified Icing Conditions". Paper presented before SAE, Los Angeles, October 2-4, 1947.

6. Patterson, D. M., "A Simplified Procedure for the Determination of Heat Requirements of Ice Protection of Fixed Areas of Aircraft". U. S. CADO, Tech. Data Digest, February 15, 1949.

7. Poppendiek, H. F., "Forced Convection Heat Transfer in Thermal Entrance Regions". Part I ORNL 913 Series A. (Physics) Oak Ridge National Laboratories, Oak Ridge, Tenn., March 1951.

8. Gelder, T. F., and Lewis, J. P., "Comparison of Heat Transfer from Airfoil in Natural and Simulated Icing Conditions". NACA TN 2480, September 1951.

9. Guibert, A. G., "Thermal Anti-Icing Survey on Mt. Washington", Trans. ASME, November 1947, p. 829.

10. Gardner, Tracy B., "Investigation of Runback", Air Materiel Command, Ice Research Base Report I.R.B. 46-36-IF, July 1946.

11. Messinger, F. L., "Design Implications of AAF Technical Report 4972, Add. I", Paper given as part of a symposium on Anti-Icing, ASME, Los Angeles, Calif., June 1946.

12. "Icing Report by the University of California, Fiscal Year 1946". AAF Tech. Report 5529.

13. Boeke, F. L., and Paselk, R. A., "Icing Problems and the Thermal Anti-Icing System". Jour. Aero. Sci., vol 13, No. 9, September 1946, p. 485.

CHAPTER VII

INTERMITTENT HEATING

In Chapter VI the design of an "anti-icing" system was considered. In this chapter we shall consider the design of a thermal "de-icing" system. The advent of higher speeds and increased knowledge about the severity of icing conditions have served to raise the known energy requirements for anti-icing. As an answer to the problem of protecting the new faster aircraft, the designers have turned to the use of intermittent heating. In an intermittently heated system the ice is permitted to form and then the ice-metal interface is heated for a short time. At 32°F the ice adhesive strength goes to zero and the wind forces pull the ice away. By keeping the water in the region of primary impingement until the ice is released, the formation of runback is avoided.

A de-icing system (as opposed to an anti-icing system) compromises the performance of the airplane, since the surfaces are no longer kept aerodynamically clean. The amounts of ice permitted to form are small, however, and it seems well worthwhile to sacrifice some performance in icing conditions for the sake of a lower installed weight. This point of view is justified in airline-type operations, for example, since icing conditions account for but 5 to 8 per cent of flying time.

Intermittent Thermal De-Icers

Propellers have used electrical de-icers with success. In a propeller system the centrifugal forces are available to cast off the ice. The centrifugal forces put a limitation on the allowable "off" time (the time during which the ice is permitted to form) since the ice, when released, may be cast off with considerable force and large pieces of ice may damage the fuselage.

The only intermittent de-icers for which descriptions are available are those which have been used with propellers. Figure VII-1 shows an example of an exterior de-icer[1,2,3] and Figure VII-2 shows the type of construction used in a de-icer mounted in the propeller blade interior.[4,5] The placing of the heating elements inside the blade reduces maintenance problems but increases the energy required for de-icing, as will be shown later.

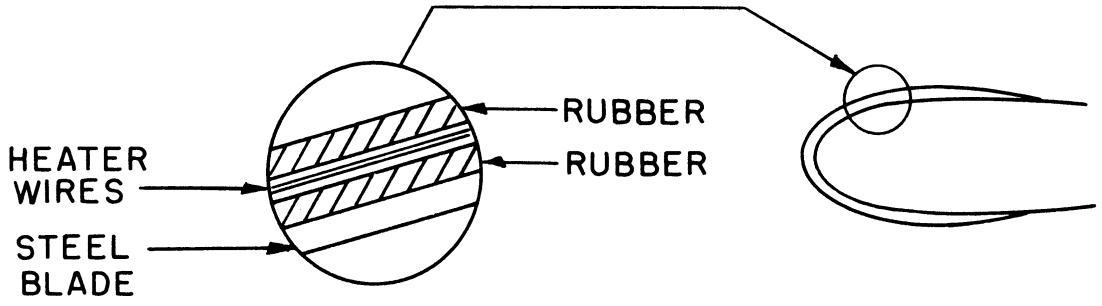

Figure VII-1. Layer details of heaters used in propeller tests by Lewis. This construction is typical of presently used heaters.

Calculating the Performance of an Intermittent De-Icer

In an intermittently operated electric de-icer the heat balance equation must be written:

The Heat from the Electric Heaters = {The heat required to raise the structure temperature
+ {the heat required to melt an ice interface
+ {any heat loss through the ice and the exterior surface during the above process

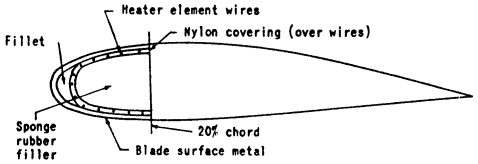

Figure VII-2. Construction of interior de-icer.

References 4 and 6 present analyses of propeller de-icing systems in which the first term on the right (above) predominates, the second term is negligible, and the third term forms 30 to 40 per cent of the total.

At the exterior surface of the ice the modes of energy transfer described in Chapter V are considered to occur.

The heat transfer beneath the ice depends on the type of construction used. Two systems will be considered here in order to illustrate the method of calculation.

Because of the complextiy of the interior construction of a typical intermittent de-icer it is convenient to use an electrical analog for computing the heat-flux distribution. The use of the analog will be shown for the case of a propeller, though the method is general and suitable for wings or other surfaces.

In the electrical analogy to heat flow the following correspondences are used.

TABLE I

Quantity	Electrical	Thermal
CAPACITANCE	C, Farad, $\left(\frac{\text{coulomb}}{\text{volt}}\right)$	$W C_p$ BTU/°F
RESISTANCE	R, ohm $\left(\frac{\text{volt sec}}{\text{coulomb}}\right)$	R_t °F hr/BTU
POTENTIAL	E, volt	T °F
CHARGE	Q, coulomb	Q BTU
FLUX	I, ampere $\left(\frac{\text{coulomb}}{\text{second}}\right)$	q BTU/hr
TIME	t, second	θ hour

The equations descriptive of heat flux and current flow bear a similarity. Thus, consider steady heat flux through a slab of thickness Δx, thermal conductivity k, and area A. The flux is given by

$$q = \frac{k A (T_2 - T_1)}{\Delta x}$$

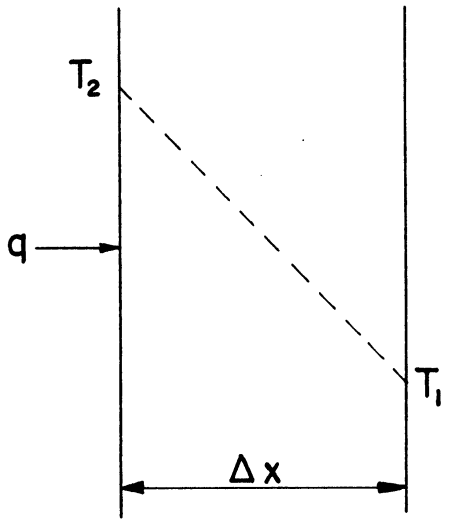

Figure VII-3

which may be rewritten

$$q = \frac{T_2 - T_1}{(\Delta x/kA)} = \frac{T_2 - T_1}{R_t} .$$

The resemblance to Ohm's law

$$I = \frac{E}{R} ,$$

with the correspondence

$$I \longrightarrow q$$

$$E \longrightarrow T_2 - T_1$$

$$R \longrightarrow R_t = \Delta x/k\Lambda$$

permits one to draw a thermal network using electrical symbols. In a complicated network one may construct the analogous electrical network and determine the behavior experimentally.

If the flow is unsteady and the slab undergoes changes in temperature, the energy absorbed is given by

$$q = W C_p \frac{dT}{d\theta} ,$$

which resembles

$$I = C \frac{dE}{dt} ,$$

with

$$I \longrightarrow q$$

$$E \longrightarrow T$$

$$t \longrightarrow \theta$$

$$C \longrightarrow W C_p .$$

If the capacity of the slab is considered as concentrated at its center, the thermal network is:

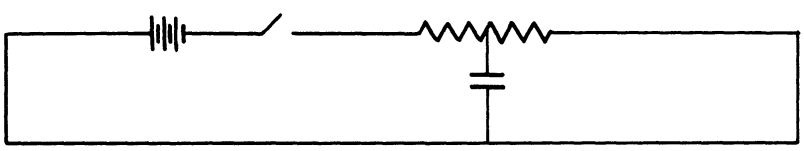

Figure VIII-4

If the slab is considered as composed of several "sub-slabs" a better approximation is obtained.

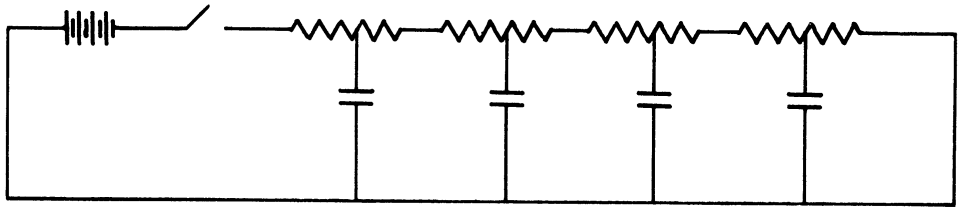

Figure VII-5

The sum of the resistances equals R_t, and the sum of capacitances equals W C_p in Figure VII-5.

The behavior of the thermal network of Figure VII-5 may be found experimentally by building an analogous electrical network and measuring its behavior. If the heat flux is in more than one dimension, additional circuit elements are required.

We now turn to the examination of the thermal network representative of a propeller and its de-icer while operating in icing conditions.

Figure VII-1 shows a typical present-day de-icer attached to a conventional propeller. Figure VII-6 shows the heat-flux paths and the thermal network which approximates the propeller conduction field. A thermal analyzer was used in this case to "solve" the network behavior. The thermal analyzer contains resistors and capacitors which may be quickly combined to form a desired network. Figure VII-7 shows a view of the thermal analyzer* with associated recorders, timers, power supplies, and nonlinear elements.

The heat production at the propeller's electrical resistance elements is relatively independent of the temperature in the propeller. To simulate this behavior a constant current network is needed. A good approximation to such a network is a high-voltage source monitored by a pentode operating on the flat part of its characteristic curve.

AT the surface of the propeller the heat flow is nonlinear with temperature, hence a simple combination of nonlinear elements cannot be utilized. Figure VII-8 shows a network capable of simulating the heat-flux current versus temperature (voltage) characteristic of a surface in icing. Figure VII-9 compares the thermal and electrical systems.

* University of California, Los Angeles

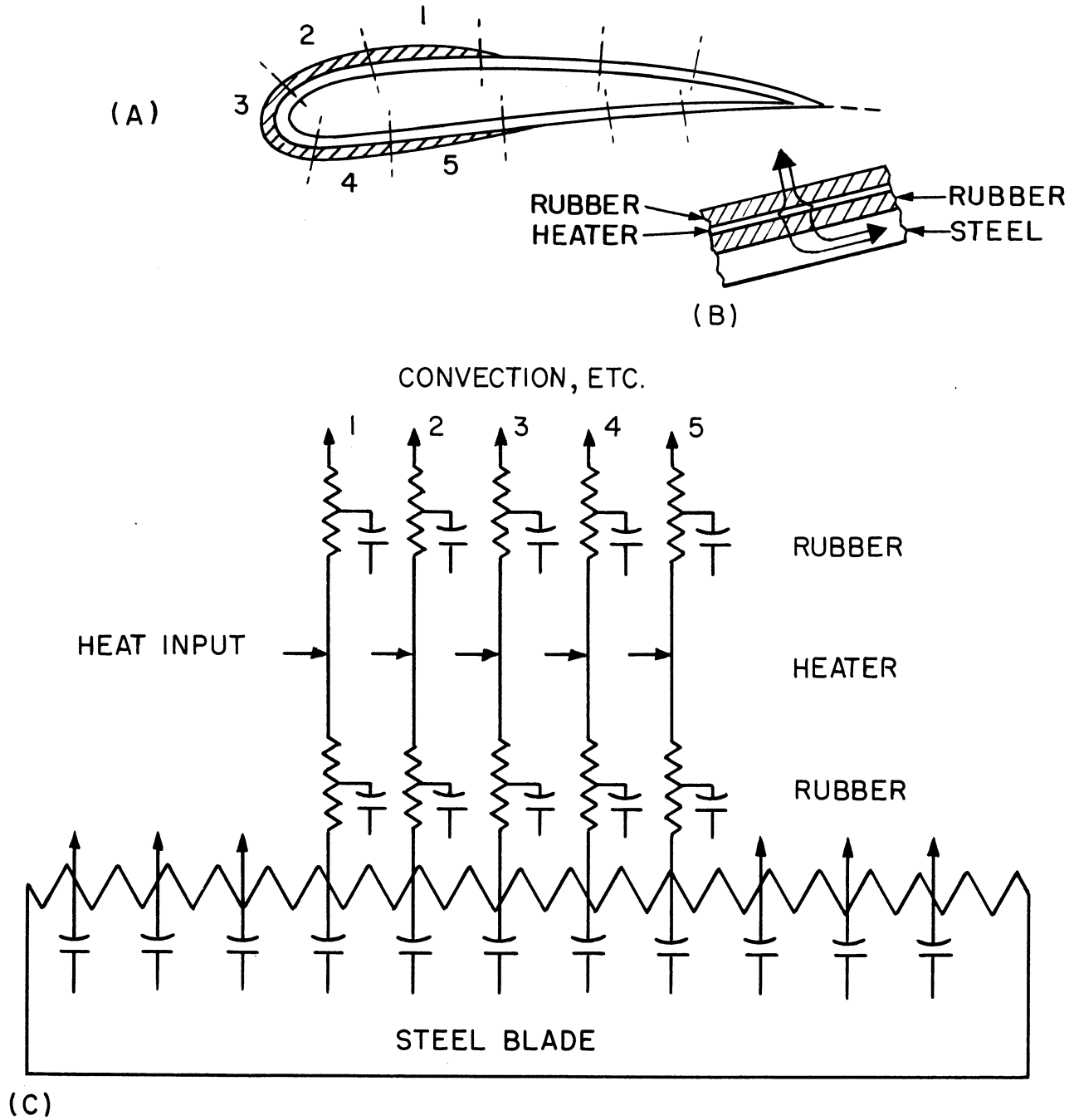

Figure VII-6. Network representative of the idealized heat flow indicated by the arrows in (B) above.

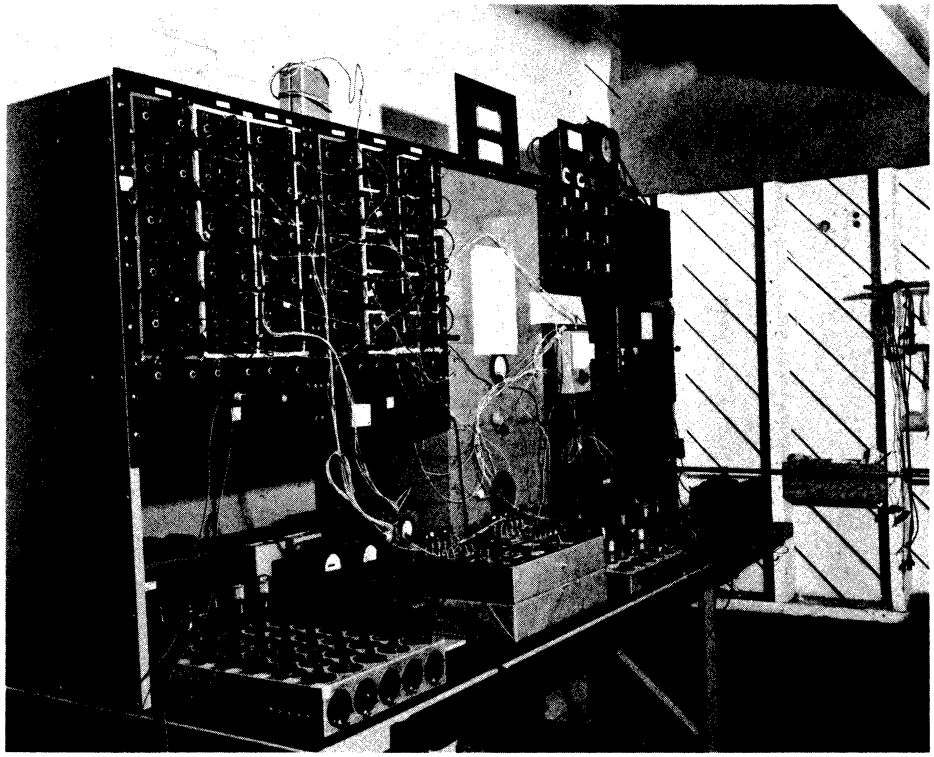

Figure VII-7. Thermal analyzer. (Courtesy University of California, Los Angeles)

The heat-balance equations derived in Chapters IV and V refer to the surface where the ice is forming. The ice layer represents a resistance and capacitance which is small compared to the characteristics of the propeller section in Figure VII-6. For example an ice layer 0.16 inches thick represents a resistance approximately 16 per cent as great as the convective resistance. To simplify the network this ice resistance term has been omitted here.*

Figure V-9 shows a typical set of time-temperature variations measured on a propeller. This figure shows clearly the contributions of the various terms which enter the energy balance. At the left of the figure we see the contribution of aerodynamic heating. When the tunnel sprays are turned on, we see the heat-of-fusion contribution. Then, as the heaters are energized intermittently, we see the rise and fall of blade temperature. In Figure IV-2 similar data are shown in which the heat-of-fusion term is more pronounced.

---

* A network element which has a servo-controlled variable resistor has since been developed to simulate the growing ice layer. In some de-icers this approximation would be seriously in error. See, for example, the discussion at the end of Reference 4.

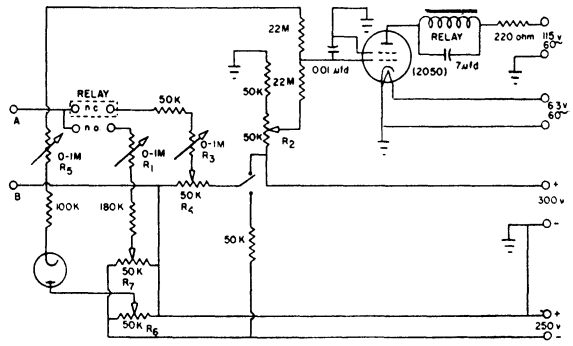

Figure VII-8. Non-linear network used to represent energy flux at the ice surface.

Figures VII-10a to VII-10d show comparisions between the results of the analyzer calculations and the measurements in the wind tunnel.[4,6]

The analyzer is a convenient tool for exploring the behavior of an intermittently operated de-icer. Figure VII-11 shows the results of operating the de-icer at constant energy but with shorter "on" times (i.e., higher powers). The reason for the increased effectiveness of shorter bursts of power is found in Figure VII-12, which shows how much of the heat flows inward to the propeller blade rather than outward to melt the ice.

A simplified view of the behavior of an intermittently heated de-icer is shown in Figure VII-13, where the entire propeller thermal capacitance is lumped in one capacitor.

The nonlinear character of the heat flux is replaced by a linear element. The resulting simple RC circuit fed by a constant current source has the behavior shown in Figure VII-14. The minimum energy occurs at short bursts

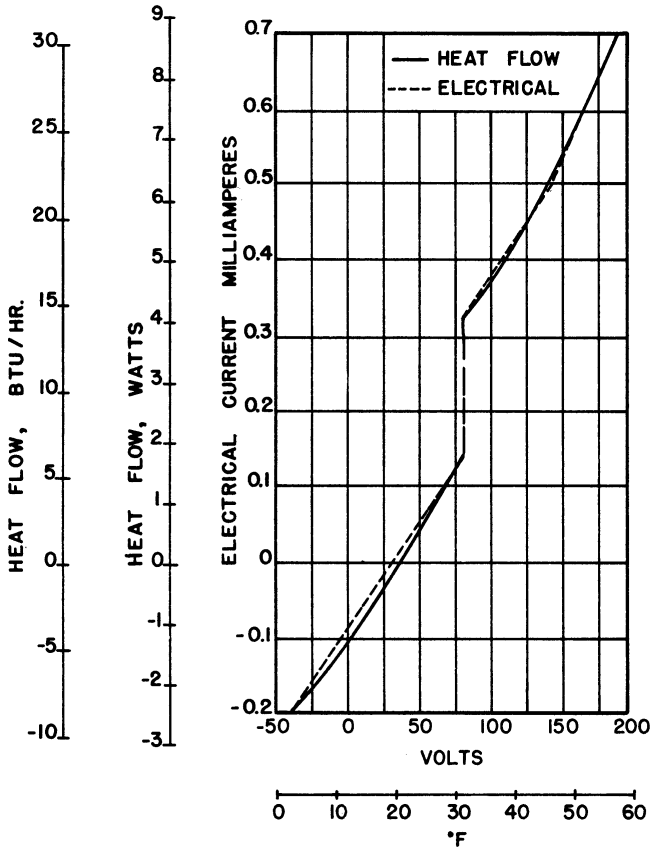

Figure VII-9. Behavior or non-linear network shown when the parameters are adjusted to approximate the heat transfer characteristics of straight dashed line segments represent the electrical network current-voltage characteristics.

of high power and is limited by the thermal capacity, i.e., from Figure VII-14, the energy input has as its lowest value

$$q\theta = W C_p \Delta T \ ,$$

$$\text{(power)(time)} = \text{(thermal capacity)(temp. rise)} \ .$$

The minimum energy requirements occur when the time of heating is vanishingly small and the thermal capacity of the heaters has been reduced to zero.

A second and important characteristic of intermittently operated systems is the diminished heat requirements at increasing water concentrations. Figures IV-2a, b, and c demonstrate the effect very well. In Figure IV-2c the temperature rise due to water impingement is greater than the temperature rise caused by the heaters.

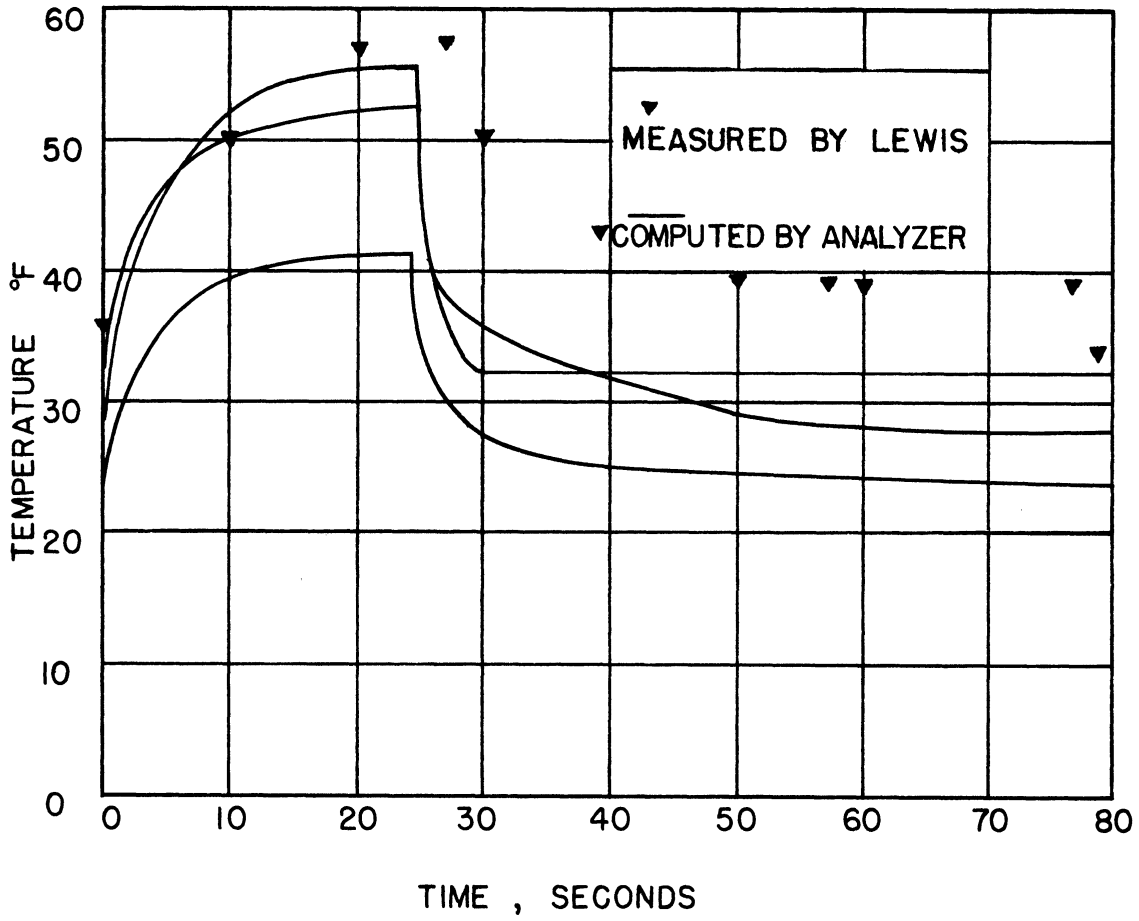

Figure VII-10a. Tunnel temperature 11°F, 925 rpm.

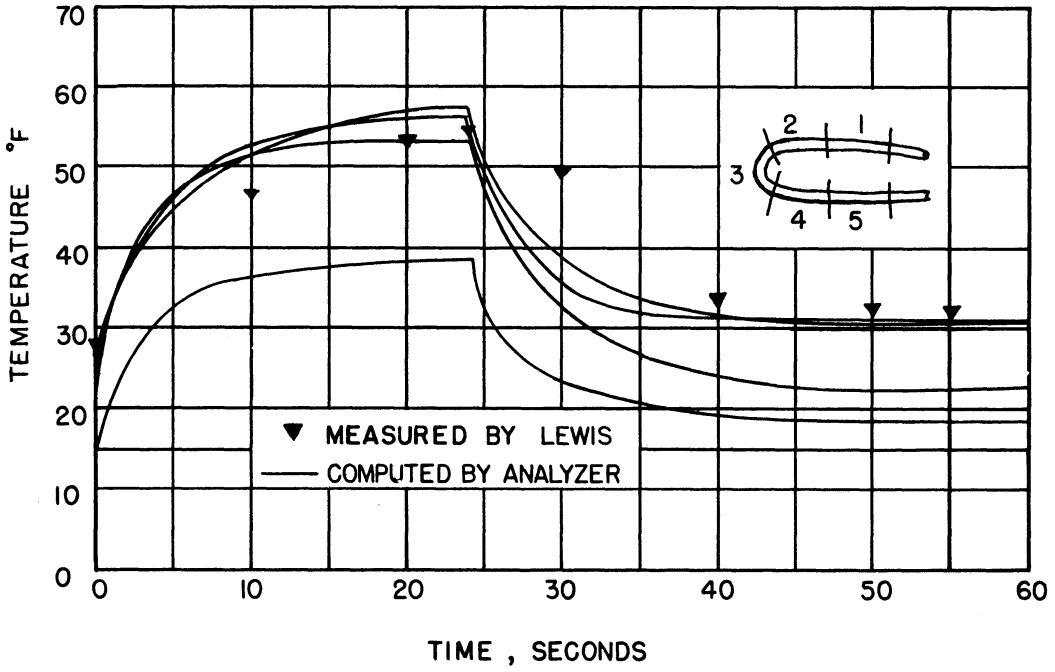

Figure VII-10b. Comparison between data of Lewis and Thermal Analyzer. (τ_∞ = 2°F, 925 rpm, 9 watts/in^2 at seg 3, 8 watts/in^2 on 1, 2, 4, 5, r/R = 0.81). Points correspond to highest curve.

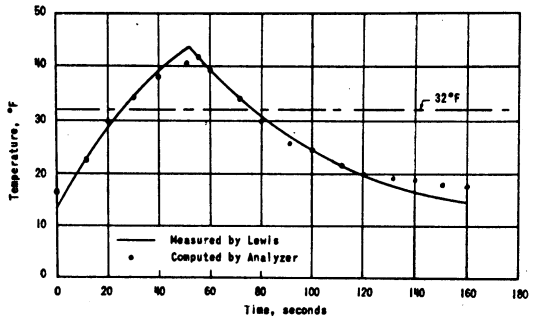

Figure VII-10c. Typical data obtained from thermal analyzer showing time-temperature variations on leading edge of heated propeller blade with comparison to data of Lewis (tunnel temperature 4°F, propeller rpm 800, r/R 0.33.

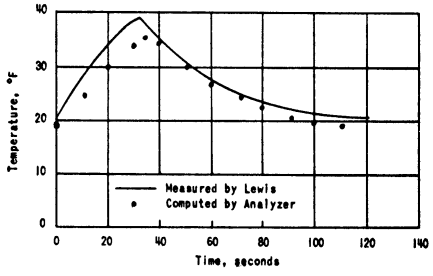

Figure VII-10d. Comparison between data of Lewis and thermal analyzer (tunnel temperature 5°F, propeller rpm 800, r/R 0.33.

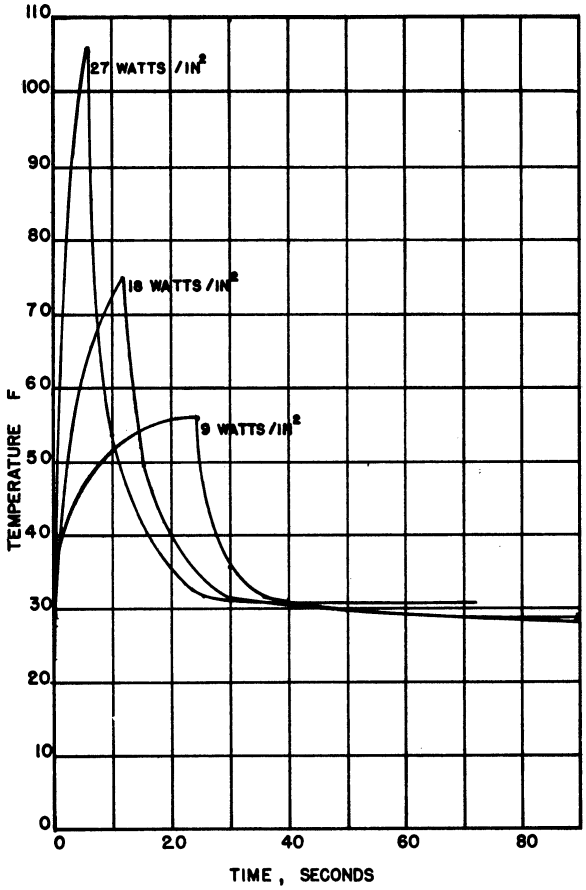

Figure VII-11. Effect of varying power density at constant energy.

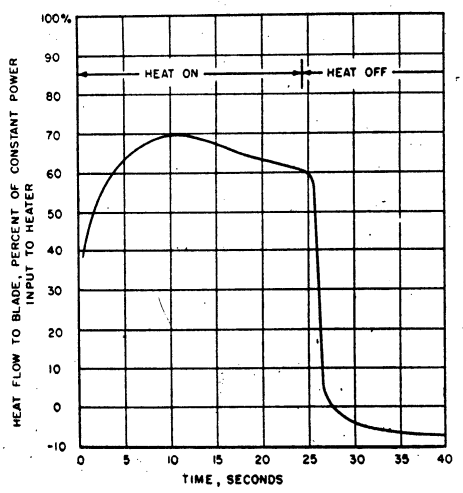

Figure VII-12. Thermal analyzer data on heat flow inward to blade during a cycle.

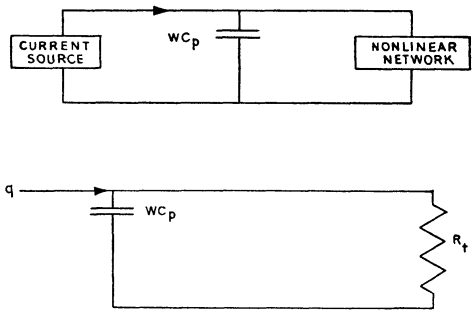

Figure VII-13. Simplified view of intermittent de-icer (above) and a further simplification (below).

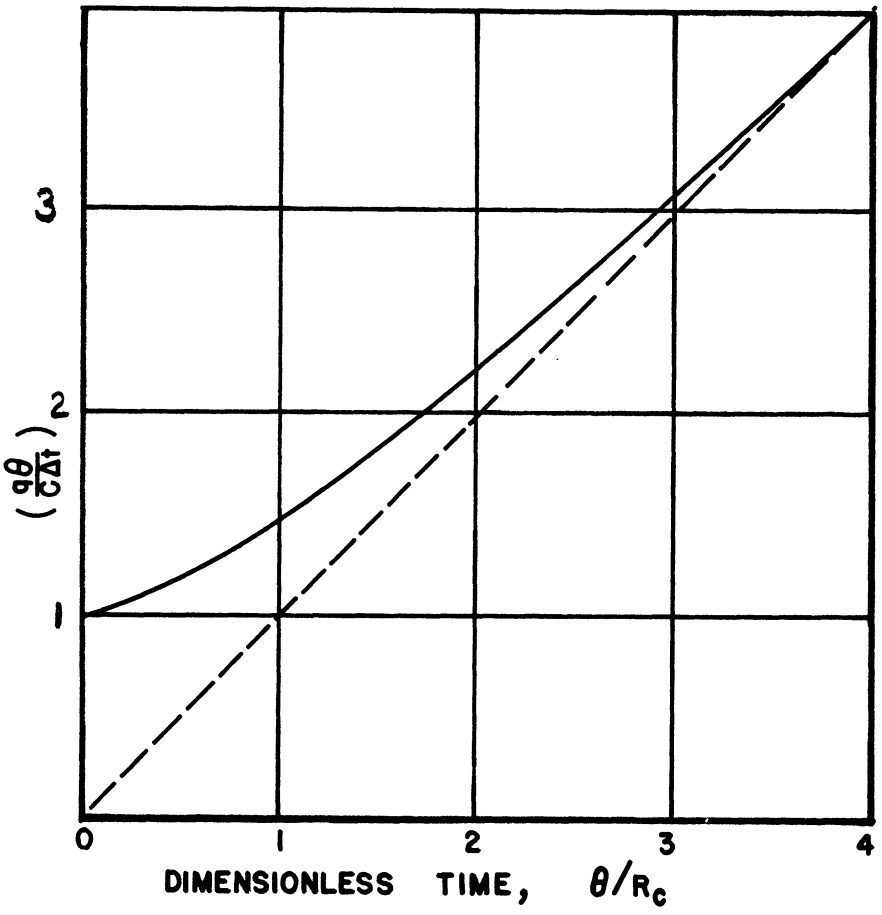

Figure VII-14. Energy requirements for de-icing as a function of heating time.

The Design of an Intermittent De-Icer

An examination of the above data shows that the minimum energy for de-icing is governed by the equation

$$q\theta = W C_p (t_s - t_o) \quad .$$

In this equation, $q\theta$ is the total energy required for de-icing, WC_p is the thermal capacity of the heated structure (and the ice), t_s is the temperature at which the ice sheds (somewhere just above 32°F), and t_o is the temperature of the surface when q = o. The actual energy required will exceed this amount because of the loss of heat to the airstream, but as noted in Figure VII-13, the excess losses may be minimized by short bursts of power.

The allowable "off" times will be set by the maximum allowable ice buildup. At low temperatures, where icing is usually less severe, the allowable "off" times may be increased. Under these conditions also the initial temperature, t_o, will be low, hence a larger value of $q\theta$ will be needed. An automatic timer which changes the cycle times in accordance with the outside air temperature is described in Reference 7.

The lowest temperatures at which icing data have been evaluated are above -40°F (Reference 8). Thus, a temperature rise of 32 - (-40) = 72°F in clear air, provided the rise occurs within on tenth of the time constant of the system (as determined from cooling curves), should provide de-icing over the important range of icing conditions.

In an intermittent de-icing system the rate of water catch determines the allowable "off" periods, and the area of impingement determines the extent of heated area required. The water catch rate has a lesser influence upon the design energy requirements for ice release, since the design is established when the icing rate is low, rather than at the other end of the icing intensity scale, as is the case with anti-icing systems.

In a wing de-icer a continuously heated region at the nose must be maintained as a "parting strip" to prevent ice capping. The minimum necessary size of parting strip has not yet been determined and most probably is a function of the airfoil shape. The energy required by the parting strip may be calculated from data used in conventional anti-icer design((Chapter VI).

REFERENCES

1. Loughlin, W., "Propeller Electrical De-icing System for the P-82 Airplane". AAF Tech. Report 5442, March 22, 1946.

2. Anon. "Hydromatic Propellers: Electric De-Icing System". Brochure No. 171 by Hamilton Standard Propellers, Division of United Aircraft Corporation, East Hartford, Conn.

3. Lewis, J. P., "De-Icing Effectiveness of External Electric Heaters for Propeller Blades". NACA TN 1520, February 1948.

4. Weiner, F. W., "Further Remarks on Intermittent Heating for Aircraft Ice Protection". Trans. ASME, November 1951, p. 1131.

5. Lewis, J. P., and Stevens, H. C., "Icing and De-Icing of a Propeller with Internal Electric Blade Heaters". NACA TN 1691, August 1948.

6. Tribus, M., "Intermittent Heating for Aircraft Ice Protection wtih Application to Propellers and Jet Engines". Trans. ASME, November 1951, p. 1117.

7. Tribus, M., "A Review of Some German Developments in Airplane Anti-Icing". Trans. ASME, July 1947, p. 505.

8. Ambrosio, A., "Statistical Analysis of Meteorological Icing Conditions". Department of Engineering, University of California, Los Angeles.

CHAPTER VIII

METEOROLOGICAL CONDITIONS FOR DESIGN

The problem of choosing the proper meterological conditions for the design of an ice-prevention system involves a fine balance between the allowable weight and maintenance penalties and the probability of encountering an icing storm which exceeds the design conditions. Heated wing equipment is still too new for the adequacy of the designs to be properly assessed. The gathering of data has been hindered until now by the lack of suitable instruments for measuring and reporting liquid-water contents and drop sizes encountered in the atmosphere.

The nature of the equipment used for ice prevention tends to set the design condition almost as much as do the meteorological data. For example, a heated wing anti-icing system fails to give adequate protection whenever the impinging moisture is not evaporated and runback begins to form. A small amount of runback is not dangerous, hence the design condition for an air heated wing anti-icer will be set, not only by the maximum water catch but also by the horizontal extent of the icing condition, i.e., how long the airplane will be in the icing conditions and how much runback can be tolerated.

On the other hand, an intermittent de-icer will be designed primarily on the basis of low-temperature icing.

The de-icing of a jet engine inlet will depend on the liquid-water content and temperature and only to a lesser extent on drop size, since the collection efficiencies of the engine components are usually high. A failure of the de-icing system of a jet engine is more serious and can lead to disaster more quickly than a wing anti-icer; hence, the horizontal extent of the icing condition becomes less important compared to the instantaneous severity.

Natural icing conditions vary greatly in intensity not only from point to point but also from time to time. A cloud is a dynamic thing; the water drops are constantly growing or evaporating. Indeed, in a particular region of the cloud, the small drops may be evaporating while the big ones grow. The measurement of liquid-water content and drop size is therefore made difficult, and simultaneous independent measurements can rarely be made. Figure VIII-1 shows a record made during an icing flight and shows the variations in icing intensity recorded on the leading edge of a flat disc in the icing airstream.[10]

Most measurements of icing have been made using the multicylinder method described in Chapter II. Reference 1 presents a statistical analysis of all icing observations available up to 1950. Approximately 3600 observations were analyzed, about 30 per cent being flight observations. William Lewis, in a sequence of NACA reports[2-7] has gathered and studied flight data taken by NACA. He has sorted the observations with respect to clouds of stratoform type, which extend over large areas, and cumuloform type, which generally display a lesser horizontal extent but greater severity. In Reference 4 Lewis proposed to use a classification system for icing conditions as follows:

Trace of Ice
Light Ice
Moderate Ice
Heavy Ice

Originally these quantities were defined in terms of the ice accretion rate on a 3-inch diameter circular cylinder at 200 mph. Lewis converted the Weather Bureau definitions to zones on a graph of liquid-water content versus mean effective drop size. These classifications have apparently been accepted by the aircraft industry, though obviously the same icing cloud may produce different ice characteristics on a slow, large cargo airplane as compared to a small high-speed fighter.

Later, Lewis and Jones[6] suggested classifications for icing conditions. These classifications are best summarized by Table I, taken directly from Reference 6. At the present date, the classification appears rational though probably some of the recommended drop sizes and liquid-water contents may be expected to change as more data become available.

Figures VIII-2 and VIII-3 are taken from a recent report by Hacker and Dorsch,[8] which shows a method of selecting the design condition for a particular heated-wing anti-icing system. The collection of water is cross-plotted on a tabulation of the number of icing observations known at each combination of drop size and liquid-water content. The stratoform clouds are considered separately from the cumuloform clouds. The designer may use such a cross plot to visualize the degree of protection afforded by various systems.

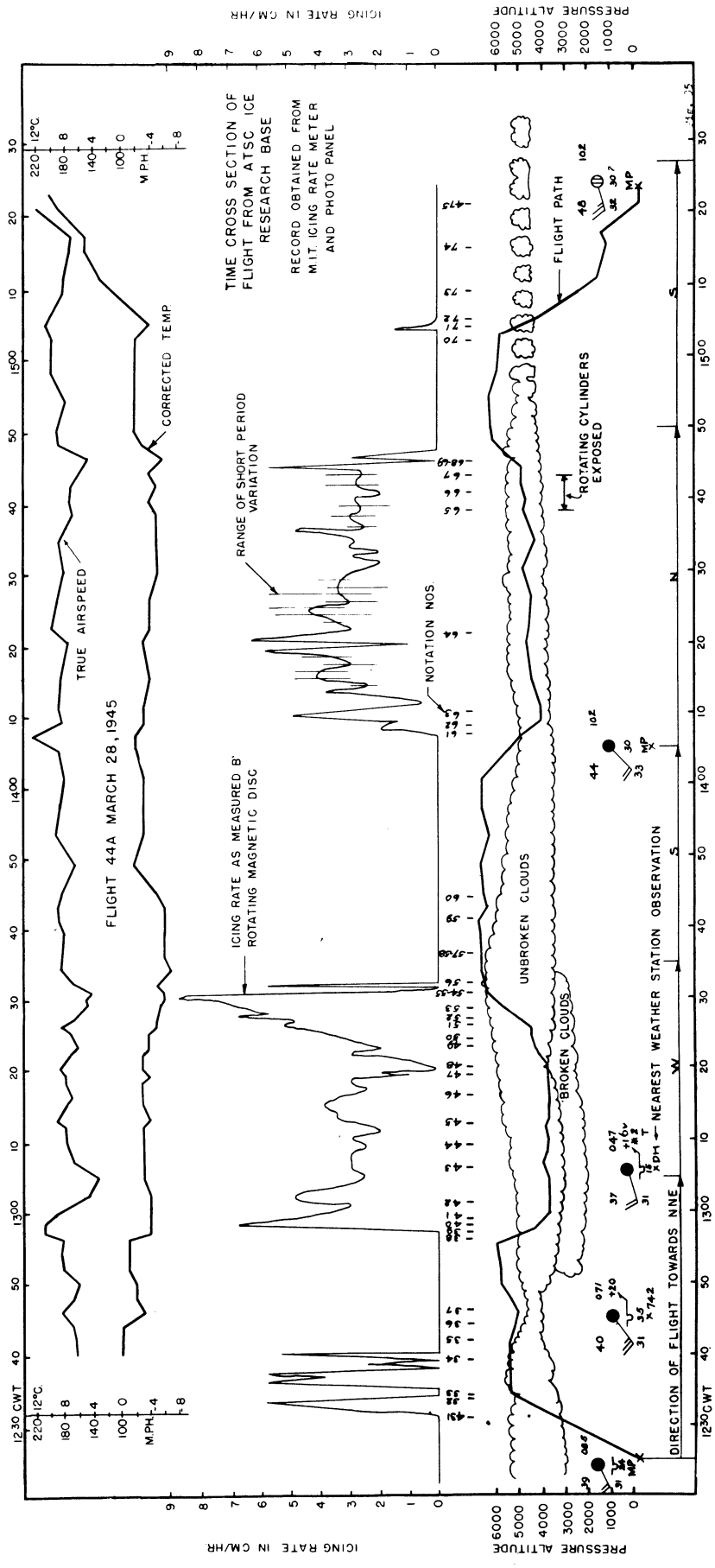

Figure VIII-1. Typical flight record as made with rotating disc instrument.

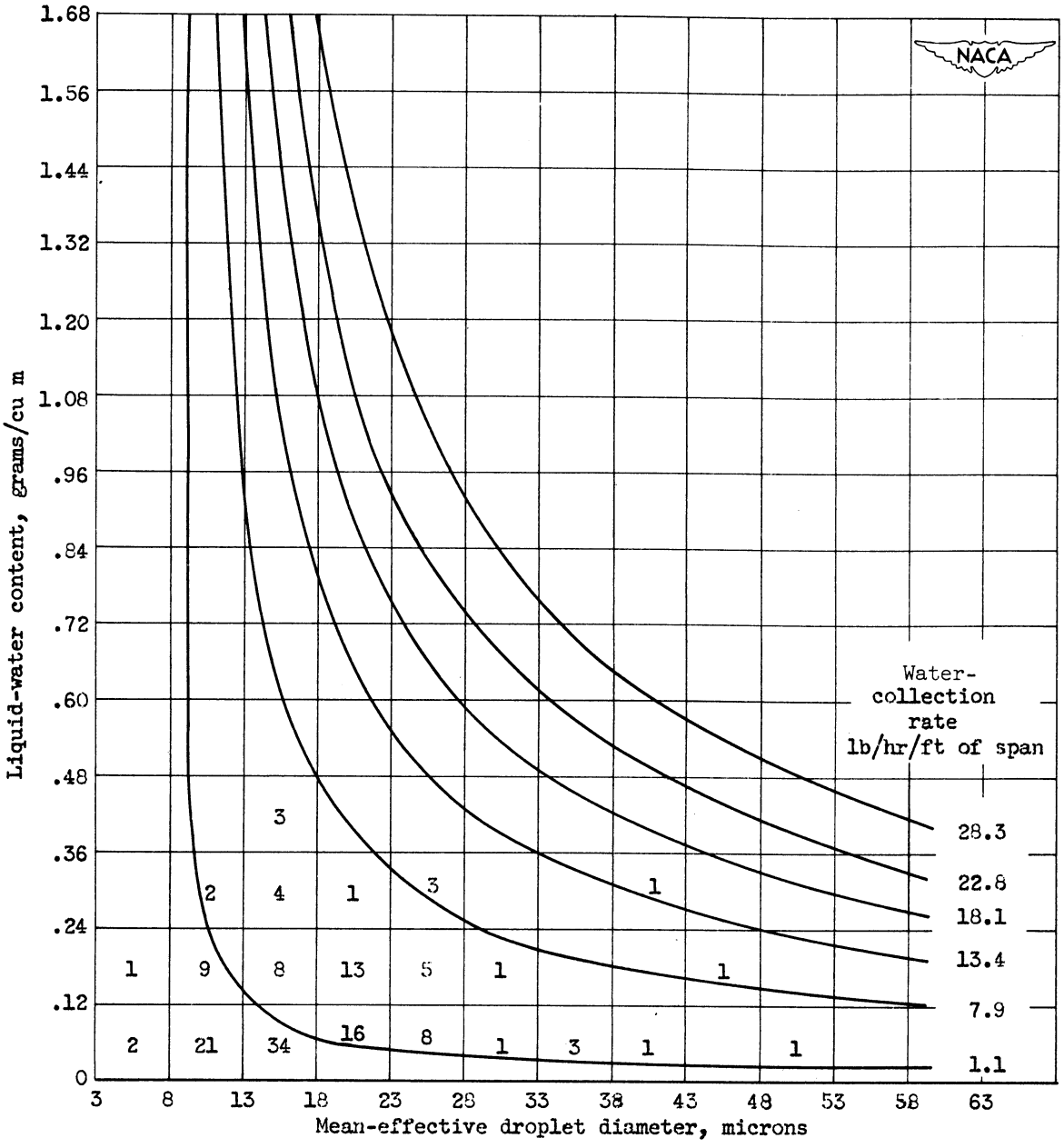

Figure VIII-2. Constant water-collection-rate curves for hypothetical airfoil superimposed on frequency distribution of icing observations: Stratiform clouds between pressure altitudes of 10,000 and 20,000 feet.

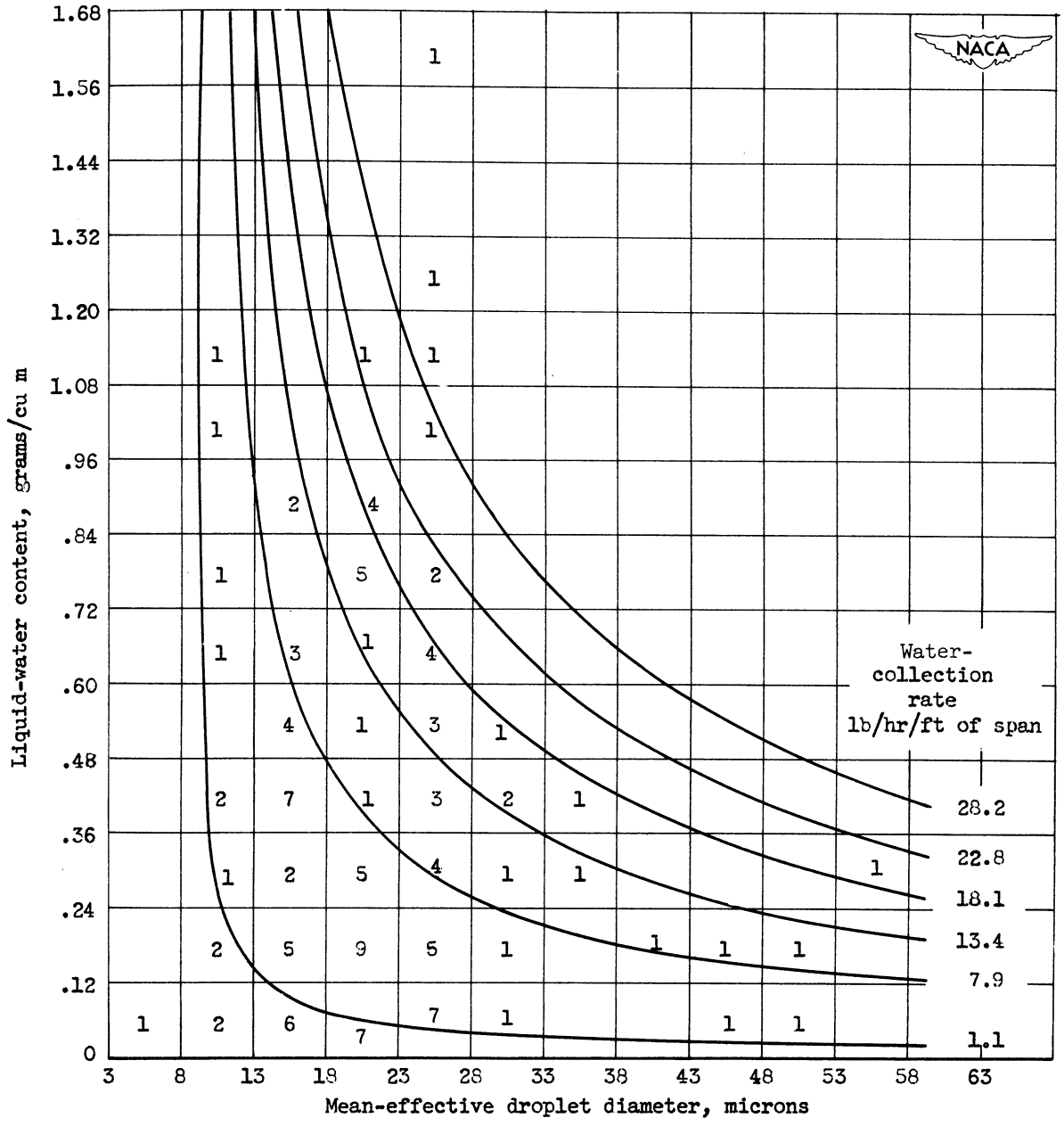

Figure VIII-3. Constant water-collection-rate curves for hypothetical airfoil superimposed on frequency distribution of icing observations: Cumuliform clouds between pressure altitudes of 10,000 and 20,000 feet.

TABLE I.- RECOMMENDED VALUES OF METEOROLOGICAL FACTORS FOR CONSIDERATION IN THE DESIGN OF AIRCRAFT ICE-PREVENTION EQUIPMENT

Class	Item	Air temp. (°F)	Liquid water content (g/m^3)	Drop diameter (microns)	Pressure altitude (ft)	Remarks
I - M Instantaneous, Maximum	1	32	5.0	25	18,000 to 20,000	Horizontal extent: 1/2 mile. Duration at 180 mph: 10 seconds. Characteristic: Very high liquid water content. Applicable to: Any part of the airplane, such as guide vanes in inlet ducts, where a sudden large mass of supercooled water would be critical, even though of short duration. Example: Induction systems, particularly turbine-engine inlets.
	2	14	4.0	25	22,000 to 25,000	
	3	-4	3.0	25	25,000 to 30,000	
	4	-22	2.0	20	20,000 to 30,000	
	5	-40	.5	15	20,000 to 30,000	
I - N Instantaneous, Normal	6	32	1.0	20	10,000 to 20,000	
	7	14	1.0	20	10,000 to 25,000	
	8	-4	.6	18	12,000 to 30,000	
	9	-22	.2	15	15,000 to 30,000	
	10	-40	<.1	13	15,000 to 30,000	
II - M Intermittent, Maximum	11	32	2.5	20	10,000 to 15,000	Horizontal extent: 3 miles Duration at 180 mph: 1 minute Characteristic: High liquid water content Applicable to: Any critical component of the airplane where ice accretions, even though slight and of short duration could not be tolerated. Example: Induction systems, windshields when continuous visibility is required.
	12	14	2.2		10,000 to 20,000	
	13	-4	1.7		12,000 to 30,000	
	14	-22	1.0		15,000 to 30,000	
	15	-40	.2		15,000 to 30,000	
	16	32	1.3	30	8,000 to 15,000	
	17	14	1.0		8,000 to 20,000	
	18	-4	.8		10,000 to 30,000	
	19	-22	.5		15,000 to 30,000	
	20	-40	.1		15,000 to 30,000	
	21	32	.4	50	8,000 to 15,000	
	22	14	.3		8,000 to 20,000	
	23	-4	.2		10,000 to 30,000	
	24	-22	.1		15,000 to 30,000	
	25	-40	<.1		15,000 to 30,000	
II - N Intermittent, Normal	26	32	.8	20	8,000 to 12,000	
	27	14	.6	20	8,000 to 15,000	
	28	-4	.4	18	12,000 to 20,000	
	29	-22	.1	15	15,000 to 25,000	
	30	-40	<.1	13	15,000 to 25,000	
III - M Continuous, Maximum	31	32	.8	15	3,000 to 20,000	Horizontal extent and duration: Continuous. Characteristic: Moderate to low liquid water content for an indefinite period of time. Applicable to: All components of the airplane; that is, every part of the airplane should be examined with the question in mind, "Will this part be affected seriously by accretions during continuous flight in icing conditions?" Example: Wings and tail surfaces.
	32	14	.6			
	33	-4	.3			
	34	-22	.2			
	35	-40	..05			
	36	32	.5	25		
	37	14	.3			
	38	-4	.15			
	39	-22	.10			
	40	-40	.03			
	41	32	.15	40		
	42	14	.10			
	43	-4	.06			
	44	-22	.04			
	45	-40	.01			
III - N Continuous, Normal	46	32	.3	15		
	47	14	.2			
	48	-4	.1			
	49	-22	<.1			
IV - M Freezing Rain	50	25 to 32	.15	1000	0 to 5,000	Horizontal extent: 100 miles. Duration at 180 mph: 30 minutes. Characteristic: Very large drops at near-freezing temperatures and low values of liquid water content. Applicable to: Components of the airplane for which no protection would be supplied after considering classes I, II, and III. Example: Fuselage static pressure airspeed vents.

S. S. Schaetzel[9] has suggested a different method of calculating. In his method, for a particular airfoil, one makes a three-dimensional plot. The three variables are (1) drop size, (2) liquid-water content, and (3) rate of catch. The resultant surface is defined by an airfoil at a particular speed altitude and angle of attack. Using the recommendations of Lewis and Jones[6] Schaetzel postulates a relation between drop size and liquid-water content as a function of temperature. This relation permitted the plotting of isothermals on the above surface. Figure VIII-4 shows the resultant graph. These isothermals are lines of equal energy required for anti-icing; hence, the most severe design conditions can be selected readily.

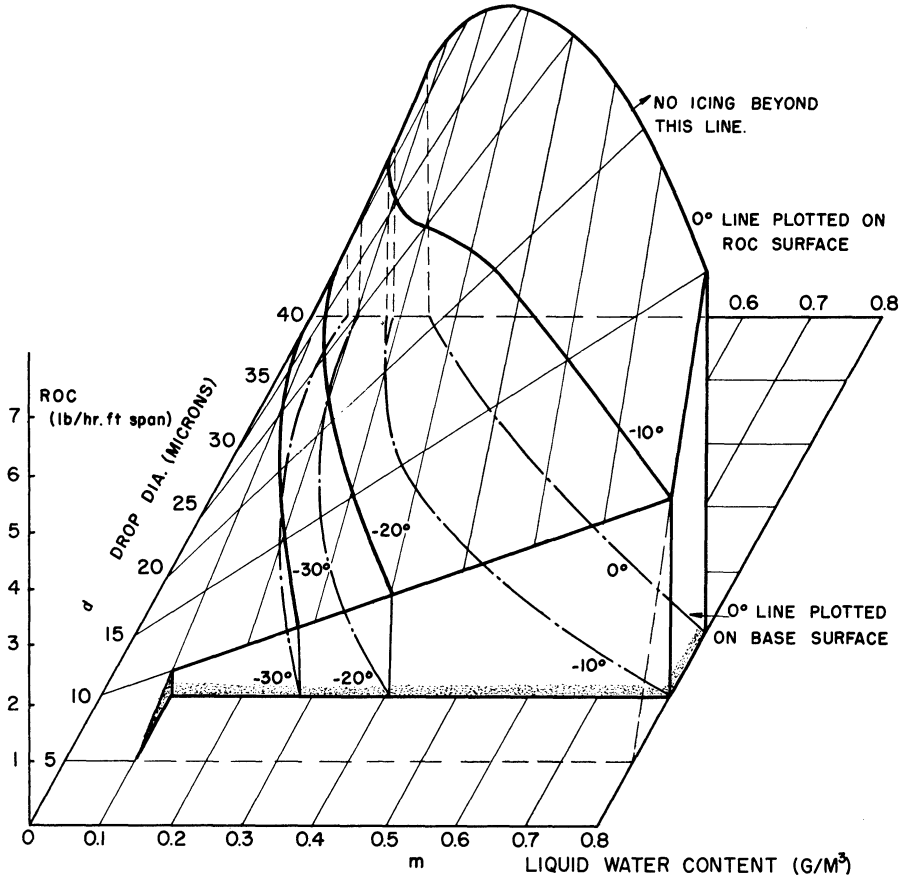

Figure VIII-4. Roc* versus drop diameter and liquid water content at various temperatures. (NACA 0012 wing 12' $\bar{c}$, 362 f.p.s. tas 20,000 ft.) The roc at any temperature is given by the vertical intercept between the temperature lines plotted on the base and the temperature line on the roc surface.

*Rate of catch.

REFERENCES

1. Ambrosio, A., "Statistical Analysis of Meteorological Icing Conditions". Department of Engineering, University of California, Los Angeles, December 1950.

2. Lewis, Wm., "Icing Properties of Noncyclonic Winter Stratus Clouds". NACA, TN 1391, September 1947.

3. Lewis, Wm., "Icing Zones in a Warm Front System with General Precipitation". NACA, TN 1392, July 1947.

4. Lewis, Wm., "A Flight Investigation of the Meteorological Conditions Conducive to the Formation of Ice on Airplanes". NACA, TN 1393, August 1947.

5. Lewis, Wm., Kline, D. B., and Steinmetz, C. P., "A Further Investigation of the Meteorological Conditions Conducive to Aircraft Icing". NACA, TN 1424, October 1947.

6. Lewis, Wm., and Jones, A. R., "Recommended Values of Meteorological Factors to be Considered in the Design of Aircraft Ice-Prevention Equipment". NACA, TN 1855, March 1949.

7. Lewis, Wm., and Hoecker, W. H., "Observations of Icing Conditions Encountered in Flight During 1948". NACA, TN 1904, June 1949.

8. Hacker, P. T., and Dorsch, R. G., "A Summary of Meteorological Conditions Associated with Aircraft Icing and a Proposed Method of Selecting Design Criterions for Ice Protection Equipment". NACA, TN 2569, November 1951.

9. Schaetzel, S. S., "A Rapid Method of Estimating the Severity of Icing". Aircraft Engineering, July 1950, p. 186.

10. Tribus, M., and Tessman, J., "Report on the Development and Application of Heated Wings". AAF, TR 4972, Add. I. January 9, 1946.